

**FAULT PATTERNS, FAULT ACTIVITY
RECONSTRUCTIONS AND A NEW SOURCE CANDIDATE
FOR TSUNAMIS IN THE MESSINA STRAIT, SOUTHERN
ITALY**

DISSERTATION

in fulfilment of the requirements for the degree “Dr. rer. nat.”

of the Faculty of Mathematics and Natural Sciences

at Kiel University

submitted by

Lili Fu

Kiel, 2015

First referee: Prof. Dr. Sebastian Krastel-Gudegast

Second referee: Prof. Dr. Jan-Hinrich Behrmann

Date of the oral examination: 21.09.2015

Approved of publication: 22.09.2015

Hiermit erkläre ich, dass die vorliegende Dissertation – abgesehen von der Beratung durch meine Betreuer – nach Inhalt und Form meine eigene Arbeit ist. Weder diese noch eine ähnliche Arbeit wurde an einer anderen Abteilung oder Hochschule im Rahmen eines Prüfungsverfahrens vorgelegt, veröffentlicht oder zur Veröffentlichung vorgelegt. Ferner versichere ich, dass die Arbeit unter Einhaltung der Regeln guter wissenschaftlicher Praxis der Deutschen Forschungsgemeinschaft entstanden ist.

Lili Fu

ABSTRACT

Submarine hazards, such as earthquakes, submarine slope failures, and resulting tsunamis, on the continental margins pose great threats to coastal communities and have received much concern in scientific research. The 1908 Messina earthquake and tsunami, the deadliest event in Europe since then, is a typical event of this kind. However, no general agreement has been archived on the seismogenic/tsunamigenic faults, mainly because the tectonics of the Messina Strait is still unclear.

In order to contribute to this open question, new multi-beam bathymetry data, sediment echo sounding data, and high-resolution 2D reflection seismic data were collected during RV Meteor Cruise M86/2 off Southern Italy (including the Messina Strait) from December 27th, 2011 to January 17th, 2012. Based on the new data, many near-surface faulting structures have been identified for the first time in the Messina Strait. The fault patterns of the Messina Strait were built up and analysed, fault activities in the outer Messina Strait were reconstructed, and numerical tsunami modelling was done. Central questions of this thesis include:

- i) What types of faults have been identified in the Messina Strait?
- ii) How do they fit to the overall tectonic framework of the Messina Strait?
- iii) Were the faults in the outer Messina Strait active recently?
- iv) Can the faults in the outer Messina Strait generate tsunamis and how large may they get?

The new data suggest that the inner Messina Strait is an angular graben. Near-surface faults in the graben strike in N-S and E-W directions. The N-S-trending near surface faults are right-lateral transtensional faults and distribute along the Messina Canyon and the coastline off southern Calabria, dipping toward the Messina Canyon; E-W-trending near-surface faults are left-lateral transtensional faults and located in the northern inner Messina Strait off Calabria. Most of them dip toward the south. The apparent dip angles of all near-surface faults are less than 50 degrees. Several newly-discovered near-surface faults fit to the suggested focal mechanisms of the 1908 Messina earthquake, but we were not able to identify the master fault of this event. The lengths of the fault planes (< 15 km) are too small to generate an earthquake of 7 Mw. The inferred Taormina Fault (TF) was considered as one of the most hazardous and largest seismic gaps in Italy. However, this fault has not been imaged on any seismic data set including our new seismic data. Hence, the existence of the TF is doubted.

In the outer Messina Strait, a prominent fault zone has been discovered and named as the Fiumefreddo - Melito di Porto Salvo Fault Zone (F-MPS_FZ). It is located in the source area proposed for the 1908 Messina tsunami. The F-MPS_FZ is a E-W-trending left-lateral transtensional fault zone, which shows ongoing tectonic activity and supports a transtensional regime in the outer Messina Strait. Most of the faults in this zone dip toward the south at apparent dip angles around 60 degrees. The dominant scarp-like structure (DSS) represents the surface expression of the master fault of the F-MPS_FZ. The F-MPS_FZ may be a STEP-Connector Fault, linking the two postulated Subduction-Transform Edge Propagator (STEP) faults: the Ionian Fault and the Alfeo-Etna Fault. This STEP-Connector Fault may have formed in two ways: in a pull-apart basin style or in a fault-termination basin style. Based on our data, the pull-apart basin style model is more reasonable for this newly-discovered fault zone.

The F-MPS_FZ reach down to the acoustic basement. It has been active during the entire regional tectonic evolution of the outer Messina Strait. During its evolution, the fault activity alternated between tranpressional and transtensional with varying apparent displacements. Currently, the F-MPS_FZ is an active transtensional fault zone. Based on the results of the tsunami modelling, the F-MPS_FZ could generate tsunamis, and an assumed slip rate of up to 15 m could generate a tsunami comparable to the 1908 Messina tsunami, but the F-MPS_FZ may not be a candidate source for the 1908 Messina tsunami, because an E-W-trending fault is not in agreement with seismological data of the 1908 Messina earthquake, and a 15 m slip event is highly unlikely. However, the F-MPS_FZ is still a highly potential hazard source in Southern Italy, because it shows the most obvious vertical displacement in the entire Messina Strait and seems to be active.

ZUSAMMENFASSUNG

Untermeerische Naturgefahren wie Erdbeben und Hangrutschungen im Bereich von Kontinentelhängen sowie damit einhergehende Tsunamis haben in den letzten Jahrzehnten einen hohen Grad an Aufmerksamkeit in der Forschung erhalten. Dies liegt darin begründet, dass solche teilweise katastrophal verlaufenden Ereignisse eine hohe Zahl an Todesopfern fordern können und immense Schäden in Küstenregionen mit sich bringen können.

Das bis heute schwerwiegendste Ereignis dieser Art in Europa war 1908 das Messina-Erdbeben und der nachfolgende Tsunami, ein typisches Beispiel für eine solche Katastrophe. Jedoch herrscht bisher kein eindeutiger Konsens über die Lokation der Störungen die die Quelle für das Erdbeben und den Tsunami waren, hauptsächlich weil die tektonischen Gegebenheiten der Straße von Messina noch nicht genau bekannt sind.

Um einen Beitrag zur Beantwortung der bisher ungeklärten Frage nach den Quellregionen für das Erdbeben und den Tsunami leisten, wurde während der Forschungsausfahrt M86/2 (FS METEOR) vom 27. 12. 2011 bis zum 17. 01. 2012 in Süditalien und der Straße von Messina, neue hochauflösende Fächerecholot-, Sedimentecholot-, und Mehrkanalseismik- Daten aufgezeichnet. Mithilfe der gewonnenen Daten war es nun es erstmals möglich einige unbekannte Störungzonen im Untergrund der Straße von Messina zu lokalisieren.

Basierend auf diesen neuen hydroakustischen und seismischen Daten, war es möglich, zahlreiche, bisher unbekannte oberflächennahen Verwerfungssysteme in und südlich der Straße von Messina zu identifizieren, Aktivitäten entlang dieser Störungzonen zu rekonstruieren und die numerische Modellierung eines möglichen Tsunami südlich der Straße von Messina durchzuführen. Die Hauptfragestellungen, die in dieser Arbeit behandelt werden lauten dementsprechend:

- i) Welche Typen von von tektonischen Verwerfungen sind in der Straße von Messina vorhanden?
- ii) Wie ist hängen diese Verwerfungen mit dem regionalen Störungssystem der Straße von Messina und von Süditalien zusammen?
- iii) Sind die neu entdeckten Verwerfungen südlich der Straße von Messina aktiv?
- iv) Könnten die Verwerfungen südlich der Straße von Messina eine Quelle für einen zukünftigen Tsunami darstellen und wenn ja, welche Ausmaße könnte ein solcher Tsunami haben?

Auf Grundlage der neu gewonnenen Daten ist zu vermuten, dass die innere Straße von Messina ein verkippter Graben ist. Oberflächennahe Verwerfungen im Bereich des Grabens entlang des Messina Canyons und der Küstenlinie des südlichen Kalabrien streichen N-S und fallen in Richtung des Messina Canyons ein, während im Bereich der nördlichen inneren Straße von Messina vorhandene sinistrale Transtensionsstörungen O-W streichen und hauptsächlich nach Süden einfallen. Der scheinbare Einfallswinkel aller oberflächennahen Störungen ist kleiner als 50° . Einige neu entdeckte oberflächennahe Verwerfungen passen zum vorgeschlagenen Herdmechanismus des 1908 Messina Erdbebens, jedoch war es nicht möglich anhand unserer Daten die Hauptstörungsfläche zu identifizieren. Die Länge der Störungsflächen (<15 km) wären zu gering um ein Erdbeben mit der Magnitude 7 zu erzeugen. Die vermutete Taormina Verwerfung (TF) wird in dieser Arbeit als die westliche Begrenzung des Grabens der Straße von Messina vorgeschlagen. Es wird angenommen, dass sie einer der größten Gefahrenherde auf Grund ihrer seismischen Kluft für Erdbeben in Italien darstellt. Jedoch konnte die TF bis heute, auch mit Hilfe der hier beschriebenen neuen seismischen Daten, nicht eindeutig nachgewiesen werden.

Das hier erstmals beschriebene Fiumefreddo - Melito di Porto Salvo Störungssystem (F-MPS_FZ) wurde in der äußeren Straße von Messina identifiziert und befindet sich ebenfalls in der vorgeschlagenen Quellregion des Messina- Tsunamis von 1908. Beim F-MPS_FZ handelt es sich um ein rezent aktives Verwerfungssystem, welches als links-laterale transtensive Verwerfungszone in der (äußeren) Straße von Messina identifiziert werden kann. Die meisten Verwerfungen dieser Verwerfungszone fallen in Richtung Süden mit einem scheinbaren Winkel von $\sim 60^\circ$ ein. Die dominierende stufenähnliche Struktur (DSS) repräsentiert die oberflächennahe Ausprägung der Hauptverwerfung des F-MPS_FZ. Das F-MPS_FZ stellt eventuell eine STEP-Connector Verwerfung dar, die die zwei vorgeschlagenen Transform Edge Propagator (STEP) Verwerfungen verbindet: Die Ionian Fault und die Alfeo-Etna Fault. Diese STEP-Connector Verwerfung könnte sich auf zwei verschiedene Arten ausgebildet haben: dem Pull-Apart Becken Stil oder dem Verwerfungsabschluss-Becken Stil. Anhand unserer Datengrundlage erscheint jedoch eine Bildung als Pull-Apart Basin plausibler.

Das F-MPS_FZ ist ein Ost-West streichendes Verwerfungssystem, das bis in das akustische Basement verfolgt werden kann. Es war während der gesamten tektonischen Entwicklung der äußeren Straße von Messina aktiv. Während seiner Entwicklung wechselten transpressive und transtensive Deformationsphasen, und damit einhergehend ergaben sich Variationen in der Sprunghöhe. Rezent stellt das F-MPS_FZ ein aktives transtensives Verwerfungssystem dar. Daher wird diese

Verwerfungszone als eine mögliche Quelle für zukünftige Tsunamis, die die italienischen Küsten treffen könnte, erachtet. Mit einem angenommenen vertikalen Versatz von bis zu 15 m könnte ein Tsunami ausgelöst werden, dessen Ausmaße mit denen des Tsunami von 1908 vergleichbar wären. Jedoch ist nicht davon auszugehen, dass der Tsunami von 1908 an dieser Verwerfung ausgelöst wurde, da ein Ost-West streichendes Verwerfungssystem den gemessenen seismologischen Daten von 1908 nach nicht die Ursache des Erdbebens war. Zudem ist ein Versatz von 15 m während eines einzigen seismischen Ereignisses sehr unwahrscheinlich. Jedoch ist zu vermuten, dass es sich bei diesem Störungssystem um einen potentiellen Gefahrenherd handelt, da es die eindeutigsten und größten bekannten Sprunghöhen in der gesamten Straße von Messina aufweist.

DEDICATIONS

The 1908 Messina earthquake and tsunami, which occurred in the Messina Strait, is the deadliest event in Europe since then. However, no general agreement has been archived on the seismogenic/tsunamigenic fault [AMORUSO *et al.* 2002a; TINTI and ARMIGLIATO 2003b; ARGNANI *et al.* 2009a]. One of the obstacles may be the unclear neo-tectonic setting of the Messina Strait. To bridge this gap, ARGNANI *et al.* [2009a] obtained the first high-resolution seismic grid in the Strait and successfully identified some single neo-tectonic features, but did not construct the neo-tectonic patterns of the Strait.

Inspired by ARGNANI *et al.* [2009a]'s work and ideas, an additional survey was carried out by members of the Kiel Cluster of Excellence 'The Future Ocean' and colleagues from Italy. We recognized numerous faulting structures that were unknown before, and based on these newly-discovered faults, we are able to construct the near-surface fault patterns of the Messina Strait for the first time. The fault with the most remarkable surface expression is exactly located in the source area proposed by BILLI *et al.* [2008] for the 1908 Messina tsunami; this fault aroused our greatest interest. It is the master fault of the Fiumefreddo - Melito di Porto Salvo Fault Zone (F-MPS_FZ). This fault zone is located between two Subduction-Transform Edge Propagator (STEP) faults: the Ionian Fault [POLONIA *et al.* 2014] and the Alfeo-Etna Fault [GALLAIS *et al.* 2013; POLONIA *et al.* 2014]. It may work as a connector of the two STEP faults. The three form a larger faulting system. This kind of system has not been described before. It may classify a new type of fault -- a STEP-Connector Fault.

We think that we have opened a new way of investigating submarine hazards off Southern Italy, but this new direction may even make the research more complicated.

TABLE OF FIGURES

Figure 1 (a) Source models for the 1908 Messina earthquake and tsunامي. Modified after *BILLI et al. [2008]*; *FAVALLI et al. [2009a]*; *PINO et al. [2009b]*. DSS, dominated scarp-like structure. The stars are epicentres proposed for the earthquake. The coloured straight lines together with the black rectangles show the possible seismogenic faults of the earthquake. The coloured straight lines indicate the intersections of the fault planes and the earth surface (cut-off lines). The black rectangles represent the surface projections of the fault planes. The dashed segments of the fault planes show the uncertain parts of those faults. The straight lines connected to the ellipses indicate the moving directions of landslides. The blue bars perpendicular to the frame of the figure represent the tsunami run-up heights of some cities. The numbers beside these bars are the values of the run-up heights in metres. (b) Overview of the Messina Strait. MS, Messina Strait. 21

Figure 2 Distribution of tidal height, amplitude and phase, and the tidal current speed through the Messina Strait. Computed by *DEFANT [1940]*. 24

Figure 3 Schematic representation of the longitudinal distribution of currents at the sill of the Messina Strait, during a tidal period, from *DEFANT [1940]*. Water mass in green is the Levantine Intermediate Water. Water mass in orange is the Tyrrhenian Surface Water. 25

Figure 4 SAR image for the Internal Wave in the Messina Strait. Data from RADARSAT1 satellite with a clear internal solitary waves train signature seen on 21 October 2006, 16:48 UTC. Taken from *CASAGRANDE et al. [2009]*. 27

Figure 5 Evolution of the African-Eurasian plate convergence zone over the last 35 Ma. Image was taken and modified from *FACCENNA et al. [2004]* and *FACCENNA et al. [2001]*. 28

Figure 6 Sketch of the consequences of the recent tectonic change on the Sicily–Calabrian area. Lines and fills are explained in the legend. Taken from *GOES et al. [2004]*. 30

Figure 7 Overall tectonic setting of the Messina Strait, Southern Italy. The red box in (b) shows the range of (a). Modified from *[ARGNANI and BONAZZI 2005; GUARNIERI 2006; CATALANO et al. 2008; ARGNANI et al. 2009a; POLONIA et al. 2011a; VITI et al. 2011a; DOGLIONI et al. 2012; GALLAIS et al. 2013]*. MS, Messina Strait. SL, Sangineto line; TL, Tindari-Letojanni faults/Taormina Line. RIF, Rosolini–Ispica faults; AF, Avola fault; WF, Western Ionian Fault; EF, Eastern Ionian Fault; ASF, Acireale–S. Alfio faults; PF, Piedimonte fault; TF, Taormina fault; RCF, Reggio Calabria fault; ARF, Armo fault; SF, Scilla faults; SEF, S. Eufemia fault; CF, Cittanova fault; SRF, Serre fault; VF, Vibo fault; CVF, Capo Vaticano fault. SCF, Southern Calabria fault; FA, fault discovered by *ARGNANI et al. [2009a]*; MSF, Messina Straits fault. 31

Figure 8 (a) 3D sketch of the Sicilian-Ionian Sea transition zone, where the Etna volcano is emplaced along the dextral transtensional fault due to differential slab roll-back. (b) 2D view from above on the plate boundary zone. The differential trench migration, as well as the measured dips of the subducted slabs is displayed, showing a gentler dip west of the Malta escarpment and a steeper dip east of it. Images from *DOGLIONI et al. [2001]*. 32

Figure 9 Bathymetry of the Messina Strait with 2D seismic and hydro-acoustic survey lines (orange and yellow lines). Survey lines in yellow are selected to be shown in this thesis. 43

Figure 10 2D seismic processing flow chart. 45

Figure 11 Velocity correction in bathymetry processing. **[Left]** Uncorrected bathymetry grid generated by “mbeditviz” with the corresponding editing window (underneath). At least three seafloor surfaces can be observed, due to the strong downward dip of the outer beams. **[Right]** Same area and editing window as on the left images, but velocity corrected using a SVP-file. Only one seafloor is visible. 47

Figure 12 Frequency adjustment before migration. **[Upper]** migrated profile with an OBPF low cut frequency of 10/20 Hz before migration. **[Lower]** migrated profile with an OBPF low cut frequency of 20/40 Hz before migration. An artificial reflector can be noticed above the seafloor reflector in the lower image. No increase/decrease of the S/N-ratio within the sediment strata is observable comparing the upper and lower image. 48

Figure 13 “Kill Trace” in 2D seismic processing. The upper image displays the data after 2D despiking. The middle image shows how the kill trace was applied to the data set. In the lower image, the result can be observed, showing a strong increase of the S/N-ratio as most of the assembly lines are erased. 49

Figure 14 Cross-section restoration flow chart, taken from Cukur et al. (2011) 51

Figure MI- 1 (a) Overall tectonic framework of Southern Italy. Modified from *ARGNANI and BONAZZI [2005]*, *GUARNIERI [2006]*, *CATALANO et al. [2008]*, *ARGNANI et al. [2009a]*, *POLONIA et al. [2011a]*, *VITI et al. [2011a]*, *DOGLIONI et al. [2012]*, and *GALLAIS et al. [2013]*. MS, Messina Strait. SL, Sanginetto line; TL, Taormina Line. RIF, Rosolini–Ispica faults; AF, Avola fault; WF, Western Ionian Fault; EF, Eastern Ionian Fault; ASF, Acireale–S. Alfio faults; PF, Piedimonte fault; TF, Taormina fault; RCF, Reggio Calabria fault; ARF, Armo fault; SF, Scilla faults; SEF, S. Eufemia fault; CF, Cittanova fault; SRF, Serre fault; VF, Vibo fault; CVF, Capo Vaticano fault; SCF, Southern Calabria fault; FA, fault identified by *ARGNANI et al. [2009a]*; MSF, Messina Straits fault. Red box shows the ranges of Fig. MI-2 and Fig. MI-7a. (b) Overview map of central Mediterranean Sea. Red box shows the range of (a). The meanings of the symbols used in the figure are shown in the LEGEND..... 56

Figure MI- 2 Bathymetry (slope gradient) of the inner Messina Strait. MC, Messina Canyon [*COLANTONI 1987*]; SCC, South Calabria Canyon [*RIDENTE et al. 2014*]. Orange and yellow lines show the location of the seismic profiles. The profiles shown in this manuscript are marked in yellow. The red boxes show the ranges of Fig. MI-7b and Fig. MI-7c, respectively..... 63

Figure MI- 3 (a) Seismic Profile P207 and (b) line drawing. Pink and black solid lines mark major surface faults and basement faults, respectively. Brown solid lines mark minor faults. Dashed lines show inferred continuations of faults. Vertical exaggeration is 8. See Fig. MI-2 and small inset map for location of profile. nfs_wMC, negative flower structure west of the Messina Canyon; nfs_uMC, negative flower structure under the Messina Canyon. 65

Figure MI- 4 (a) Seismic Profile P219 and (b) line drawing. Pink and black solid lines mark major surface faults and basement faults, respectively. Brown solid lines mark minor faults. Dashed lines show inferred continuations of faults. Vertical exaggeration is 8. See Fig. MI-2 and small inset map for location of profile. 66

Figure MI- 5 (a) Seismic Profile P1101 and (b) line drawing. Pink and black solid lines mark major surface faults and basement faults, respectively. Brown solid lines mark minor faults. Dashed lines show inferred continuations of faults. Vertical exaggeration is 8. See Fig. MI-2 and small inset map for location of profile. 67

Figure MI- 6 (a) Seismic Profile P231 and (b) line drawing. Pink and black solid lines mark major surface faults and basement faults, respectively. Brown solid lines mark minor faults. Dashed lines show inferred continuations of faults. Vertical exaggeration is 8. See Fig. MI-2 and small inset map for location of profile. 68

Figure MI- 7 (a) Newly-discovered near-surface faults (pink solid lines) in the tectonic framework of the inner Messina Strait. The location of faults previously described (in chapter 1.2.2) are shown in black: TL, Taormina Line; TF, Taormina Fault; RCF, Reggio Calabria Fault; ARF, Armo Fault; SF, Scilla Faults; SEF, S. Eufemia Fault; CF, Cittanova Fault; SCF, Southern Calabria Fault; MSF, Messina Straits Fault. Gray lines are seismic profiles. (b) Horizontal distributions of the newly-discovered near-surface faults (pink solid lines). (c) Horizontal distribution of the newly-discovered basement faults. See Fig. MI-2 for locations of maps shown on Fig. MI-7a and MI-7b. 70

Figure MII- 1 (a) Overall tectonic framework of Southern Italy. Modified from *GOVERS and WORTEL [2005]; ARGNANI and BONAZZI [2005]; GUARNIERI [2006]; CATALANO et al. [2008]; ARGNANI et al. [2009a]; POLONIA et al. [2011b]; POLONIA et al. [2014]; VITI et al. [2011b]; DOGLIONI et al. [2012]; GALLAIS et al. [2013]*. The green and blue lines show the location of Subduction-Transform Edge Propagator (STEP) faults. Dashed lines are inferred fault locations. MS, Messina Strait. SL, Sanginetto line; TL, Taormina Line. RIF, Rosolini–Ispica faults; AF, Avola fault; WF, Western Ionian Fault; EF, Eastern Ionian Fault; ASF, Acireale–S. Alfio faults; PF, Piedimonte fault; TF, Taormina fault; RCF, Reggio Calabria fault; ARF, Armo fault; SF, Scilla faults; SEF, S. Eufemia fault; CF, Cittanova fault; SRF, Serre fault; VF, Vibo fault; CVF, Capo Vaticano fault; SCF, Southern Calabria fault; FA, fault identified by *ARGNANI et al. [2009a]*; MSF, Messina Straits fault. (b) General map of central Mediterranean Sea..... 85

Figure MII- 2 (a) Bathymetry of the outer Messina Strait with 2D seismic profiles. Location of map is shown on Fig. MII-1. DSS, dominant scarp-like structure; NSS_N, northern N-S trending scarp-like structure; NSS_S, southern N-S trending scarp-like structure; SCC, South Calabria Canyon [*RIDENTE et al. 2014*]; SC, South Canyon; LM: large meander. Orange and yellow solid lines are 2D seismic survey lines. (b) Fault pattern of the outer Messina Strait reconstructed based on the selected seismic profiles. The DSS is the surface expression of fault SF21. Light blue dashed curves circle out the source area proposed by *BILLI et al. [2008]* for the 1908 Messina tsunamis. See text for details..... 91

Figure MII- 3 (a) Sediment echo sounder data interpretation of profile P234. Red arrows indicate the surface expressions of major faults. Vertical exaggeration is 6. (b) Uninterpreted and (c) interpreted seismic sections of P234. Faults in pink are major surface faults. Faults in brown are minor surface faults. The dashed lines show the uncertain lower parts of the major surface faults. Colored solid lines show the picked horizons. TWT, Two-Way-Travel-Time. Vertical exaggeration is 6. See Fig. MII-2 for location of profile..... 93

Figure MII- 4 (a) Sediment echo sounder data interpretation of profile P807. Red arrows indicate the surface expressions of major faults. Vertical exaggeration is 6. (b) Uninterpreted and (c) interpreted seismic sections of P807. Faults in pink are major surface faults. Faults in brown are minor surface faults. The dashed lines show the uncertain lower parts of the major surface faults. Colored solid lines show the picked horizons. TWT, Two-Way-Travel-Time. Vertical exaggeration is 6. See Fig. MII-2 for location of profile..... 94

Figure MII- 5 (a) Sediment echo sounder data interpretation of profile P242. Red arrows indicate the surface expressions of major faults. Vertical exaggeration is 6. (b) Uninterpreted and (c) interpreted seismic sections of P242. Faults in pink are major surface faults. Faults in brown are minor surface faults. The dashed lines show the uncertain lower parts of the major surface faults. Colored solid lines show the picked horizons. TWT, Two-Way-Travel-Time. Vertical exaggeration is 6. See Fig. MII-2 for location of profile..... 95

Figure MII- 6 Fiumefreddo - Melito di Porto Salvo Fault Zone (F-MPS_FZ) in the regional tectonic framework of the outer Messina Strait. See figure 1a for location of map. Modified from *GOVERS and WORTEL [2005]*; *ARGNANI and BONAZZI [2005]*; *GUARNIERI [2006]*; *CATALANO et al. [2008]*; *ARGNANI et al. [2009a]*; *[POLONIA et al. 2011b]*; *POLONIA et al. 2014*; *VITI et al. [2011b]*; *DOGLIONI et al. [2012]*; *GALLAIS et al. [2013]*. TL, Taormina Line; WF, Western Ionian Fault; EF, Eastern Ionian Fault; TF, Taormina fault; RCF, Reggio Calabria fault; SF, Scilla faults; SEF, S. Eufemia fault; ARF, Armo fault; SCF, Southern Calabria fault; FA, fault identified by Argnani; MSF, Messina Straits fault; ME, Malta Escarpment. The green and blue lines show the location of Subduction-Transform Edge Propagator (STEP) faults. Dashed lines are inferred fault locations. (b) Pull-apart basin and (c) fault-termination basin style models for the patterns of the “H” faulting system in the outer Messina Strait. PDZ, principle displacement zone. See text for details. 99

Figure MIII- 1 (a) Bathymetry of the Messina Strait and proposed source models for the 1908 Messina earthquake and tsunamis. Modified after *BILLI et al. [2008]*; *FAVALLI et al. [2009a]*; *PINO et al. [2009b]*; *POLONIA et al. [2011b]*; *GALLAIS et al. [2013]*. The coloured straight lines together with the black rectangles show the possible seismogenic faults of the 1908 Messina earthquake. The coloured straight lines indicate the intersections of the proposed fault planes and the earth surface (cut-off lines). The black rectangular represent the surface projections of the fault planes. The dashed segments of the fault planes show the uncertain parts of those faults. The straight lines connected to the ellipses indicate the moving directions of landslides. The blue bars perpendicular to the frame of the figure represent the observed run-up heights of the 1908 Messina tsunami in some cities. The numbers beside these bars are the values of the run-up heights in metres. The red box marks the research area of this study and the range of Fig. MIII-2. DSS, dominate scarp-like structure. (b) Overall tectonic evolution of the central Mediterranean Sea (Southern Italy). Modified after *NERI et al. [2009]*. (c) Present tectonic setting of Southern Italy. Please see the LEGEND to know the meanings of the symbols used in the figure. 106

Figure MIII- 2 Horizontal distributions of the newly-discovered Fiumefreddo - Melito di Porto Salvo Fault Zone in the outer Messina Strait. SCC, South Calabria Canyon [*RIDENTE et al. 2014*]; SC, South Canyon. Pink lines show the faults. Light blue dashed closed curves show the source area proposed by *BILLI et al. [2008]* for the 1908 Messina tsunami. Yellow lines mark the locations of the selected seismic profiles, P807 and P242. See Fig. MIII-1a for location of map. 111

Figure MIII- 3 (a) Uninterpreted and (b) interpreted seismic sections of profile P807. Faults in brown are minor surface faults; faults in other colours are the major surface faults. The dashed lines show the uncertain lower parts of the faults. Solid coloured horizontal lines show the picked horizons. TWT, Two-Way Travel Time. The vertical exaggeration is 6. See Fig. MIII-2 for location of the profile. 112

Figure MIII- 4 (a) Uninterpreted and (b) interpreted seismic sections of profile P242. Faults in brown are minor surface faults; faults in other colours are the major surface faults. The dashed lines show the uncertain lower parts of the faults. Solid coloured horizontal lines show the picked horizons. TWT, Two-Way Travel Time. The vertical exaggeration is 6. See Fig. MIII-2 for location of the profile. 113

Figure MIII- 5 Reconstructions of fault activities of the F-MPS_FZ, based on profile P807 that runs across the central part of the F-MPS_FZ. Stage 1. See Fig. MIII-2 for the location of the profile. F807-1, F807-2, and F807-3 are minor

surface faults on the section P807. From the acoustic basement to sequence 9, no water column is included, as the water column has already been decompacted when reconstructing the sequence 9 from the present phase. We set the depth to 0, as we do not have any evidences for the paleo-water depths at the time of the sequences' deposition. ... 115

Figure MIII- 6 Reconstructions of fault activities of the F-MPS_FZ, based on profile P242 that runs across the western part of the F-MPS_FZ. Stage 1. See Fig. MIII-2 for the location of the profile. F242-1 and F242-2 are minor surface faults on the section P242. From the acoustic basement to sequence 9, no water column is included, as the water column has already been decompacted when reconstructing the sequence 9 from the present phase. We set the depth to 0, as do not have any evidence for the paleo-water depths at the time of the sequences' deposition. 118

Figure MIII- 7 Results of tsunami simulations for four scenarios with slips of 2 m (a), 5 m (b), 10 m (c) and 15 m (d) and comparisons with observed wave heights. The red and blue contours represent the uplift and subsidence due to the tectonic source, respectively. The colour maps show the distribution of maximum tsunami amplitudes due to each source scenario. The parameter K shows the quality of fit between observations and simulations according to Equ. (1). 123

Figure MIII- 8 Tsunami travel times in minutes for scenario (d) shown in Fig. MIII-7. The contours are in minutes and show the arrivals of first tsunami waves. The side plots compare the observed arrival times with the first noticeable peak (with amplitude > 0.5 m) in simulations. The right panel shows some of the simulated waveforms. The parameter K shows the quality of fit between observations and simulations according to Equ. (1). 124

Figure A1 Sketch of the tectonic evolution of the central-western Mediterranean, based on *GOES et al. [2004]*, with the reconstruction of subducted plate geometry. Bold lines mark the reconstructed paleogeography from 35 Ma to present, relative to a fixed Europe. For reference, dotted lines show present-day geography in all panels. The dipping part of the slab is shaded in dark gray, the part that lies flat above 660 km in light gray. A gap (in white) develops in this slab after 15–10 Ma, starting just south of Sardinia. The bold gray line indicates the approximate location of the trench axis (not the deformation front). Extension in the Sicily Channel started around 5–6 Ma. 134

Figure A2 [Left] Principal axes of the horizontal strain rate tensor (in blue) and associated 1 sigma errors (red bars). **[Right]** The orientation of uniform faulting that can accommodate the strain rate field shown in the left figure. Red lines are faults with a left-lateral component; blue lines are faults with a right-lateral component. Line lengths are equal to the magnitude of the difference between the principal strain rates. Taken from *D'AGOSTINO and SELVAGGI [2004]*. 135

Figure A3 Geodetic strain rate field of Southern Italy computed over a regular $0.2^\circ \times 0.2^\circ$ grid. Taken from *SERPELLONI et al. [2010]*. **[Left]** Red and blue arrows show extensional and compressional strain rates, respectively. Grey crosses display 1σ uncertainties. **[Right]** Rotation rates and 1σ uncertainties (grey wedges). Red wedges show clockwise rotations, whereas blue wedges show counter-clockwise rotations. Grey arrows in both panels show GPS velocities with respect to the Nubian plate. 135

TABLE OF TABLES

Table MI- 1 Fault geometries in the inner Messina Strait. See locations in Fig. MI-7b. na, north azimuth; rhr, right hand rule; aada, average apparent dip angle; dd, dip direction; E. S. P., Equal-area stereo-graphic plots of the fault planes (strike, dip (rhr)).....	72
Table MII- 1 Fault geometries in the outer Messina Strait.	96
Table MIII- 1 Fault geometries of the major surface faults in the newly-discovered Fiumefreddo - Melito di Porto Salvo Fault Zone in the outer Messina Strait. Details are given in Fu et al. (this thesis) (chapter 5 4.2).....	114
Table MIII- 2 Reconstructed amounts of the apparent displacements of the faults in the outer Messina Strait at the end of the formation of each sequence. Negative and positive signs indicate the normal and the reverse slip components, respectively.	120

TABLE OF CONTENTS

ABSTRACT	4
ZUSAMMENFASSUNG	6
DEDICATIONS	9
TABLE OF FIGURES.....	10
TABLE OF TABLES	15
TABLE OF CONTENTS	16
OUTLINE OF THE DISSERTATION	18
1 INTRODUCTION	20
1.1 MOTIVATION	20
1.2 INTRODUCTION TO THE STRAIT OF MESSINA (STRETTO DI MESSINA)	23
1.2.1 <i>Hydrology</i>	24
1.2.2 <i>Tectonic Settings of the Messina Strait</i>	28
1.2.3 <i>Turbidity Currents in the Messina Strait</i>	36
1.3 PREVIOUS RESEARCH ON ACTIVE TECTONIC STRUCTURES IN THE MESSINA STRAIT	37
1.4 PREVIOUS RESEARCH ON THE SOURCE OF THE 1908 MESSINA EARTHQUAKE AND TSUNAMI.....	38
1.4.1 <i>Possible Source Models for the 1908 Messina Earthquake</i>	39
1.4.2 <i>Possible Sources for the 1908 Messina Tsunami</i>	40
2 OBJECTIVES	42
3 DATA AND METHODOLOGY.....	43
3.1 ACQUISITION AND PROCESSING OF SEISMIC AND HYDRO-ACOUSTIC DATA.....	43
3.1.1 <i>Bathymetric Multi-Beam Echo Sounding Data</i>	44
3.1.2 <i>Sediment Echo Sounding Data</i>	44
3.1.3 <i>High-Resolution 2D Reflection Seismic Data</i>	45
3.1.4 <i>Special Processing of the Hydro-Acoustic Data</i>	46
3.2 METHODS FOR DATA INTERPRETATIONS.....	50
3.3 CROSS-SECTION RESTORATION	51
3.4 NUMERICAL TSUNAMI MODELING	52
4 MANUSCRIPT I.....	53
ABSTRACT	54
1 INTRODUCTION	55
2 TECTONIC SETTING.....	59
3 DATA AND METHOD.....	61
4 RESULTS	63
4.1 <i>Multi-beam swath bathymetry</i>	63
4.2 <i>High-resolution 2D multi-channel seismic data</i>	65
5 DISCUSSION	76
5.1 <i>General seafloor morphology of the Messina Strait</i>	76
5.2 <i>Characterization of tectonic features and their structural relevance to the tectonic framework of the Messina Strait</i>	77

5.3 <i>The graben structure of the Messina Strait</i>	79
5.4 <i>The Taormina Fault</i>	79
6 CONCLUSIONS	81
5 MANUSCRIPT II.....	82
ABSTRACT	83
1 INTRODUCTION	84
2 TECTONIC SETTINGS.....	87
2.1 <i>The inner Calabrian Arc and the Siculo-Calabrian Rift Zone</i>	87
2.2 <i>The STEP faults</i>	88
3 DATA AND METHOD.....	90
4 RESULTS	91
4.1 <i>Seafloor morphology</i>	91
4.2 <i>Fault pattern in the outer Messina Strait</i>	93
5 DISCUSSION	98
5.1 <i>The characteristics of the Fiumefreddo - Melito di Porto Salvo Fault Zone (F-MPS_FZ) in the outer Messina Strait</i>	98
5.2 <i>How do the newly-discovered Fiumefreddo - Melito di Porto Salvo Fault Zone (F-MPS_FZ) in the outer Messina Strait fit to the regional tectonic framework?</i>	99
6 CONCLUSIONS	103
6 MANUSCRIPT III.....	104
ABSTRACT	105
1 INTRODUCTION	106
2 TECTONIC SETTINGS.....	108
3 DATA AND METHOD.....	109
4 RESULTS	111
4.1 <i>Fault pattern in the outer Messina Strait</i>	111
4.2 <i>Reconstructions of fault activities in the outer Messina Strait</i>	115
4.3 <i>Numerical modelling of tsunamis</i>	122
5 DISCUSSION	125
5.1 <i>Quality of the fault reconstruction</i>	125
5.2 <i>Evolution of the newly-discovered Fiumefreddo - Melito di Porto Salvo Fault Zone in the outer Messina Strait</i>	125
5.3 <i>Implications from tsunami modelling</i>	126
5.4 <i>Do submarine landslides tsunami triggers exist in the outer Messina Strait?</i>	127
6 CONCLUSIONS	129
7 FINAL CONCLUSIONS AND OUTLOOK.....	130
7.1 CONCLUSIONS	130
7.2 OUTLOOK	133
APPENDIXES.....	134
BIBLIOGRAPHY	136
ACKNOWLEDGEMENTS	147
CURRICULUM VITAE	149

OUTLINE OF THE DISSERTATION

Chapter 1 introduces the survey area – the Messina Strait. General information on the geographic and tectonic characteristics of the Strait are presented. Previous research on the tectonics and submarine hazards of the Messina Strait are also included.

Chapter 2 presents the objectives of this thesis.

Chapter 3 summarizes the used data and methodology. It briefly introduces the parameters used during acoustic data acquisition and interpretation. Methods and parameters of cross-section restoration and numerical tsunami modelling are also presented.

Chapter 4 Manuscript I

Assessing the fault pattern of the inner Messina Strait, Southern Italy, by means of high-resolution 2D reflection seismics

This chapter presents a map of the near-surface fault pattern of the inner Messina Strait based on the new high-resolution 2D reflection seismic data. The general fault pattern is analysed and discussed in the overall tectonic framework of the survey area.

Chapter 5 Manuscript II

An active transtensional fault zone between two STEP faults in the outer Messina Strait, Southern Italy

This chapter focusses on a newly-discovered near-surface fault zone in the outer Messina Strait, namely the Fiumefreddo - Melito di Porto Salvo Fault Zone (F-MPS_FZ). This fault zone is interpreted as a transtensional fault zone connecting two Subduction-Transform Edge Propagator (STEP) faults in the outer Messina Strait. When analysing the relationship between the new fault zone and the regional tectonic framework of the outer Strait, two models for this new fault zone will be discussed: the pull-apart basin style and the fault-termination basin style.

Chapter 6 Manuscript III

Tsunami potential for Southern Italy related to a newly-discovered active fault zone in the outer Messina Strait, based on fault activity reconstructions and tsunami modelling.

The reconstructions of the activity of the newly-discovered Fiumefreddo - Melito di Porto Salvo Fault Zone will be presented in this chapter. Numerical tsunami modelling based on derived fault parameters will also be presented.

Chapter 7 will present some final conclusions and give a short outlook for the work.

1 INTRODUCTION

1.1 Motivation

Submarine hazards, such as earthquakes, submarine slope failures, and resulting tsunamis on the continental margins is a current focus of scientific research. These hazards pose great threats to coastal communities, which are homes to over sixty percent of humankind and locations of most major industrial installations, including increasingly offshore installations. Once these hazards strike the coastline, lives and properties in the coastal areas may experience severe damage. The 1908 Messina earthquake and tsunami is a typical event of this kind.

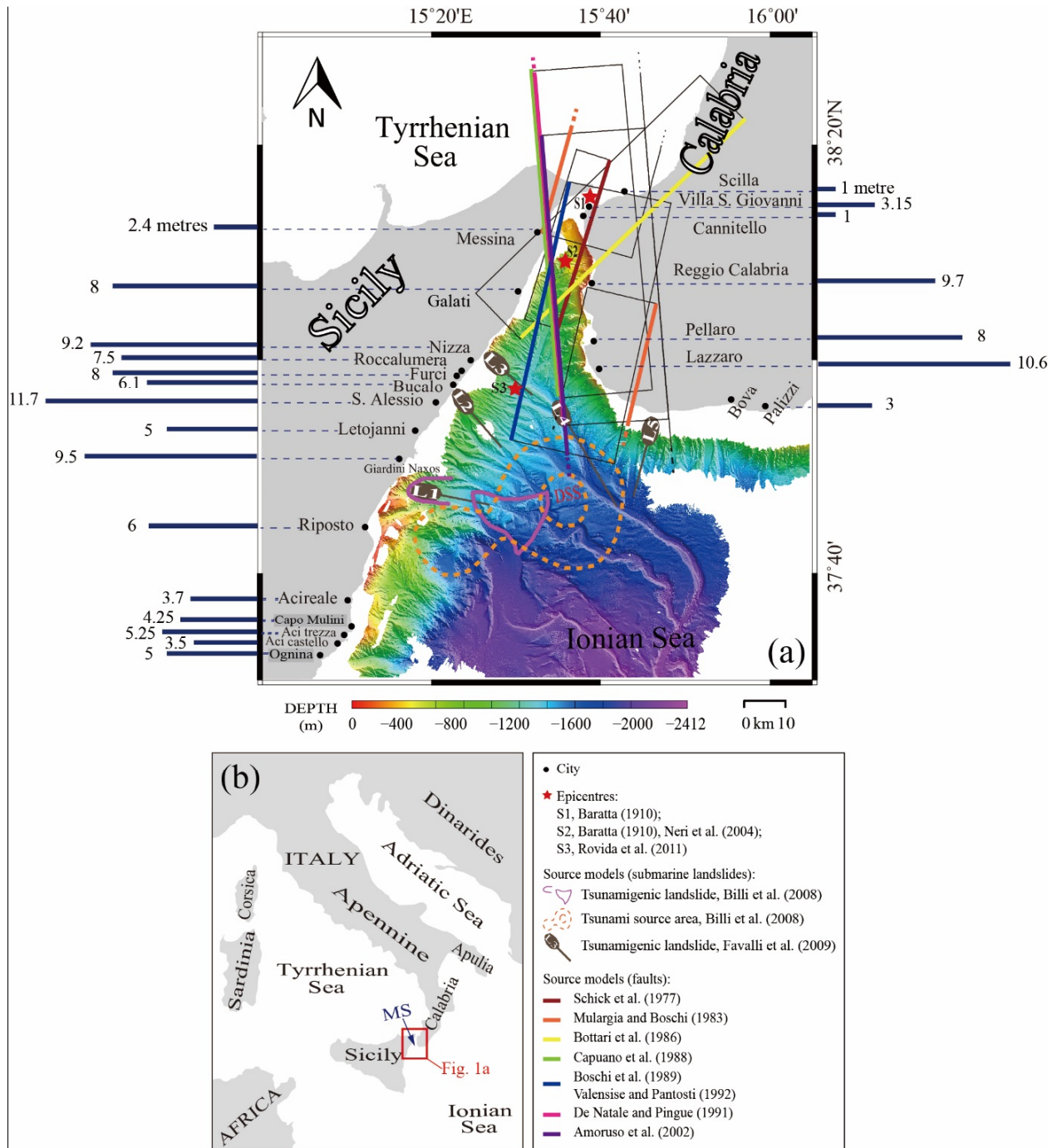


Figure 1 (a) Source models for the 1908 Messina earthquake and tsunami. Modified after *BILLI et al. [2008]*; *FAVALLI et al. [2009a]*; *PINO et al. [2009b]*. DSS, dominated scarp-like structure. The stars are epicentres proposed for the earthquake. The coloured straight lines together with the black rectangles show the possible seismogenic faults of the earthquake. The coloured straight lines indicate the intersections of the fault planes and the earth surface (cut-off lines). The black rectangles represent the surface projections of the fault planes. The dashed segments of the fault planes show the uncertain parts of those faults. The straight lines connected to the ellipses indicate the moving directions of landslides. The blue bars perpendicular to the frame of the figure represent the tsunami run-up heights of some cities. The numbers beside these bars are the values of the run-up heights in metres. (b) Overview of the Messina Strait. MS, Messina Strait.

On December 28th, 1908, a devastating earthquake, $M_w=7.1$ [PINO *et al.* 2000; CPTIWORKINGGROUP. 2004], occurred in the Messina Strait (Fig. 1). Many cities located in the coastal areas of the Strait were badly destroyed, especially Messina and Reggio di Calabria (Fig. 1a). The earthquake was accompanied by a tsunami [PLATANIA 1909] (Fig. 1a). About 80,000 [BARATTA 1910] to 100,000 [MERCALLI 1909] people were killed, making the event the deadliest one in Europe since then.

Intensive investigations have been carried out by many researchers [OMORI 1910; DENATALE and PINGUE 1991; ANZIDEI *et al.* 1998; AMORUSO *et al.* 2002a; GERARDI *et al.* 2008; GUARNIERI and PIRROTTA 2008; ARGNANI *et al.* 2009a], based on various data sets, such as seismological data, geodetic measurement data (levelling surveys and GPS velocity analyses), tide gauge data, data from geological surveys, and macroseismic observations including P-wave polarities [BOTTARI *et al.* 1989b; DENATALE and PINGUE 1991; TORTORICI *et al.* 1995; ANZIDEI *et al.* 1998; MONACO and TORTORICI 2000a], as well as the tsunami run-up heights (Fig. 1a) and arrival times [TINTI *et al.* 1999a; BILLI *et al.* 2008].

So far, various seismogenic fault models have been proposed for the 1908 Messina event. They vary from a central position in the Strait to the coasts, dipping toward the west or east to southeast (Fig. 1a). Although a NNW-SSE-trending, E-dipping normal fault, which is located in the northern central part of the Strait, was approved to be the seismogenic fault by many authors, no general agreement has been archived on the seismogenic fault of the 1908 Messina earthquake [AMORUSO *et al.* 2002b; TINTI and ARMIGLIATO 2003b; ARGNANI *et al.* 2009a].

The 1908 Messina tsunami occurred following the earthquake hit the entire coastline of the Messina Strait. Field surveys were conducted immediately after the event. The records in the harbour of Naples showed that this tsunami has been the largest one ever recorded in Italy in historical time, both in terms of run-up height (>10 m) [PLATANIA 1909] (Fig. 1a) and impacted area. The run-up heights in the southern part of the Messina Strait (5 - 10 m) were significantly higher than those in the north (1 - 3 m) (Fig. 1a). The extreme values exceed 11 m (Fig. 1a).

Since the 1908 Messina tsunami was assumed to be triggered by seismic activity, tsunami modellers [TINTI *et al.* 1999b; TINTI and ARMIGLIATO 2003a; FAVALLI *et al.* 2009b] constructed numerical models on some most common fault solutions, but no one came up with a consistent explanation for both earthquake and tsunami [TINTI *et al.* 1999b; GERARDI *et al.* 2008]. Hence, BILLI *et al.* [2008] postulated that the 1908 Messina tsunami was caused by a submarine landslide. They used triangulation methods to determine a possible source area, which is located in the western Ionian Basin, offshore to the southwest of the southwestern tip of Calabria and to the east of Giardini Naxos city (Sicily) (Fig. 1a).

However, several authors [ARGNANI *et al.* 2009b; GROSS *et al.* 2014] doubt the interpretation of BILLI *et al.* [2008], as no ~100 yr old landslide deposits can be identified on high-resolution bathymetric and seismic data in this area. Additionally, modelling results presented by GERARDI *et al.* [2008] conflict with the landslide-generated tsunami hypothesis. The length of the inundated coast seems to be the key factor in discriminating the tsunami source. Tsunamis caused by dislocation propagated over a wider area with respect to those caused by submarine landslides [TINTI *et al.* 2007].

What are the main reasons for the existence of these disputes? The unclear neo-tectonic setting of the Messina Strait is probably the most important aspect. This shortcoming is mainly based on the lack of high-resolution and high-quality seismic data, leading to an insufficient and biased knowledge on the tectonics of the Messina Strait. Hence, the main objective of this thesis is to map and analyse neo-tectonic features in the Messina Strait based on a newly-collected high-resolution acoustic and seismic data set. Special emphasis will be drawn on the general fault patterns, its relationship to the overall tectonic setting of Southern Italy, and the tsunami hazard related to selected fault patterns.

1.2 Introduction to the Strait of Messina (Stretto Di Messina)

The Messina Strait is a NNE-SSW striking channel, located in the central Mediterranean Sea (Fig. 1), between latitude 37°40'N to 38°20'N and longitude 15°20'E to 15°50'E. It separates the Italian Peninsula (Calabria) (east) and Sicily (west) and links the Tyrrhenian Sea (north) and the Ionian Sea (south) (Fig. 1). The Strait is a fan-shaped channel (Fig. 1). It is ~40 km long, ~3 km wide in the north, and ~16 km wide in the south.

1.2.1 Hydrology

1.2.1.2 Tide and current

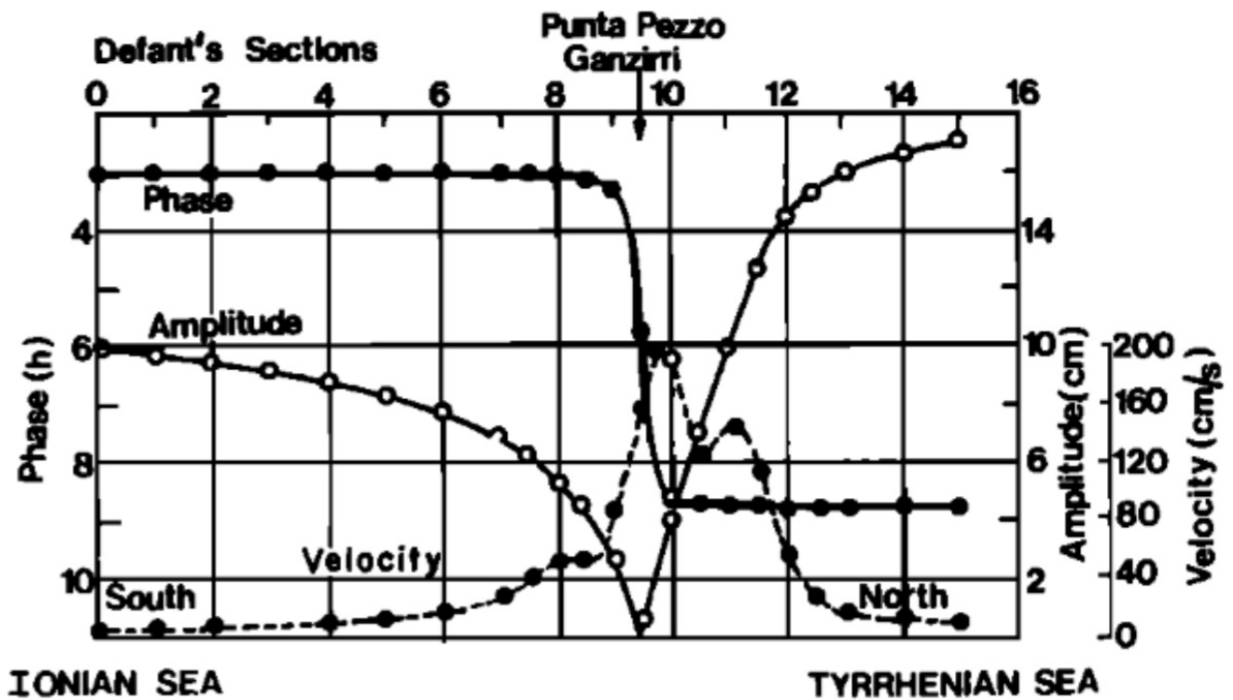


Figure 2 Distribution of tidal height, amplitude and phase, and the tidal current speed through the Messina Strait. Computed by DEFANT [1940].

The Messina Strait is characterised by irregular hydrodynamic conditions. Tyrrhenian and Ionian tides are practically opposite in phase, so that sea level oscillations are almost null in the Strait, while currents are very high (Fig. 2). On the sill, currents as high as 2.00 m/s were measured. From the harmonic analysis, the K1 (Lunar diurnal constituent) and M2 (Principal lunar semidiurnal constituent) components turned out to be the most significant. The former ranged roughly between 0.10 and 0.35 m/s, the latter between 0.40 and 1.40 m/s. Direction of such velocities varied slightly with depth and location, but was predominantly aligned with the Strait's axis.

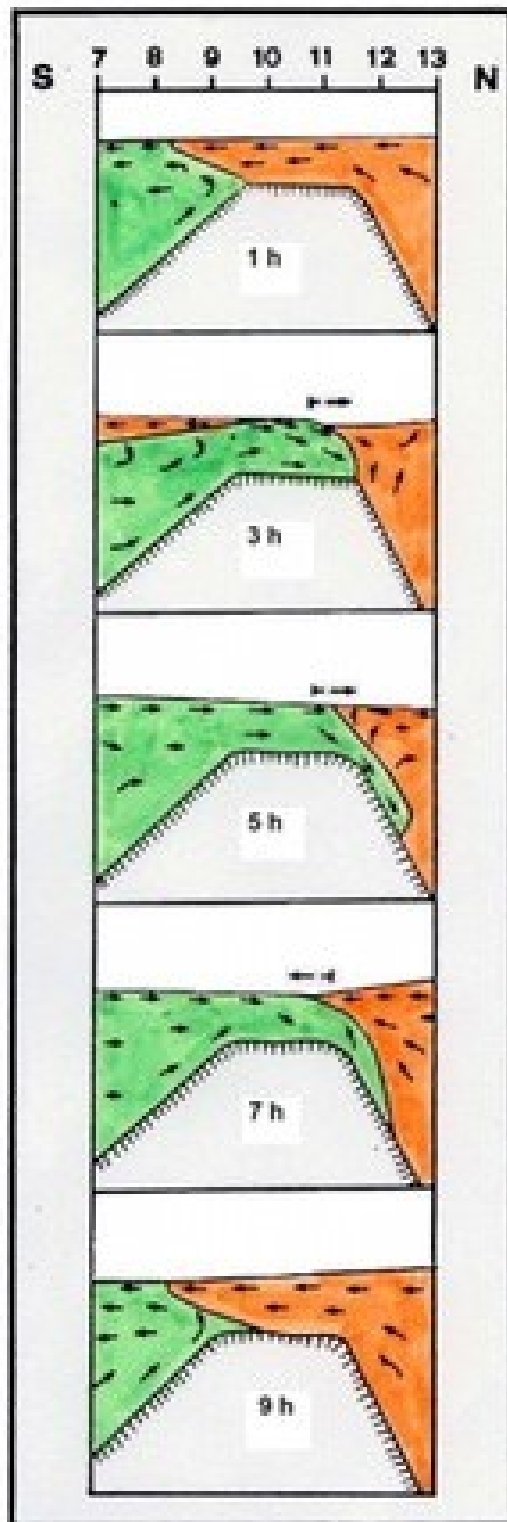


Figure 3 Schematic representation of the longitudinal distribution of currents at the sill of the Messina Strait, during a tidal period, from *DEFANT [1940]*. Water mass in green is the Levantine Intermediate Water. Water mass in orange is the Tyrrhenian Surface Water.

Two water masses, the Tyrrhenian Surface Water and the colder and saltier Levantine Intermediate Water, encounter at the sill in the narrowest part of the Strait (Fig. 3). During the maximum tidal flow, the heavier Levantine Intermediate Water crosses the sill from the Ionian Sea to the Tyrrhenian Sea (3h to 5h in Fig. 3). The pycnocline is thus lifted at the sill and then depressed north of the sill. The depression generates a southward and a northward propagating bore. The northward propagating bore keeps propagating in the Tyrrhenian Sea; the southward bore is stopped by the sill. When the semi-diurnal tide reverses to the maximum tidal flow from the Tyrrhenian Sea to the Ionian Sea, the southward propagating bore undergoes a hydraulic jump over the sill and into the south of the sill and propagates away from the sill [CASAGRANDE *et al.* 2009] (7h to 9h in Fig. 3).

The wind causes both strong drift currents at the surface and upwelling of the waters from the Ionian Sea or from the Tyrrhenian Sea [SANTORO *et al.* 2002]. Moreover, the presence and the variable width of the sill result in a nonhomogeneous hydrodynamic regime along the Strait's axis in terms of current strength and direction [SANTORO *et al.* 2002].

1.2.1.3 Internal wave

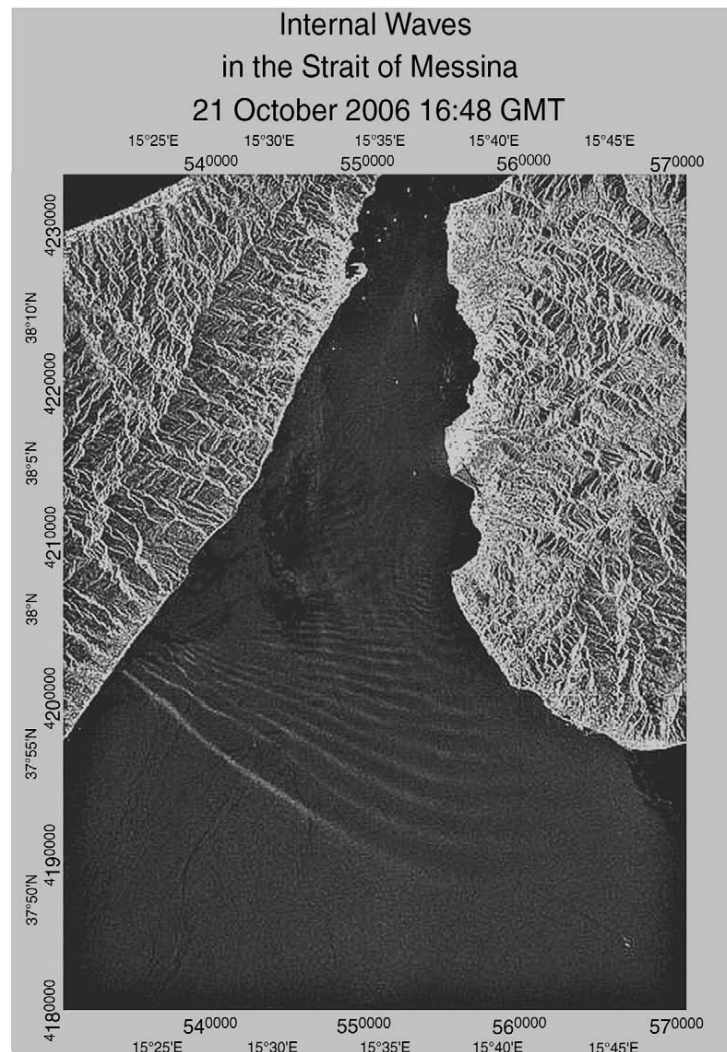


Figure 4 SAR image for the Internal Wave in the Messina Strait. Data from RADARSAT1 satellite with a clear internal solitary waves train signature seen on 21 October 2006, 16:48 UTC. Taken from *CASAGRANDE et al. [2009]*.

Strong barotropic tidal flow, steep bathymetry, and stable stratified environment are the three required ingredients for internal wave generation [ZEILON 1912]. In the Messina Strait, when the southward propagating bore (chapter 1.2.1.3), propagates away from the sill, its leading edge will be steepen, because of the nonlinear effects, until disintegrating into a “train” of interfacial nonlinear short internal waves (Fig. 4), due to frequency and amplitude dispersions [WARN-VARNAS et al. 2007]. A well pronounced wave train may consists of 4 - 10 internal solitary waves with periods of 8 to 30 min. Propagation speed of the internal waves varies between 0.80 and 1.15 m/s [ALPERS and SALUSTI 1983; CASAGRANDE et al. 2010].

1.2.2 Tectonic Settings of the Messina Strait

1.2.2.1 Evolution of the African-Eurasian plate convergence zone over the last 35 Ma

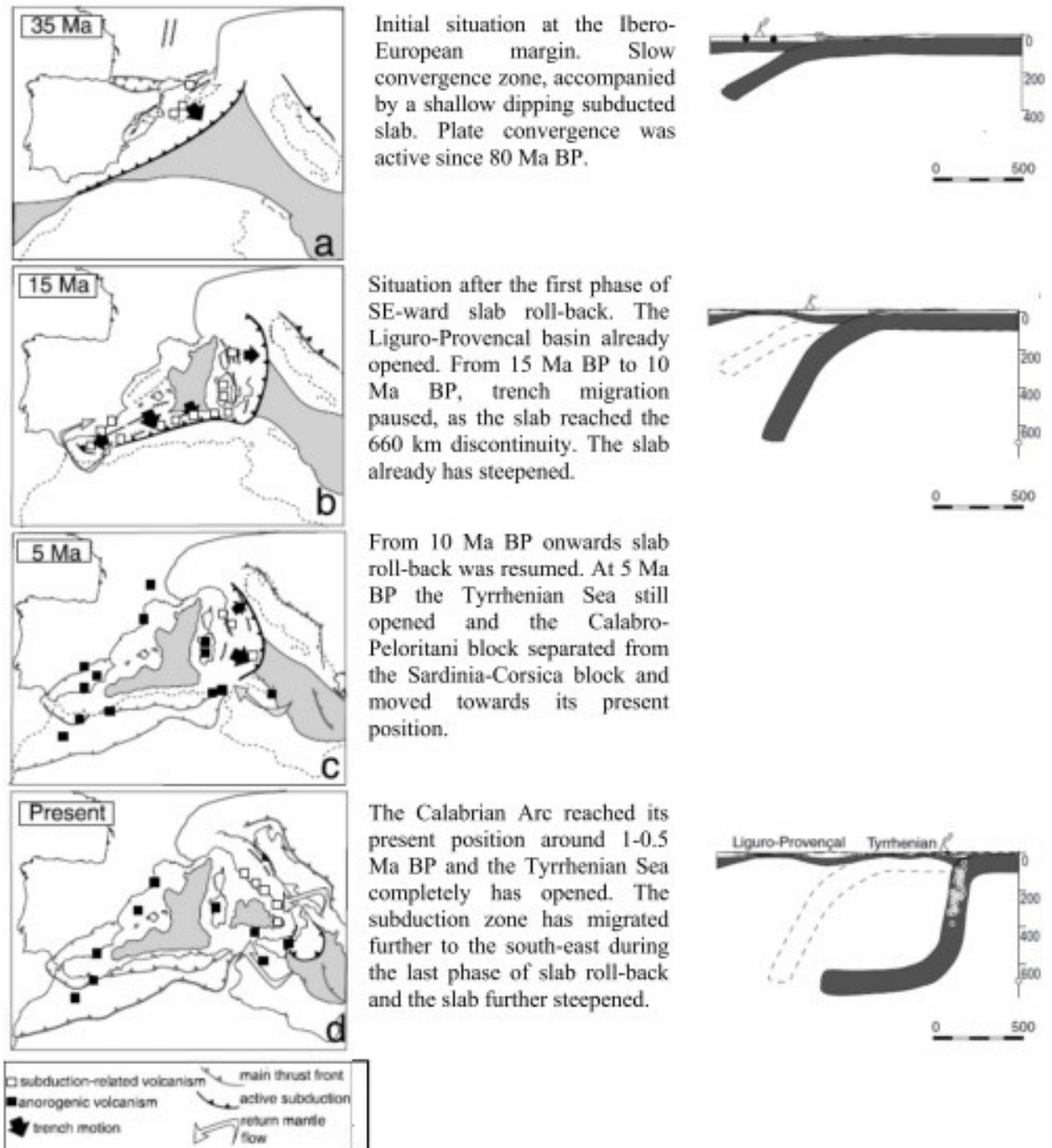


Figure 5 Evolution of the African-Eurasian plate convergence zone over the last 35 Ma. Image was taken and modified from *FACCENNA et al. [2004]* and *FACCENNA et al. [2001]*.

The evolution of the African-Eurasian plate boundary zone can be dated back to 35 Ma to the Late Oligocene [GUEGUEN *et al.* 1998; FACCENNA *et al.* 2001; FACCENNA *et al.* 2003; FACCENNA *et al.* 2004; GOES *et al.* 2004; GUARNIERI and PIRROTTA 2008] (Fig. 5a). Since then, the western Mediterranean Sea progressively opened from its initial location at the Ibero-European margin toward the southeast as a result of the trench retreat and slab roll-back [GUEGUEN *et al.* 1998; FACCENNA *et al.* 2001; FACCENNA *et al.* 2003; FACCENNA *et al.* 2004; GOES *et al.* 2004]. The trench retreat and slab roll-back process was probably initiated by a gravitational pull of the subducted slab [GOES *et al.* 2004], which was generated by an adequate amount of lithospheric material subducted at the Ibero-European margin since ~80 Ma [GUEGUEN *et al.* 1998; FACCENNA *et al.* 2001]. As a result, a system of slow African-Europe convergence, and fast subduction was developed [GUEGUEN *et al.* 1998; GOES *et al.* 2004].

During the southeastward trench retreat and slab roll-back, the overriding plate was lengthened, accompanied by strong extensional forces [GOES *et al.* 2004], leading to the opening of the Liguro-Provencal and the Tyrrhenian back-arc basins [FACCENNA *et al.* 2003]. Oceanic spreading started [GUEGUEN *et al.* 1998; FACCENNA *et al.* 2001]. The subducted slab, which was previously characterised by a shallow dip, became continuously steeper with the evolution of the plate boundary zone [FACCENNA *et al.* 2001; FACCENNA *et al.* 2003; FACCENNA *et al.* 2004].

From ~10 Ma (Late Miocene) onwards, the trench retreat was strongly enhanced (Fig. 5b). With the opening of the Tyrrhenian Sea [MONACO *et al.* 1996; GOES *et al.* 2004], the Calabro-Peloritani block, which builds up the present Calabrian Arc, moved away from the Sardinia-Corsica block toward its present position [GUEGUEN *et al.* 1998; FACCENNA *et al.* 2001; GOES *et al.* 2004]. As a part of the overriding plate, compressional and extensional forces already affected the Calabro-Peloritani block [MONACO *et al.* 1996; GOES *et al.* 2004].

Between ~5 Ma to ~2 Ma (Pliocene) (Fig. 5c-d), the trench migrated rapidly [GOES *et al.* 2004]. The thrust process already shifted to the Ionian offshore [MONACO *et al.* 1996].

1.2.2.2 Recent tectonic reorganization

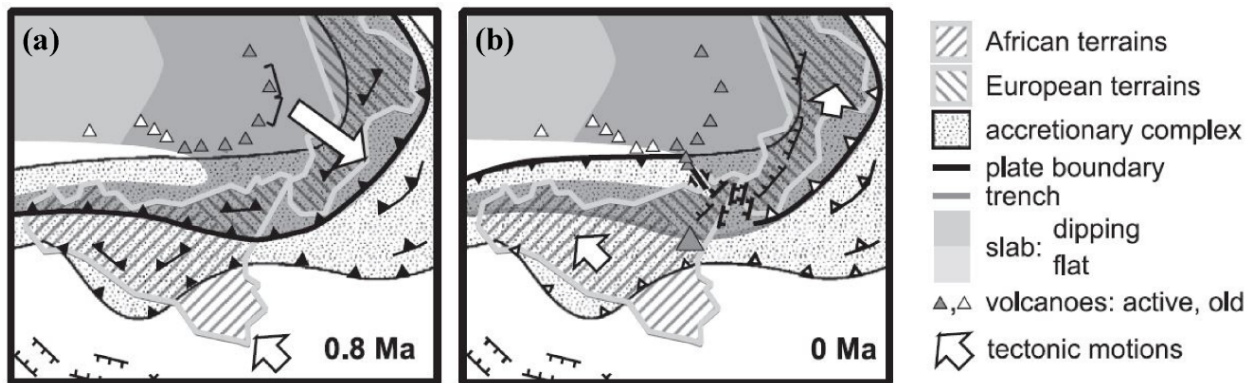


Figure 6 Sketch of the consequences of the recent tectonic change on the Sicily–Calabrian area. Lines and fills are explained in the legend. Taken from *GOES et al. [2004]*.

During the last phase (1 – 0.5 Ma) of trench migration, tectonics of the south-central Mediterranean changed [*GOES et al. 2004*] (Fig. 6). To the north of Sicily, Africa–Europe convergence has transferred to a back thrust, in response to the arrival of African continental lithosphere at the trench. When Calabria docked between Apulia and Sicily, Calabrian trench migration and accompanying Tyrrhenian back-arc extension essentially almost stalled. A northeastward divergence between the Ionian section and the rest of the African plate -- manifesting itself as extension in eastern Sicily and the Sicily Channel -- may control the current eastward motions of Calabria and Apulia relative to Africa, now that large roll-back displacements have ceased. Very strong deformation is recorded in the region between Europe, Africa, and Calabria, as plate boundaries are readjusting [*GOES et al. 2004*].

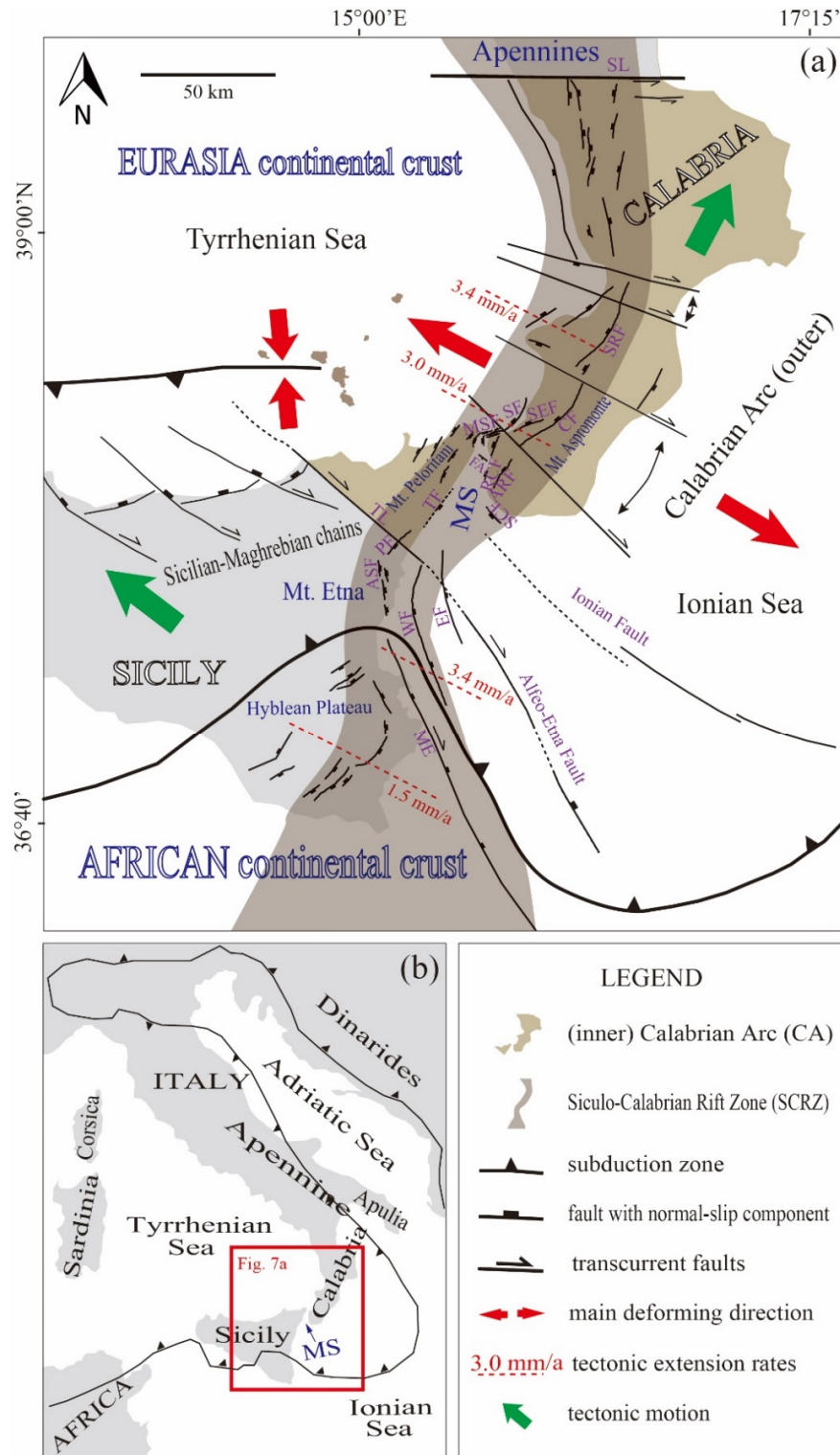


Figure 7 Overall tectonic setting of the Messina Strait, Southern Italy. The red box in (b) shows the range of (a). Modified from [ARGNANI and BONAZZI 2005; GUARNIERI 2006; CATALANO et al. 2008; ARGNANI et al. 2009a; POLONIA et al. 2011a; VITI et al. 2011a; DOGLIONI et al. 2012; GALLAIS et al. 2013]. MS, Messina Strait. SL, Sangineto line; TL, Tindari-Letojanni faults/Taormina Line. RIF, Rosolini-Ispica faults; AF, Avola fault; WF, Western Ionian Fault; EF, Eastern Ionian Fault; ASF, Acireale-S. Alfio faults; PF, Piedimonte fault; TF, Taormina fault; RCF, Reggio Calabria fault; ARF, Armo fault; SF, Scilla faults; SEF, S. Eufemia fault; CF, Cittanova fault; SRF, Serre fault; VF, Vibo fault; CVF, Capo Vaticano fault. SCF, Southern Calabria fault; FA, fault discovered by ARGNANI et al. [2009a]; MSF, Messina Straits fault.

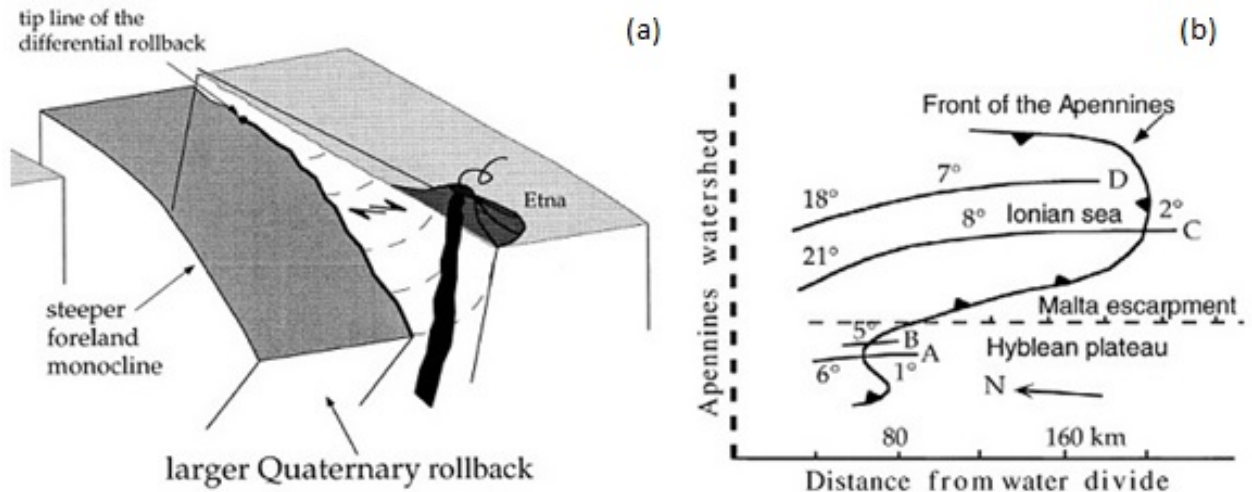


Figure 8 (a) 3D sketch of the Sicilian-Ionian Sea transition zone, where the Etna volcano is emplaced along the dextral transtensional fault due to differential slab roll-back. (b) 2D view from above on the plate boundary zone. The differential trench migration, as well as the measured dips of the subducted slabs is displayed, showing a gentler dip west of the Malta escarpment and a steeper dip east of it. Images from *DOGLIONI et al. [2001]*.

The segment of the plate convergence zone, which is between the Hyblean Plateau (Sicily) and Apulia, moved further southeast compared to the other parts (Figs. 6, 7a, 8). This displacement has been assumed to be a result of a differential plate motion [*DOGLIONI et al. 2001; GOES et al. 2004*], which is a consequence of the development of a variable dip of the subducted slab caused by a different composition of the subducted lithosphere [*DOGLIONI et al. 2001; D'AGOSTINO and SELVAGGI 2004*] (Figs. 6, 7a, 8). This differential plate motion is supposed to be regulated by the Malta Escarpment (Figs. 7a, 8), an old, re-activated and N-S oriented Mesozoic passive margin [*DOGLIONI et al. 2001*], and by the Tindari-Letojanni faulting system (Fig. 7a), a dextral transtensional zone formed across northeastern Sicily, to accommodate the differential motion between Sicily (Africa) and Calabria (Fig. 7a). Motion along this zone decouples Sicily's Peloritani corner from the Calabrian block, with which it has migrated across the Tyrrhenian basin (Fig. 7a).

FACCENNA et al. [2001] and *GUEGUEN et al. [1998]* estimated a total amount of up to ~780 km lengthening/extension of the overriding plate, due to the trench migration in the last 35 Ma. They also calculated an average migration rate of 2.6 cm/a, with a maximum rate exceeding 5.6 cm/a during the last phase of the trench retreat and slab roll-back [*FACCENNA et al. 2004*].

This young and changing tectonics seems to be associated with diffuse, strongly time-dependent and sometimes devastating seismicity, but details are not well understood due to the lack of the information concerning the comprehensive tectonic framework.

1.2.2.3 The Calabrian Arc (CA)

The Messina Strait is situated in the inner Calabrian Arc (CA) (Fig. 7a), which is on the convergent boundary of the Africa-Eurasia plate [MONACO *et al.* 1996; D'AGOSTINO and SELVAGGI 2004; GOES *et al.* 2004; BILLI *et al.* 2008]. The Ionian lithosphere is subducted north-westward underneath the CA, resulting in complex deformation and the formation of an accretionary wedge, with foreland fold-and-thrust belts extending along the entire plate boundary zone, since at least Neogene [TORTORICI *et al.* 1995; MONACO *et al.* 1996; ANZIDEI *et al.* 1998; FACCENNA *et al.* 2003; FACCENNA *et al.* 2004; FERRANTI *et al.* 2007; BILLI *et al.* 2008; GUARNIERI and PIRROTTA 2008].

The CA (Fig. 7a) is a Cenozoic–Quaternary curved orogeny running from the NW-SE-trending Southern Apennines to the E-W-trending Sicilian Maghrebides [MALINVERNO and RYAN 1986; CATALANO *et al.* 1996; MARIOTTI and DOGLIONI 2000; FACCENNA *et al.* 2004; PATACCA and SCANDONE 2007; POLONIA *et al.* 2011a; CARMINATI *et al.* 2012]. The central part of the CA is located on top of a narrow subduction zone, whose activity is now close to cessation [NERI *et al.* 2009], but still slowly retreating [D'AGOSTINO *et al.* 2011]. The Neogene–Quaternary evolution, southeastward migration, and curvature development of the CA have been all controlled by the migration and roll-back, respectively, of the subduction zone and Ionian slab, a fragment of oceanic lithosphere between the continental domains of the Adriatic to the northeast and Africa to the west [MALINVERNO and RYAN 1986; CARMINATI *et al.* 1998; WORTEL and SPAKMAN 2000; FACCENNA *et al.* 2001; SCROCCA *et al.* 2005; ASCIONE *et al.* 2012].

The CA consists of two main orogenic domains (Fig. 7a): i) the outer domain, including the Southern Apennines and Sicilian Maghrebides, and ii) the inner domain, including the Calabro-Peloritan belt, which occupies the regions of Calabria, northeastern Sicily, and parts of southern Tyrrhenian.

The outer domain is mainly composed of deformed Meso-Cenozoic platform and basin sediments derived from the margins of the African and Adriatic continents and from the Neogene–Quaternary foredeep and thrust-top basins. Contractual phases in the Southern Apennines and Sicilian Maghrebides started in late Miocene time and lasted until early Pleistocene time as demonstrated by lower Pleistocene sediments suturing the outer front of the thrust-fold belt in the Sicily Channel [BUTLER and GRASSOT 1993]. Contraction may be still active as demonstrated, for instance, by the 1968 Belice earthquake in central-western Sicily [MONACO *et al.* 1996; LAVECCHIA *et al.* 2007]. Post-

orogenic extension followed the contractional phases since late Pliocene time in the Southern Apennines, where this tectonic regime is still active [MONTONE *et al.* 2004].

The inner domain of the CA is mainly composed of crystalline and metamorphic rocks overlain by a Mesozoic sedimentary cover. These units are, in places, unconformably overlain by Neogene sedimentary sequences. The inner units drifted away toward the southeast from the Sardinia–Corsica block during early Miocene time and accreted onto the outer domain of the CA [BONARDI *et al.* 2001; VIGNAROLI *et al.* 2008; OLIVETTI *et al.* 2010]. Since late Tortonian time, most of this tectonic edifice was subsequently stretched apart during the extensional phases that led to the formation of the Tyrrhenian back-arc domain [PEPE *et al.* 2000].

Recent GPS data show a rather heterogeneous velocity field along the CA for present times [HOLLENSTEIN *et al.* 2003; D'AGOSTINO and SELVAGGI 2004; SERPELLONI *et al.* 2007; BILLI *et al.* 2008; DEVOTI *et al.* 2008; BILLI *et al.* 2011; PALANO *et al.* 2011] with a marked kinematic divergence between Calabria and Sicily and active shortening in the Ionian section of the CA and in the south-Tyrrhenian (Fig. 7a). Several sectors of the CA and adjacent areas are seismically active as demonstrated by recent and historical earthquakes [CHIARABBA *et al.* 2005; BASILI *et al.* 2008; GALLI *et al.* 2008].

1.2.2.4 The Siculo-Calabrian Rift Zone (SCRZ)

The recent extension of the inner Calabrian Arc mainly occurred in the Siculo-Calabrian Rift Zone (SCRZ) (Fig. 7a). The SCRZ extends from the Tyrrhenian side of Calabria to the Ionian coast of Sicily [MONACO and TORTORICI 2000b]. An indicator for this extension is the ~370 km long seismogenic belt, well developed in the entire zone [TORTORICI *et al.* 1995; MONACO and TORTORICI 2000b; CATALANO *et al.* 2008]. It extends on both sides of the Messina Strait and is considered continuous throughout the water arm [TORTORICI *et al.* 1995; MONACO and TORTORICI 2000b].

Various normal fault segments of 10 to 45 km length are part of this zone, which is supposed to be responsible for major seismic events in the region [MONACO and TORTORICI 2000b; CATALANO *et al.* 2008] (Fig. 7a). Most of the faults show a NE-SW to NNE-SSW orientation, for example the Reggio Calabria fault and the Capo Vaticano fault [TORTORICI *et al.* 1995; MONACO and TORTORICI 2000b] (Fig. 7a). The faults striking ENE-WSW, e.g., the S. Eufemia fault and the Scilla fault (Fig. 7a), were interpreted as sinistral faults [TORTORICI *et al.* 1995; MONACO and TORTORICI 2000b]. In these areas,

differential extensions between the Aspromonte area and the Messina Strait are balanced [MONACO and TORTORICI 2000b] (Fig. 7a). In the same manner, a dextral behaviour was attributed to NW-SE and NNW-SSE trending faults, which occurred in the inner side of the inner CA and between Mt. Etna and the Hyblean Plateau [MONACO and TORTORICI 2000b] (Fig. 7a). Recent activities of the faults in the SCRZ are indicated by deformed upper Pleistocene sediments, as the faults typically border Plio-Pleistocene basins [TORTORICI et al. 1995; MONACO and TORTORICI 2000b].

1.2.2.5 Tectonic activity in the Messina Strait area

The extension in the Messina Strait can be dated back to 0.8 - 0.6 Ma, which is in agreement with the start of regional uplift [TORTORICI et al. 1995; MONACO and TORTORICI 2000b; CATALANO et al. 2008; ARGNANI et al. 2009a]. From fault investigations as well as GPS velocity measurements, an overall extensional strain at a rate of 1.5 - 3.4 mm/a in a WNW-ESE to NW-SE direction can be assumed [D'AGOSTINO and SELVAGGI 2004; FERRANTI et al. 2007] (Fig. 7a). The region is generally viewed as a graben structure, as a subsidence of 1 mm/a has been measured in the Strait and numerous faults border the Strait [BOTTARI et al. 1989a; DE NATALE and PINGUE 1991; AMORUSO et al. 2002a]. Nevertheless, the graben structure theory is still under discussion due to the lack of investigations, especially in the offshore area [BOTTARI et al. 1989a; ANZIDEI et al. 1998; ARGNANI et al. 2009a].

Different theories for the active extension have been proposed. In all cases, extension is considered to be strongly associated with the development of differential trench retreat and slab roll-back at the plate boundary zone [D'AGOSTINO and SELVAGGI 2004; GOES et al. 2004; BILLI et al. 2008] (Fig. 7a, 8). Based on this, the differential motion of Calabria in comparison to Sicily as well as the active rifting of the Messina Strait may be the result of slip partitioning in the overlying forearc [D'AGOSTINO and SELVAGGI 2004]. A similar theory assumes that the Sicilian plate boundary zone and thrust front may have shifted into the Tyrrhenian Sea [D'AGOSTINO and SELVAGGI 2004; GOES et al. 2004] (Fig. 7a). This assumption is based on observations of recent volcanic activity of the Aeolian Islands to the north of Sicily [GOES et al. 2004]. Within this system, the Strait area may act as a diffuse transfer zone, where dextral deformation outbalanced the differential motion of the plate boundary zone [GOES et al. 2004]. An extension of 1 - 2 mm/a would be a result, which is very similar to the observed amount of extension in the Messina Strait [GOES et al. 2004]. Furthermore, this theory also explains the differential motion of Calabria in comparison to Sicily [GOES et al. 2004]. However, the differential motion between

Calabria and Sicily is a matter of ongoing debate. On one hand, researchers suppose that differential motion exists based on modern GPS data [*D'AGOSTINO and SELVAGGI 2004; GOES et al. 2004*] (Fig. 7a). On the other hand, *ANZIDEI et al. [1998]* came to the conclusion that no significant difference can be identified in older GPS measurements from 1987 to 1994. Based on the extensional movement, a third theory has been put forward, which assigns the extension and the accompanying fault activities to the regional uplift [*VALENSISE and PANTOSTI 1992; MONACO et al. 1996*].

1.2.3 Turbidity Currents in the Messina Strait

The shelves of the Messina Strait are very narrow (<1 km). Short, ephemeral streams can deliver sediment from the mountain ranges of Sicily and Calabria almost directly to the submarine slopes. This can generate hyperpycnal flows [*MULDER and SYVITSKI 1995*]. Turbidity currents may originate from high sediment fluxes at river mouths during floods, resulting in hyperpycnal flows that either bypass the narrow continental shelf or become trapped on the shelf to produce deposits subsequently mobilized by slope failures [*MITCHELL 2005*]. Some cores containing turbidities have actually been retrieved in the Messina Strait [*SELLI et al. 1979*]. Evidence for the generation of one or more turbidity currents associated with the 1908 earthquake was suggested by the breakage of telegraph cables crossing submarine channels on the abyssal Messina cone [*RYAN and HEEZEN 1965*].

Many channel heads at depths shallower than 100 m can be directly linked with particular onshore streams. As the local sea level dropped by ~140 m during the LGM (Last Glacial Maximum) [*LAMBECK and PURCELL 2005*], the uppermost parts of the channels would have connected with river valleys [*SHEPARD 1972; PIPER and NORMARK 2009*]. Although slumps and slides are common, the absence of scarps at the heads of the gullies and channels suggests that they were not formed by slope failure [*FARRE 1983*] or the failure of sediment accumulations at river mouths [*CONWAY et al. 2012*]; their association with rivers suggests a hyperpycnal origin [*CASALBORE et al. 2011*], although not every river discharge must necessarily result in hyperpycnal flow. In some cases temporary deposition near river mouths may occur, the deposits being subsequently remobilised during high-energy events [*MITCHELL 2005*].

According to *GOSWAMI et al. [2014]*, the density and spatial organization of channels and gullies in the Messina Strait differ on opposite sides of the basin, channel density being higher on the Sicilian than the Calabrian side, and channel density being also more variable along the Sicilian coast (Fig. 1a). This

may at least partly relate to spatial variations in the flux of sediments from land. However, the lack of channels on the Calabrian side seems to coincide with the main fault escarpments. The evolution of these faults may have somehow impeded the development of a stable channel network. Unlike some other more enclosed rift basins (e.g. the Eilat sub-basin in the northern Gulf of Eilat/Aqaba), there is relatively little evidence of modern turbidities accumulating within the Messina Strait, a feature it has in common with the Aqaba sub-basin in the northern Gulf of Eilat/Aqaba [TIBOR *et al.* 2010]. Regional uplift in the north maintains a steep basin gradient, causing turbidity currents to bypass the basin on its way to the Ionian Trench further south.

1.3 Previous Research on Active Tectonic Structures in the Messina Strait

While the overall tectonic setting of the area around the Messina Strait has intensely studied in the past, only very limited direct observation of active tectonic structures is available in the Messina Strait itself. This is mainly caused by a very difficult setting for seismic data collection. The Messina Strait is too narrow for running straight lines across the Strait with a long streamer but such lines are needed for imaging faults parallel to the axis of the Messina Straits. Seismic data collection is further complicated by heavy ship traffic and strong currents. Hence, only a few surveys were conducted in the past.

DOGLIONI *et al.* [2012] reported a blind SE-dipping normal fault bounding the northernmost part of the Messina Strait, named Messina Strait Fault (MSF in Fig. 7a). It gradually disappears northeastward and continues as NW-dipping Scilla fault (SF in Fig. 7a). FERRANTI *et al.* [2007] thought that there is a cumulative slip rate of ~0.5 mm/yr on this Scilla fault, with coseismic slip of 1.5 - 2 m, hinting at the possibility of 6.9 - 7.0 Mw earthquakes.

In the northern part of the Messina Strait, a W-dipping fault (FA in Fig. 7a) was identified by ARGNANI *et al.* [2009a]. It is located on the Calabrian side and connected to the fault system onshore near Reggio Calabria. The fault can be dated back to Late Pliocene-Early Pleistocene.

In the southern part of the Messina Strait, approaching southwest Calabria, a 30 km-long W-dipping fault (SCF in Fig. 7a) is outcropping at the sea floor [ARGNANI *et al.* 2009a]. It trends NW-SE and represents the longest lineament within the Messina Strait. However, the undisrupted and subparallel Plio-Quaternary strata seen on seismic profiles is an indication against the occurrence of active faults.

In southern Calabria (Fig. 7a), faults were active during the Late Pleistocene-Holocene [TANSI *et al.* 2007]. Ongoing investigations by different institutions will probably cast light on this fundamental issue.

In Sicily (Fig. 7a), faults were active during the Late Pleistocene-Holocene [AZZARO and BARBANO 2000]. The Malta Escarpment is generally considered as being active [MONACO and TORTORICI 1995] during the Holocene, which was confirmed by reflection seismic data [HIRN *et al.* 1997]. This fault has been considered as a possible source of the 1693 Sicily earthquake [HIRN *et al.* 1997; SIROVICH and PETTENATI 1999; ZOLLO *et al.* 1999].

Taormina Fault has been proposed by many authors [BONFIGLIO 1981; GHISSETTI and VEZZANI 1982; SCANDONE *et al.* 1991; FIRTH *et al.* 1996; STEWART *et al.* 1997a; RUST and KERSHAW 2000; ANTONIOLI *et al.* 2003; CATALANO and DE GUIDI 2003; ANTONIOLI *et al.* 2006a; ANTONIOLI *et al.* 2006b], being located offshore northeast coastline of Sicily (TF in Fig. 7a). Based on coastal geomorphology, the TF has been inferred to be an NNE-SSW trending, E-facing, active extensional fault [GHISSETTI and VEZZANI 1982; SCANDONE *et al.* 1991; RUST and KERSHAW 2000]. It is in the Siculo-Calabrian Rift Zone (SCRZ) [BONFIGLIO 1981; FIRTH *et al.* 1996; STEWART *et al.* 1997a; RUST and KERSHAW 2000; ANTONIOLI *et al.* 2003; CATALANO and DE GUIDI 2003; ANTONIOLI *et al.* 2006a; ANTONIOLI *et al.* 2006b] (Fig. 7a).

Therefore, the TF is regarded as a structure which is responsible for the formation of the Holocene paleo-shorelines, the coastal uplift, the abrupt coastal coseismic displacements, and the steps/flights of the upper Pleistocene marine terraces along the Taormina coast.

The TF is considered as an important connecting fault in the SCRZ, linking the southern Calabria rifting branch to the southeastern Sicily rifting branch [STEWART *et al.* 1997b; MONACO and TORTORICI 2000b; CATALANO and DE GUIDI 2003; CATALANO *et al.* 2008]. This connection would let the TF be one of the most hazardous and largest seismic gaps in Italy, a potential site for a large future earthquake, [STEWART *et al.* 1997b; NERI *et al.* 2004]. A very low-level of seismicity ($M_w \leq 3.5$) [AZZARO and BARBANO 2006] and some stronger events (e.g. the March 28th, 1780 event, $I_0 = \text{VII-VIII MCS}$, $M_w = 5.6$) [AZZARO *et al.* 2007] might be evidences for this characteristic.

1.4 Previous Research on the Source of the 1908 Messina Earthquake and Tsunami

1.4.1 Possible Source Models for the 1908 Messina Earthquake

Several source models have been proposed for the 1908 Messina earthquake; these models show significant differences in fault parameters including strike, dip and length of the fault [SCHICK *et al.* 1977; CAPUTO 1979; MULARGIA and BOSCHI 1983; BOTTARI *et al.* 1986; CAPUANO *et al.* 1988; BOSCHI *et al.* 1989a; DE NATALE and PINGUE 1991; VALENSISE and PANTOSTI 1992; PIATANESI *et al.* 1999; TINTI *et al.* 1999a; PINO *et al.* 2000; AMORUSO *et al.* 2002a; MICHELINI *et al.* 2005; PINO *et al.* 2009a] (Fig. 1a).

Based on inversion of the levelling data, [MULARGIA and BOSCHI 1983] initially envisaged a model being represented by the displacement on two normal faults, a low-angle, E-dipping fault on the Sicilian side of the Strait, and a high-angle, W-dipping fault on the Calabrian side (Fig. 1a). Successively, many inversion models proposed for the causative fault show various geometric realizations of the blind low-angle E-dipping fault [CAPUANO *et al.* 1988; BOSCHI *et al.* 1989a; DE NATALE and PINGUE 1991; VALENSISE and PANTOSTI 1992; AMORUSO *et al.* 2002a; VALENSISE *et al.* 2008]. Numerical modelling simulations based on the E-dipping fault [TINTI *et al.* 2001; TINTI and ARMIGLIATO 2003b] show that the tsunamigenic earthquake source must have been placed under the Messina Strait, where it caused subsidence of the seafloor, and extends under the Ionian Sea to the south of the Strait.

AMORUSO *et al.* [2002a] applied a nonlinear approach to draw the faulting mechanism by inverting P-wave first arrivals and levelling data simultaneously. This method could improve the estimation of the strike, the dip and the slip of a source fault and determine the location, the width and the length of that fault. Their model is a ~30 km long, N-S-striking fault, right along the Straits (Fig. 1a). Moreover, in order to evaluate the expected shaking to the pillars of a planned bridge over the Straits, TAYLOR and FRANCIS [2009] proposed a summary model centred on the E-dipping fault.

Based on the macroseismic scenario and on structural and morphotectonic data, there is a different view relating the 1908 event to the rupture along NE-trending, W-dipping faults on the Calabrian side [SCHICK *et al.* 1977; GHISSETTI 1984a; BOTTARI *et al.* 1986; GHISSETTI 1992b; WESTAWAY 1992; TORTORICI *et al.* 1995; BOTTARI *et al.* 2008]. Actually, the area of the greatest damage was in Calabria, where subsidence and ground fractures were documented [MONACO and TORTORICI 2007; BLUMETTI *et al.* 2008]. This second interpretation is compatible with the geological structure of the Straits, characterized by master faults on the Calabrian side [GHISSETTI 1984a; MONTENAT *et al.* 1991; TORTORICI *et al.* 1995; FERRANTI *et al.* 2008] and by larger long- and short-term uplift patterns in southern Calabria

than in northeast Sicily [CATALANO *et al.* 2003; FERRANTI *et al.* 2007]. However, analogue modelling of the structural architecture of the Strait [BONINI *et al.* 2011] suggests that high-angle normal faults in southern Calabria represent antithetic structures and are linked to a low-angle E-dipping master fault, which is thought to be the source fault of the 1908 Messina earthquake.

ALOISI *et al.* [2013] demonstrates that levelling data alone cannot discriminate between two oppositely dipping fault models. Thus, their role as a keystone for modellers is untenable. However, new morphotectonic and geodetic data indicate that the Armo Fault (Fig. 7a) has been very active recently and is currently accumulating strain [ALOISI *et al.* 2013]. Surface observations, together with appraisal of macroseismic intensity distribution, available seismic tomography and marine geophysical evidence, give credit to the hypothesis that the Armo fault and possibly the S. Eufemia fault are part of a major crustal structure that slipped during the earthquake (Fig. 1a, 7a).

1.4.2 Possible Sources for the 1908 Messina Tsunami

Since the tsunami was assumed to be triggered by the seismic shock, tsunami modellers built up models on the most common fault solution, but showed a misfit between the simulated results and the observed data, especially that the calculated largest run-up heights appeared in the northern Messina Strait, whereas the largest observed values occurred in the south [TINTI *et al.* 1999b; TINTI and ARMIGLIATO 2003b]. Therefore, the modellers modified the fault solution, e.g. adjusting the heterogeneity [TINTI *et al.* 1999b], and obtained a more accurate model. Still, no fault solution comes up with a consistent explanation for both the earthquake and the tsunami [TINTI *et al.* 1999b; GERARDI *et al.* 2008].

Since the proposed seismogenic faults could not explain the observed run-up heights of the tsunami, BILLI *et al.* [2008] suggested an alternate solution for the triggering mechanisms of the 1908 Messina tsunami. BILLI *et al.* [2008] recalculated the possible source region of the tsunami (Fig. 1a) based on tsunami travel times and run-up values described by different scientists shortly after the event, especially by PLATANIA [1909]. For this purpose, BILLI *et al.* [2008] used a backward ray-tracing method, where tsunami travel time data are converted into distances, based on the assumption that the earthquake and tsunami were triggered more or less simultaneous [BILLI *et al.* 2008].

The predicted tsunami source area lies in the Ionian Sea off Giradini on the Sicily coast and off Lazzaro on the Calabria Coast [BILLI *et al.* 2008] (Fig. 1a). As the observed run-up heights of the tsunami cannot be explained by the suggested seismic fault solutions [TINTI and ARMIGLIATO 2003b; BILLI *et al.* 2008;

FAVALLI et al. 2009b], *BILLI et al. [2008]* strongly postulated a landslide induced tsunami. Their argument is based on a calculation method developed by *OKAL and SYNOLAKIS [2003]*, and they intended to find a massive landslide in the area of the supposed tsunami source region, visible in a seismic image and bathymetry data.

However, *ARGNANI et al. [2009a]* strongly doubts the occurrence of a large landslide in this part of the Messina Strait. They argued that the seismic image used by *BILLI et al. [2008]* is of a bad quality and that their bathymetry data do not show clear landslide evidence. New high-resolution seismic and bathymetric data clearly show that the features interpreted by *BILLI et al. [2008]* do not represent a young landslide [*ARGNANI et al. 2009b; GROSS et al. 2014*]. *GERARDI et al. [2008]* did the same calculations with slightly different data, but came up with the conclusion that the 1908 Messina tsunami was a fault induced tsunami. Despite this, *ARGNANI et al. [2009a]* did not find any reliable arguments against the backward ray-tracing method used by *BILLI et al. [2008]*.

2 OBJECTIVES

The main objective of this thesis is to analyse neo-tectonic features in the Messina Strait and associated hazards. This is done based on new dense high-resolution acoustic data set collected during RV Meteor Cruise M86/2 in Dec. 2011/Jan 2012 [KRASTEL *et al.* 2014]. Near-surface faults were mapped and analysed based on the new data. The activities of selected faults were reconstructed in order to address the current activity. Derived input parameters were used for numerical tsunami modelling.

Specific objectives of the thesis are:

i) Characterization of fault patterns and their structural relevance to the overall tectonic framework of the inner Messina Strait.

How are faults distributed in the Messina Straits? What types of faults can be identified? How do they fit to the overall tectonic framework?

ii) Assessing the graben structure of the inner Messina Strait.

Is it correct to characterize the Messina Strait as graben structure? How was this graben structure formed?

iii) Verification / Falsification of the proposed submarine Taormina Fault.

Is it possible to identify or exclude the proposed Taormina Fault on the new data?

iv) Analyzing the past and recent activity of the newly-discovered Fiumefreddo - Melito di Porto Salvo Fault Zone in the outer Messina Strait.

What was the evolution of the Fiumefreddo - Melito di Porto Salvo Fault Zone? Is it active in recent times and therefore a potential source for tsunamis? What was the relationship between Fiumefreddo - Melito di Porto Salvo Fault Zone and the overall tectonics, especially in recent time?

v) Tsunamigenic potential of the newly-discovered Fiumefreddo - Melito di Porto Salvo Fault Zone in the outer Messina Strait.

Can the newly-discovered Fiumefreddo - Melito di Porto Salvo Fault Zone generate tsunamis? How large may such tsunamis get?

3 DATA AND METHODOLOGY

3.1 Acquisition and Processing of Seismic and Hydro-Acoustic Data

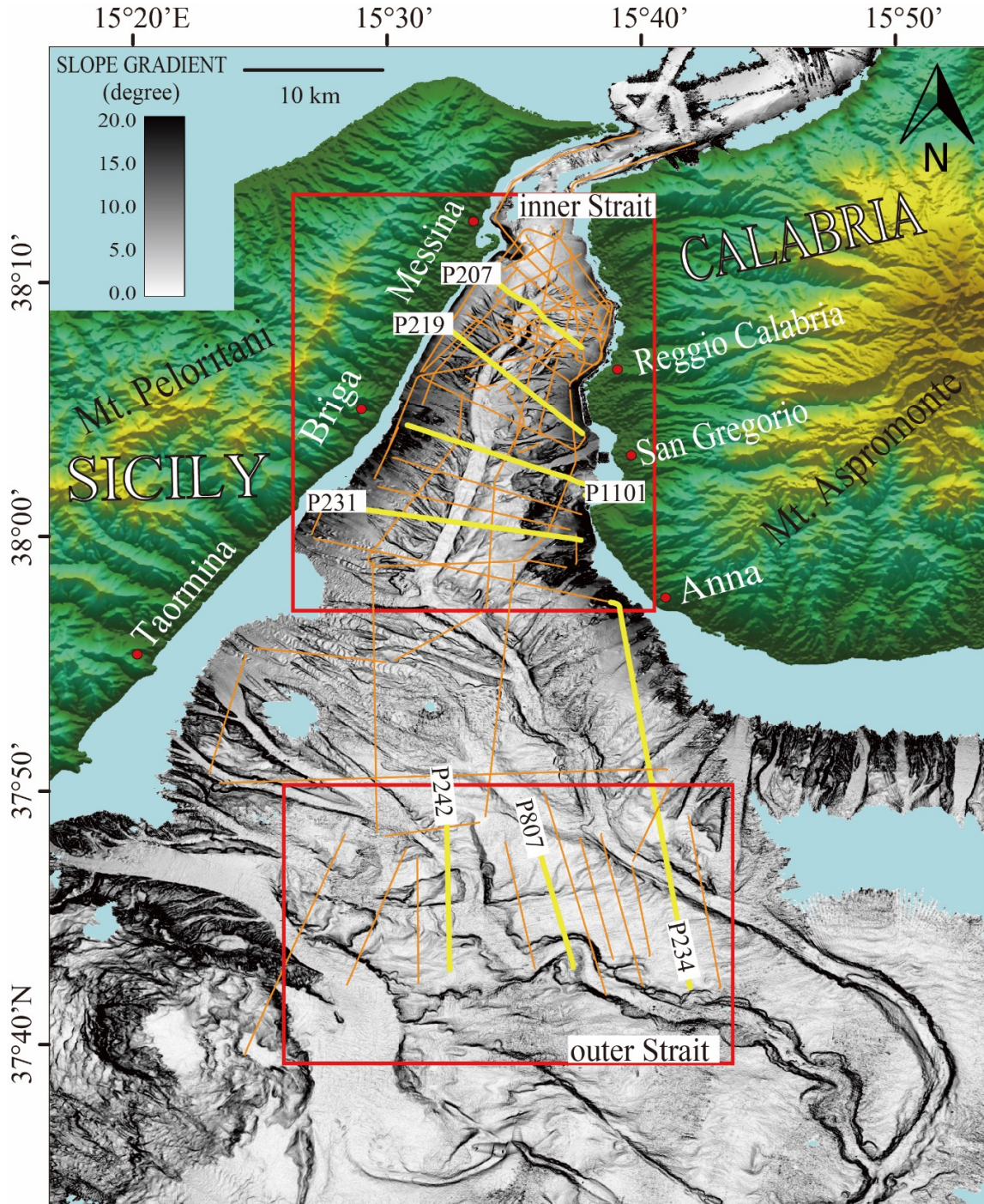


Figure 9 Bathymetry of the Messina Strait with 2D seismic and hydro-acoustic survey lines (orange and yellow lines). Survey lines in yellow are selected to be shown in this thesis.

From December 27th, 2011 to January 17th, 2012, a new high-resolution 2D seismic and hydro-acoustic dataset was acquired during RV Meteor Cruise M86/2. The Messina Strait was one of the survey targets during Cruise M86/2. Data (Fig. 9) were collected by means of a bathymetric multi-beam echo sounder, a sediment echo sounder, and a high-resolution 2D reflection seismic system. Additional high-resolution bathymetric data collected in the frame of the MAGIC project (Marine Geohazards along the Italian Coasts, *CHIOCCI and RIDENTE [2011]*) were assessed for this study as well.

3.1.1 Bathymetric Multi-Beam Echo Sounding Data

RV Meteor's hull-mounted Kongsberg-Simrad EM122 deep-water bathymetric multi-beam echo sounder was used to acquire new bathymetric data. Frequencies of 12 kHz and 432 soundings per swath can be transmitted at the Mills cross configured transducer array. The soundings per ping are duplicated by using a multi-ping mode (two swaths per ping); the pings are transmitted with a small difference in along-track tilt, thereby improving along-track resolution. An angular coverage sector of up to 150° results from this configuration, with a focal length equal to six times the water depth (assuming a flat seafloor). Bathymetric data were processed with the open source software package Multi-Beam System[®] (version 5.2) and displayed by the Generic Mapping Tool[®] (GMT, version 4.9) and Global Mapper (Blue Marble Geographics, version 12).

3.1.2 Sediment Echo Sounding Data

The sediment echo sounder system we used was the Atlas PARASOUND system P70. This system applies the so-called parametric effect. Three signals are recorded: the primary high frequency signal (18 kHz; PHF), the secondary low frequency signal (selectable 0.5 to 6.0 kHz; SLF) and the secondary high frequency (selectable 36.5 to 42 kHz; SHF). In this thesis, only the SLF signal was used in order to image the upper tens of meters of the sedimentary succession. The SLF frequency was set to 4 kHz. ps32sgy[®] (version 1.5.1) and Kingdom Suite[®] (version 8.6) were used to process and display the data, respectively.

3.1.3 High-Resolution 2D Reflection Seismic Data

High-resolution 2D reflection seismic data were collected by using 162.5 m-long, 104-channel digital Geometrics GeoEeL streamer. This streamer is capable of recording high-resolution seismic data, as its group interval is only ~1.56 m. The seismic signal was generated by a 1.7 l GI gun, operated in harmonic mode and a shot interval of 4 s. With a cruise speed of ~4 knots, this results in a shot spacing of ~8 m; sub-bottom penetration was up to 1 s TWT (Two-Way-Travel-Time). This configuration enables the collection of high-resolution data in both shallow and deep water. 90 two-dimensional seismic profiles with a total length of ~1000 km were acquired in the Messina Strait (Fig. 9).

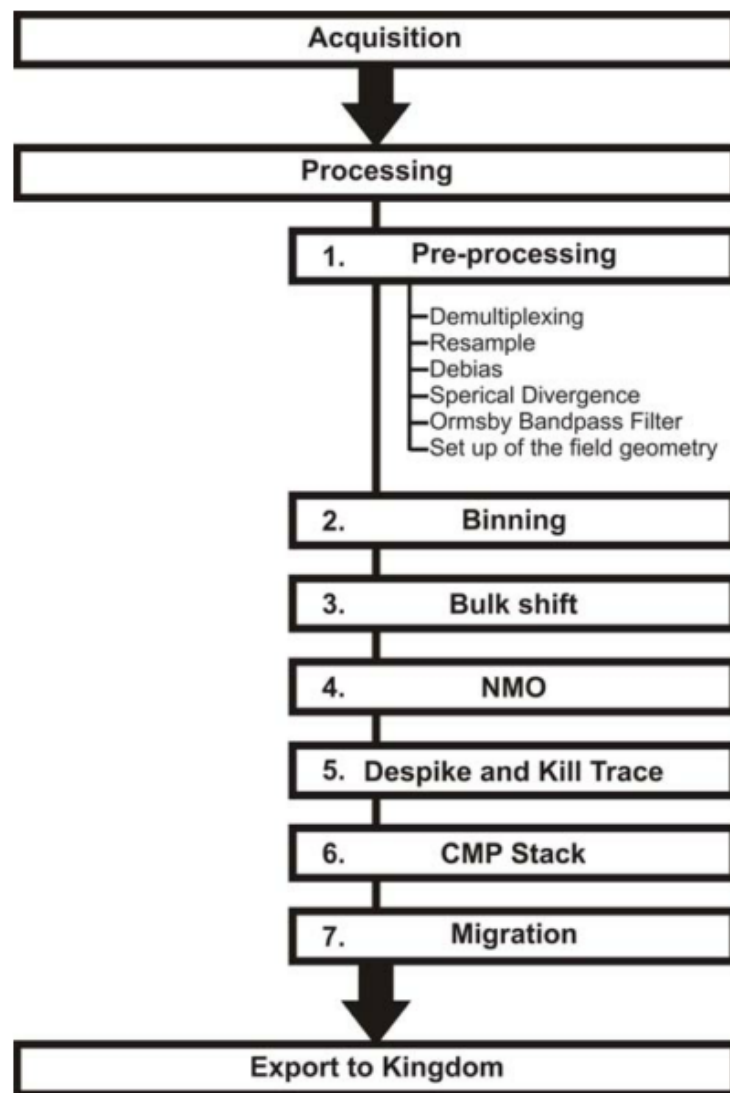


Figure 10 2D seismic processing flow chart.

The processing steps include geometry setup, binning, band-pass filtering (10/20/600/1000 Hz, assumed for low truncation frequency, low cut frequency, high cut frequency, and high truncation frequency, respectively), Normal Move-Out (NMO) corrections, despiking, stacking and time-migration (Fig. 10). The lateral bin size was set to 2 m, which results in an average fold of 14. Due to the relative short length of the streamer system, the system is not capable for a dedicated velocity analysis. Therefore, a constant sound velocity of 1500 m/s was applied during NMO corrections and data migration. Gedco Vista Seismic Processing[®] (Schlumberger, version 11) and IHS Kingdom Suite[®] (version 8.6) were used for processing and interpretation.

3.1.4 Special Processing of the Hydro-Acoustic Data

3.1.4.1 “mbeditviz” used in Multi-beam data processing

During the Cruise M86/2, parts of the multi-beam data were already processed. The automatic cleaning tool “mbclean” was used to remove noise during initial processing. Afterwards, in the lab processing, we used MB-system tool “mbeditviz” instead of “mbclean”. “mbeditviz” is an interactive and therefore time-consuming cleaning tool, but without the risk of erasing real data in contrast to “mbclean”.

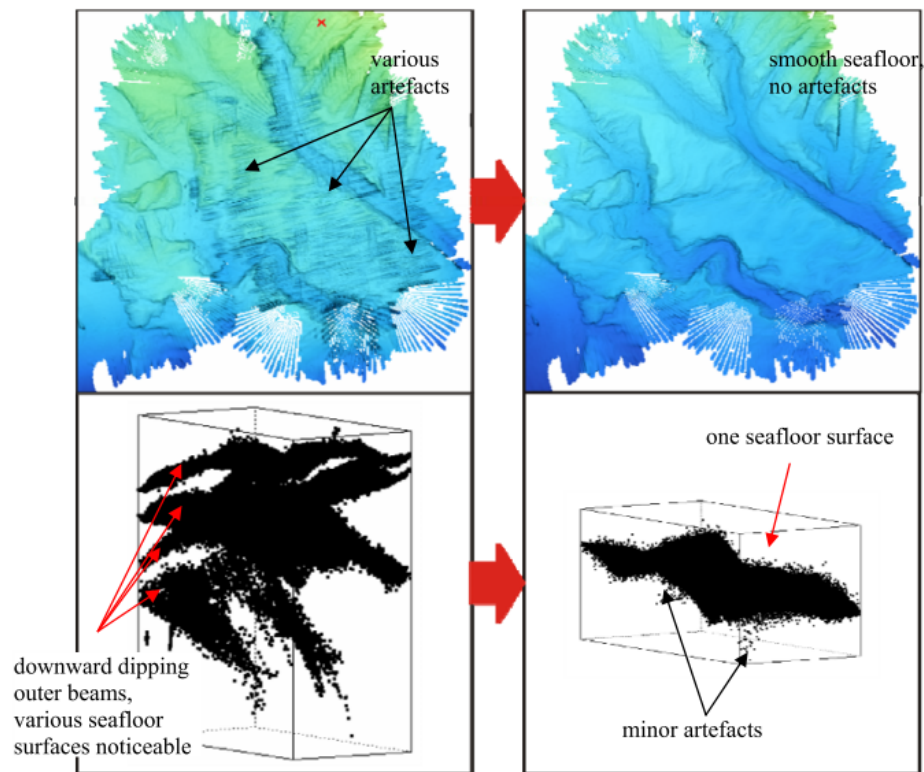


Figure 11 Velocity correction in bathymetry processing. **[Left]** Uncorrected bathymetry grid generated by “mbeditviz” with the corresponding editing window (underneath). At least three seafloor surfaces can be observed, due to the strong downward dip of the outer beams. **[Right]** Same area and editing window as on the left images, but velocity corrected using a SVP-file. Only one seafloor is visible.

“mbeditviz” is an interactive editing tool deleting noise/spikes resulting from false soundings and inaccurate overlaps of data received from multiple surveys (Fig. 11). This tool is very handy, as it visualizes every single data point received within a certain editing area. Data points are visualized as 3D data cloud that can be examined from variable perspectives. The different editing areas can be picked from a temporary bathymetry grid (Fig. 11) – generated by “mbeditviz” from the selected multi-beam data package – which in addition works as an overview map to comprehend changes while editing, as these changes are displayed on the grid immediately. “mbedit”, a predecessor of “mbeditviz”, is another possible editing tool, but only offers the possibility to check every single beam for noise/spikes. Therefore, only “mbeditviz” was used.

During editing, it was revealed that parts of the data show a huge downward dip of the outer beams (Fig. 11). This type of error is not observable in the on-board processed data, which were processed using an on-board measured sound-velocity-profile (SVP-file). Within this thesis, the ‘mbvelocitytool’

was used to check the SVP-file for its accuracy, before using it to correct the data. The result can be observed in Fig. 11, showing a successful corrected bathymetry grid.

3.1.4.2 Frequency adjustment before migration

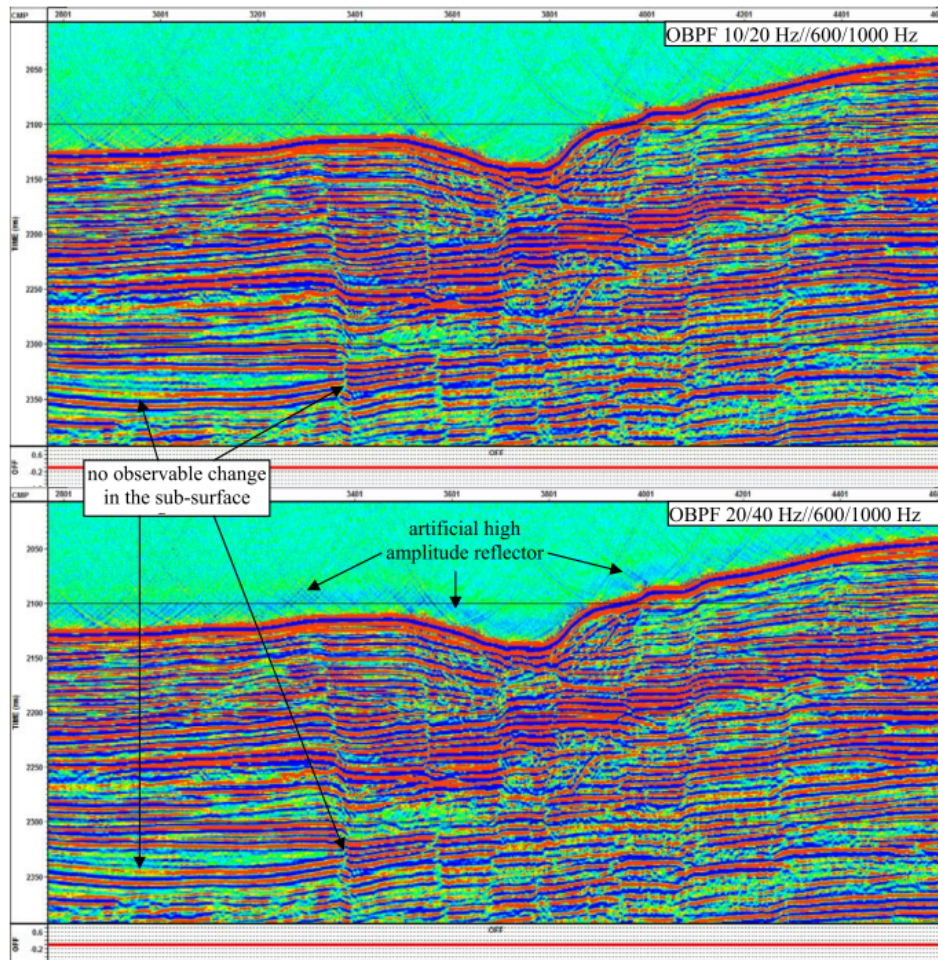


Figure 12 Frequency adjustment before migration. [Upper] migrated profile with an OBPF low cut frequency of 10/20 Hz before migration. [Lower] migrated profile with an OBPF low cut frequency of 20/40 Hz before migration. An artificial reflector can be noticed above the seafloor reflector in the lower image. No increase/decrease of the S/N-ratio within the sediment strata is observable comparing the upper and lower image.

Prior to the migration, an Ormsby Band Pass Filter (OBPF) was applied, which allows comparing the differences in the migration with varying low cut frequency values. In Fig. 12, two migrated images are presented with an OBPF of 10/20 Hz and 20/40 Hz low truncation/cut frequency and 600/1000 Hz for the high cut/truncation frequency not showing any differences within the sub-surface reflectors. The section with the 20/40 Hz low truncation/cut frequency, however, shows an artificial reflector directly

above the seafloor. Therefore, the OBPF was kept in a very wide range as already used during the pre-processing. A SEGY-file was exported after migration, which was imported to the software KINGDOM Suite for further interpretation.

3.1.4.2 “Kill Trace” in 2D seismic processing

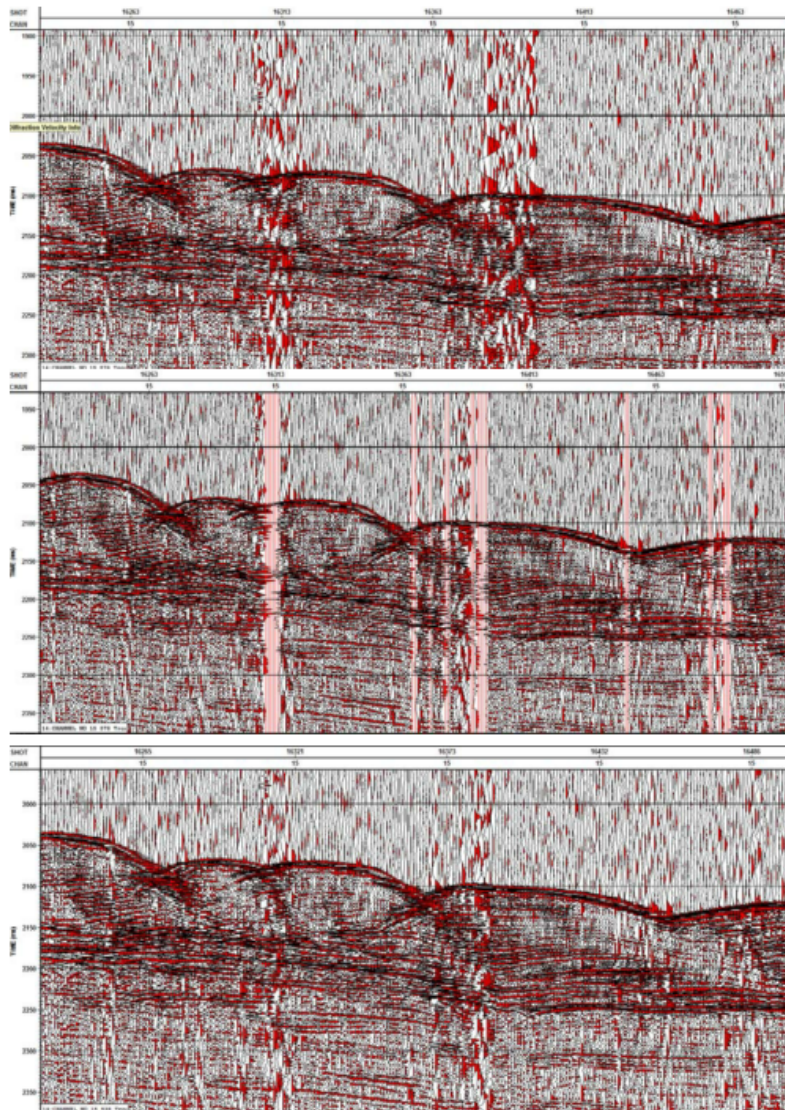


Figure 13 “Kill Trace” in 2D seismic processing. The upper image displays the data after 2D despiking. The middle image shows how the kill trace was applied to the data set. In the lower image, the result can be observed, showing a strong increase of the S/N-ratio as most of the assembly lines are erased.

After data despiking, noisy sections were still observable within the first 40 channels of the profiles P803 to P812 (Fig. 13). Therefore, noise traces were erased using the kill-trace command. This approach is

very helpful as it prevents deleting entire channels or shot-points. After the application of kill trace, a strong increase of the data quality could be noticed (Fig. 13). The noisy sections may be the result of temporarily caught fishing lines or varying noise from wave actions, as a result of slight variations of the towing depth of the streamer (temporarily shallower towing depth results in a higher noise level).

3.2 Methods for Data Interpretations

For ease of description, we divided the Messina Strait into two subareas – the inner Strait and the outer Strait (Fig. 9). Seismic profiles P207, P219, P1101 and P231 in the inner Strait and P234, P807 and P242 in the outer Strait were selected as representatives (Fig. 9) and shown in this thesis. They cover major faults and abundant minor faults and typically exhibit the seismic stratigraphic settings of the subareas as well.

Fault interpretations were based on the following criteria: (a) abrupt offset of steeply dipping strata reflections, (b) tracking of fault plane reflections, (c) sudden vertical changes of the number and shape of the reflectors.

3.3 Cross-Section Restoration

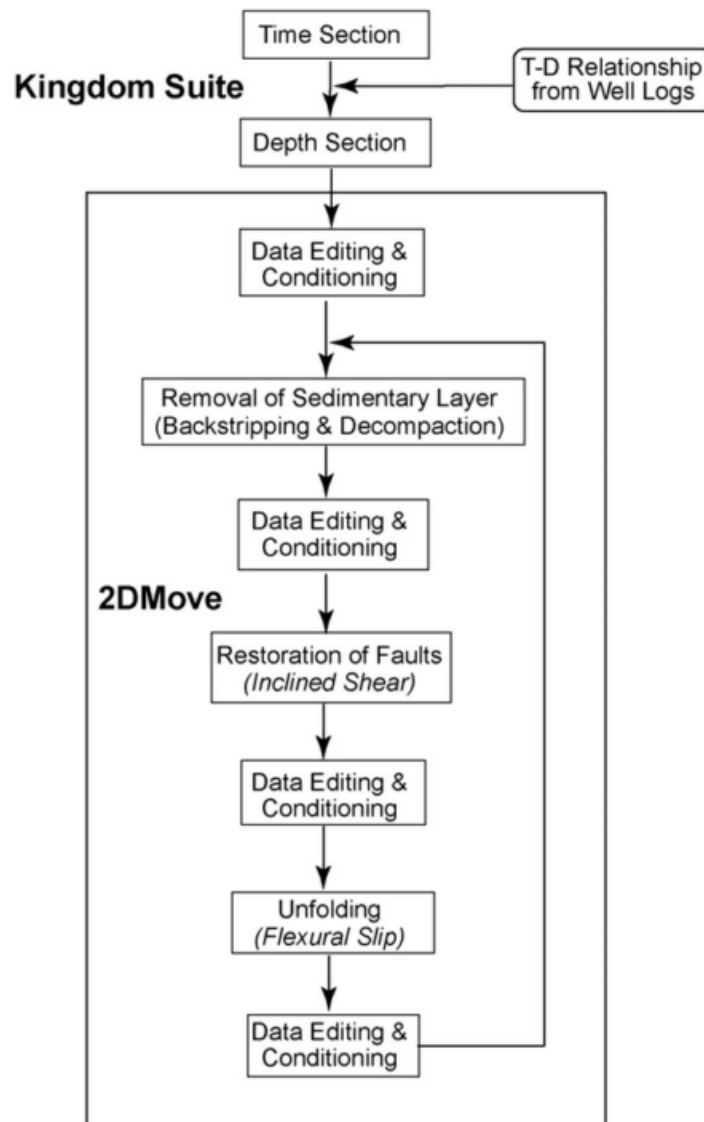


Figure 14 Cross-section restoration flow chart, taken from Cukur et al. (2011)

The cross-section restoration is involved in order to figure out whether the tectonic structures identified in the outer Strait were recently active or not. Seismic profiles were converted to the depth sections, based on an assumed well (no real well information was available), and then imported to Move 2014.2[®] to restore the cross-sections. The restoring steps include backstripping and decompacting sedimentary layers (decompaction), restoring faults (move on fault), and unfolding (Fig. 14). Details are given in Chapter 6.

3.4 Numerical Tsunami Modeling

Numerical modelling of tsunami was performed using a nonlinear shallow water code known as TUNAMI-N2 developed at the Tohoku University, Japan [GOTO *et al.* 1997]. TUNAMI-N2, which solves governing equations of water motions using the leap-frog scheme of Finite Differences on a Cartesian Coordinate system, has been validated using experimental and field data [SYNOLAKIS and BERNARD 2006] and has been applied to several world's tsunamigenic zones [YALÇINER *et al.* 2004; HEIDARZADEH *et al.* 2009; SUPPASRI *et al.* 2011]. Fault parameters used for coseismic seafloor calculations are: Strike, dip, rake angles, top depth of the fault, length and width of the fault as well as the slip amount.

4 MANUSCRIPT I

Assessing the fault pattern of the inner Messina Strait, Southern Italy, by means of high-resolution 2D reflection seismics

Lili Fu¹, Sebastian Krastel¹, Felix Gross¹, Francesco Chiocci², Domenico Ridente³, Deniz Cukur^{4,5}, Jörg Bialas⁴

¹Institute of Geosciences, University of Kiel, Kiel 24118, Germany

²Department of Earth Sciences, Sapienza University of Rome, Rome 00185, Italy

³National Research Council, Roma, Italy

⁴GEOMAR | Helmholtz Centre for Ocean Research Kiel, Kiel 24148, Germany

⁵now at Korea Institute of Geoscience and Mineral Resources, Daejeon 305-350, Korea

Abstract

The exact location of the seismogenic fault of the 1908 Messina earthquake is still under debate, because of the unclear tectonic condition of the inner Messina Strait. In order to reconstruct and shed light upon the fault pattern of the inner Messina Strait, we acquired a new high-resolution 2D reflection seismic dataset. The data suggest that the inner Messina Strait is an angular graben. Surface faults in the graben strike in N-S and E-W directions. The N-S-trending surface faults are right-lateral transtensional faults and distribute along the Messina Canyon and the coastline off southern Calabria, dipping toward the Messina Canyon; E-W-trending surface faults are left-lateral transtensional faults and located in the northern inner Messina Strait off Calabria. Most of them dip toward the south. Several of these newly-discovered surface faults fit to the suggested focal mechanisms of the 1908 Messina earthquake, but we were not able to identify the master fault of this event. The lengths of the fault planes (< 15 km) are too small to generate an earthquake of 7 Mw. The inferred Taormina Fault (TF) was considered as one of the most hazardous and largest seismic gaps in Italy. However, this fault has not been imaged on any seismic data set, even not in our new seismic data. Hence, we doubt the existence of the TF.

1 Introduction

During the last decades, submarine hazards at continental margins and their consequences to coastal communities have been addressed and investigated by the scientific community [MORGAN *et al.* 2009]. The 1908 Messina earthquake ($M_w = 7.1$) and tsunami (run-up height > 10 m) is the most fatal event in Europe since then. Large areas of Southern Italy were affected, and $\sim 80,000$ [BARATTA 1910] to $\sim 100,000$ [MERCALLI 1909] people were killed. However, no general agreement has been archived on the seismogenic/tsunamigenic fault of this event [AMORUSO *et al.* 2002a; TINTI and ARMIGLIATO 2003b; ARGNANI *et al.* 2009a]. There may be two main reasons: i) the Messina Strait shows a high geological complexity and the highest seismicity in Italy; ii) the limitation of available marine seismic data, such as the resolution of the data, the density of the data, etc, may lead to an insufficient and biased knowledge on the tectonics of the Messina Strait (Fig. MI-1).

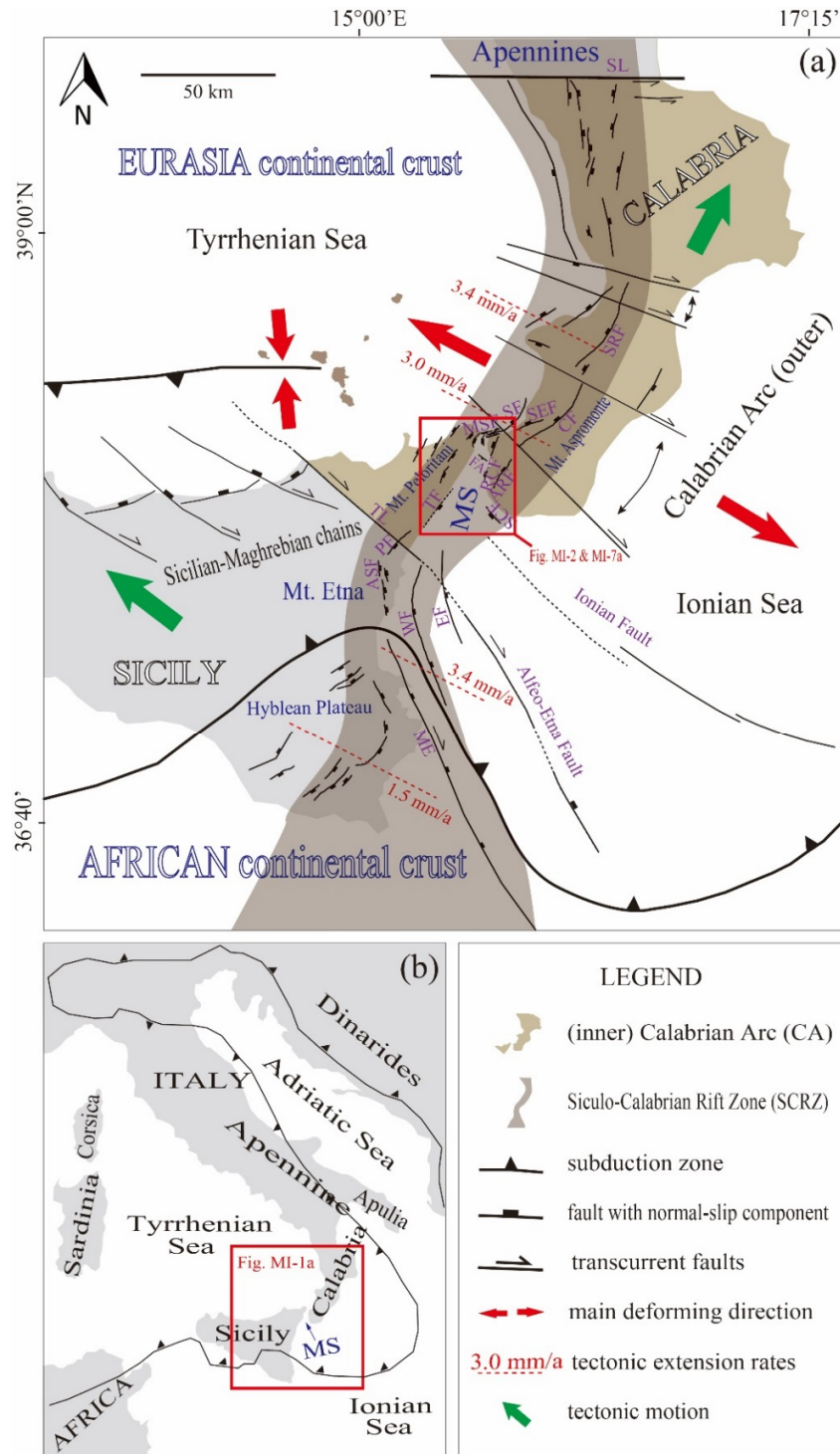


Figure MI- 1 (a) Overall tectonic framework of Southern Italy. Modified from ARGNANI and BONAZZI [2005], GUARNIERI [2006], CATALANO et al. [2008], ARGNANI et al. [2009a], POLONIA et al. [2011a], VITI et al. [2011a], DOGLIONI et al. [2012], and GALLAIS et al. [2013]. MS, Messina Strait. SL, Sangineto line; TL, Taormina Line. RIF, Rosolini–Ispica faults; AF, Avola fault; WF, Western Ionian Fault; EF, Eastern Ionian Fault; ASF, Acireale–S. Alfio faults; PF, Piedimonte fault; TF, Taormina fault; RCF, Reggio Calabria fault; ARF, Armo fault; SF, Scilla faults; SEF, S. Eufemia fault; CF, Citanova fault; SRF, Serre fault; VF, Vibo fault; CVF, Capo Vaticano fault; SCF, Southern Calabria fault; FA, fault identified by ARGNANI et al. [2009a]; MSF, Messina Straits fault. Red box shows the ranges of Fig. MI-2 and Fig. MI-7a. (b) Overview map of central Mediterranean Sea. Red box shows the range of (a). The meanings of the symbols used in the figure are shown in the LEGEND.

The Messina Strait (Stretto di Messina) is a NNE-SSW-trending channel, located in Southern Italy between the Italian Peninsula (Calabria) and Sicily (Fig. MI-1). Several hypotheses have been proposed for the structural pattern of the Messina Strait.

SEGUENZA [1880] suggested the existence of a syncline, with flanks forming from the crystalline rocks outcropping along the opposite shores of the Strait. In contrast, *DI STEFANO [1907]* and *TARAMELLI [1911]* identified a normal faulting system, running NE-SW, confirming that the Strait is a tectonic trench. *OGNIBEN et al. [1973]* pointed out that this faulting system shows a left transurrence. However, *D'AMICO et al. [1973]* proposed another hypothesis, as the position of the petrographically correlated leuco-granodiorite along the two shores of the Strait was not compatible with horizontal displacements.

The genesis of the Messina Strait was related to a tectonic graben by means of geodetic surveys [*CAPUTO et al. 1981*] before and after the 1908 Messina Earthquake, marine geology and neo-tectonic studies [*SELLI et al. 1979*], as well as mesostructural and regional feature analysis [*GHISETTI and VEZZANI 1984*]. Specifically, *GHISETTI and VEZZANI [1982]* and *MULARGIA et al. [1984b]* considered the Strait as an angular graben; *GHISETTI [1984b]* regarded the Strait as a half-graben.

As for the tectonic structures in the Strait, *DOGLIONI et al. [2012]* reported a blind SE-dipping normal fault, the Messina Strait Fault (MSF in Fig. MI-1), bounding the northeast coast of Sicily north of Messina. It gradually vanishes northeastward and transforms into the NW-dipping Scilla fault (SF in Fig. MI-1a). *ARGNANI et al. [2009a]* identified two SW-dipping faults: the FA (fault identified by *ARGNANI et al. [2009a]*) (Fig. MI-1a) and the Southern Calabria Fault (SCF in Fig. MI-1a). The FA is located near the Calabrian side and connected to the fault system onshore near Reggio Calabria [*ARGNANI et al. 2009a*]. The SCF is situated offshore near the southwestern tip of Calabria [*ARGNANI et al. 2009a*].

The existence of the Taormina Fault offshore the northeast coastline of Sicily between Taormina and Briga (TF in Fig. MI-1a) has been proposed by many authors [*BONFIGLIO 1981; GHISETTI and VEZZANI 1982; SCANDONE et al. 1991; FIRTH et al. 1996; STEWART et al. 1997a; RUST and KERSHAW 2000; ANTONIOLI et al. 2003; CATALANO and DE GUIDI 2003; ANTONIOLI et al. 2006a; ANTONIOLI et al. 2006b*]. Based on coastal geomorphology, the TF has been inferred to be a NNE-SSW-trending, E-facing, active extensional fault [*GHISETTI and VEZZANI 1982; SCANDONE et al. 1991; RUST and KERSHAW 2000*].

The inferred TF is part of the Siculo-Calabrian Rift Zone (SCRZ) (Fig. MI-1a), a high-level seismicity belt with active seismo-tectonic deformation [*BONFIGLIO 1981; FIRTH et al. 1996; STEWART et al. 1997a; RUST and KERSHAW 2000; ANTONIOLI et al. 2003; CATALANO and DE GUIDI 2003; ANTONIOLI et al. 2006a*;

ANTONIOLI et al. 2006b). Therefore, the TF is regarded as a structure which is responsible for the formation of the Holocene paleo-shorelines, the coastal uplift, the abrupt coastal coseismic displacements, and the steps/flights of the upper Pleistocene marine terraces along the Taormina coast.

The TF is considered as an important connecting fault in the SCRZ, linking the southern Calabria rifting branch to the southeastern Sicily rifting branch [*STEWART et al. 1997b; MONACO and TORTORICI 2000b; CATALANO and DE GUIDI 2003; CATALANO et al. 2008*]. This connection would let the TF be one of the most hazardous and largest seismic gaps in Italy, a potential site for a large future earthquake, [*STEWART et al. 1997b; NERI et al. 2004*]. A very low-level of seismicity ($M_w \leq 3.5$) [*AZZARO and BARBANO 2006*] and some stronger events (e.g. the March 28th, 1780 event, $I_0 = \text{VII-VIII MCS}$, $M_w = 5.6$) [*AZZARO et al. 2007*] might be evidences for this characteristic.

However, the existence and the exact location of TF has not been documented by means of geological or geophysical work, so far. *ARGNANI et al. [2009a]* was not able to image the TF by means of marine multi-channel seismic data as well.

ARGNANI et al. [2009a] obtained the first high-resolution seismic grid in the Messina Strait and have identified some neo-tectonic features, like FA and SCF [*ARGNANI et al. 2009a*] (Fig. MI-1a), but they did not construct the tectonic pattern of the Messina Strait. To make further progress on the tectonic pattern of the Messina Strait, we launched the RV Meteor Cruise M86/2 in Southern Italy and collected new data. In this study, we constructed and analysed the near-surface fault pattern of the inner Messina Strait (see the range of the red box in Fig. MI-1a) based on the new high-resolution 2D seismic data. The specific objectives are i) characterization of tectonic features and their structural relevance for the tectonic framework of the Messina Strait, ii) assessing the graben structure of the Messina Strait, and iii) verification/falsification of the proposed submarine Taormina Fault.

2 Tectonic Setting

The Messina Strait crosscuts the southern part of the inner Calabrian Arc (CA) and is situated in the Siculo-Calabrian Rift Zone (SCRZ) (Fig. MI-1a).

The CA (Fig. MI-1a), connecting the Apennines to the northeast with the Sicilian-Maghrebian chains to the southwest developed during the Neogene-Quaternary Africa-Europe collision [BARBERI *et al.* 1973; MALINVERNO and RYAN 1986; BOCCALETTI *et al.* 1990; PATACCA *et al.* 1990]. The African Plate subducts northwestward (\sim N20°W, 1-2 cm/yr following the MORVEL plate model) [DEMETS *et al.* 2010] underneath the Eurasia Plate. Since the Pliocene, compressional structures of the inner arc were superseded by extensional faults, both longitudinal and transversal with respect to the arc, causing structural highs and marine sedimentary basins [GHISETTI and VEZZANI 1982]. The CA moved (5 - 6 cm/yr) toward the east or southeast due to the roll-back of the subducting Ionian slab and the corresponding back-arc extension of the Tyrrhenian Basin [MALINVERNO and RYAN 1986; GUEGUEN *et al.* 1998; FACCENNA *et al.* 2004]. The slab roll-back velocities decreased (1-2 cm/yr) during the Middle-Late Pleistocene as a result of tectonic reorganization [FACCENNA *et al.* 2001].

The SCRZ is a \sim 370 km long normal fault system, which roughly runs N-S along the inner side of the inner Calabrian Arc, through the Messina Strait and along the Ionian coast of Sicily [TORTORICI *et al.* 1995; MONACO and TORTORICI 2000b; CATALANO *et al.* 2008] (Fig. MI-1a). Focal mechanisms of crustal earthquakes [PONDRELLI *et al.* 2006; SCARFI *et al.* 2009; D'AMICO *et al.* 2010; D'AMICO *et al.* 2011], structural analyses [TORTORICI *et al.* 1995; MONACO *et al.* 1997; MONACO and TORTORICI 2000b; JACQUES *et al.* 2001; FERRANTI *et al.* 2007; FERRANTI *et al.* 2008], and geodetic data (levelling data and GPS velocity data) [D'AGOSTINO and SELVAGGI 2004; GOES *et al.* 2004; MATTIA *et al.* 2009; D'AGOSTINO *et al.* 2011; PALANO *et al.* 2012] have documented a \sim N115°E extension of the SCRZ (Fig. MI-1a), with rates of 3.6 ± 0.6 mm/yr. This extension is still ongoing and the normal faults have developed in southern Calabria and northeastern Sicily in response to this extension [BIANCA *et al.* 1999; MONACO and TORTORICI 2000b].

Since the Middle Pleistocene, this extension has been accompanied by an intense regional uplift. The uplift is almost uniform (1.0 mm/yr) on the Calabrian and the Sicilian sides of the Strait [BIANCA *et al.* 1999; MONACO and TORTORICI 2004; CATALANO *et al.* 2008] and developed a series of marine terraces, as well as widespread raised Holocene shorelines [VALENSISE and PANTOSTI 1992; STEWART *et al.* 1997b; FERRANTI *et al.* 2007]. Moreover, local uplift may also occur at the footwalls of major faults, [CATALANO

and DE GUIDI 2003]. In southern Calabria, ~ 1.7 mm/yr of post-Middle Pleistocene uplift was partitioned into ~ 1 mm/yr due to regional processes and the residual due to displacements on the footwalls of major faults [WESTAWAY 1993; FERRANTI et al. 2007].

Various tectonic hypotheses of mechanisms, often contrasting, have been invoked to explain the extension and the uplift including : i) the back-arc stretching in the Tyrrhenian Sea; ii) the counter-clockwise rotation of the Adriatic microplate, which has generated a compressive stress field at its western margin [D'AGOSTINO and SELVAGGI 2004; D'AGOSTINO et al. 2008]; iii) the Hellenic slab dragging eastward the entire Ionian-Calabrian domain; or iv) a dynamic balancing regional, deep-induced uplift [GOES et al. 2004].

The uplift is suggested to be an isostatic response to the detachment of the Ionian slab [WESTAWAY 1993; WORTEL and SPAKMAN 2000], or the decoupling of the upper crust from the underlying slab and the convective flow in the mantle wedge [DOGLIONI et al. 2001; GVIRTZMAN and NUR 2001]. Alternatively, the uplift may be caused by the asthenospheric flow occurring at the lateral edge of the roll-back of the Ionian slab [FACCENNA et al. 2011].

Meanwhile, geodetic measurements show that a subsidence occurs in the inner Messina Strait with a rate of ~ 1 mm/yr. GPS data implied that Sicily and Calabria move toward the northwest and northeast (Fig. MI-1a) with respect to the Eurasian plate, respectively, and Sicily moves northward with respect to Calabria [GOES et al. 2004; DEVOTI et al. 2011].

Therefore, the compressional, extensional and transcurrent processes coexist in the vicinity of the Strait [FACCENNA et al. 2003; GOES et al. 2004; PONDRELLI et al. 2006], which has been widely thought to account for diffuse, strongly time-dependent and sometimes devastating disasters in Southern Italy.

3 Data and Method

From December 27th, 2011 to January 17th, 2012, a new high-resolution 2D seismic and hydro-acoustic dataset was acquired during RV Meteor Cruise M86/2 [KRSTEL *et al.* 2014]. The Messina Strait was one of the main targets during the cruise. Data were collected by means of a bathymetric multi-beam echo sounder, a sediment echo sounder, and a high-resolution 2D reflection seismic system. Additional high-resolution bathymetric data collected in the frame of the MaGIC project (Marine Geohazards along the Italian Coasts, *CHIOCCI and RIDENTE [2011]*) were assessed for this study as well. As the complex morphology of the inner Messina Strait restricted the use of sediment echo sounder data, this study is exclusively focused on bathymetric and 2D reflection seismic data.

RV Meteor's hull-mounted Kongsberg-Simrad EM122 deep-water bathymetric multi-beam echo sounder was used to acquire new bathymetric data. Frequencies of 12 kHz and up to 864 soundings per ping (2 swathes with up to 432 soundings) can be transmitted by the Mills cross-configured transducer array. An angular coverage sector of up to 150° results from this configuration, with a focal length equal to six times the water depth (assuming a flat seafloor). Bathymetric data were processed with the open source software package Multi-Beam System[®] (version 5.2) and displayed by the Generic Mapping Tool[®] and Global Mapper (Blue marble geographics).

High-resolution 2D reflection seismic data were collected by using a 162.5 m-long, 104-channel digital Geometrics GeoEeL streamer. The seismic signal was generated by a 1.7 l GI gun, operated in harmonic mode. A sub-bottom penetration of up to 1 s TWT (Two-Way-Travel-Time) was achieved. This configuration enables the collection of high-resolution data in both shallow and deep water. Data processing was carried out by using the commercial software Gedco Vista Seismic Processing[®] (Schlumberger, version 11). The data processing includes geometry setup, binning, band-pass filtering (10/20/600/1000 Hz, assumed for low truncation frequency, low cut frequency, high cut frequency, and high truncation frequency, respectively), Normal Move-Out (NMO) corrections, despiking, stacking and time-migration. The lateral bin size was set to 2 m, which results in an average fold of 14. Due to the relative short length of streamer system, the system is not capable for a dedicated velocity analysis. Therefore, a constant sound velocity of 1500 m/s was applied during NMO corrections and data migration. 90 two-dimensional seismic profiles were acquired in the Messina Strait. IHS Kingdom Suite[®] (version 8.6) was used for data processing and interpretation.

Fault interpretations were based on the following criteria: i) abrupt offset of steeply dipping strata reflections; ii) tracking of fault plane reflections; iii) sudden vertical changes of the number and shape of the reflectors. We divided faults into major faults and minor faults. Major faults are those that could be traced on at least two parallel or subparallel profiles, while those usually only recognized on one single profile are minor faults. Major faults were subdivided into surface faults (marked as 'SFxx'), intersecting the surface of the seafloor, and basement faults (marked as 'BFxx'), cutting into the deeper strata and sedimentary structures close to the acoustic basement. Some of the faults cut both the seafloor and the strata directly above the acoustic basement.

Seismic profile P207, P219, P231 and P1101 were selected as representative profiles (Fig. MI-2) covering most major faults as well as abundant minor faults.

4 Results

4.1 Multi-beam swath bathymetry

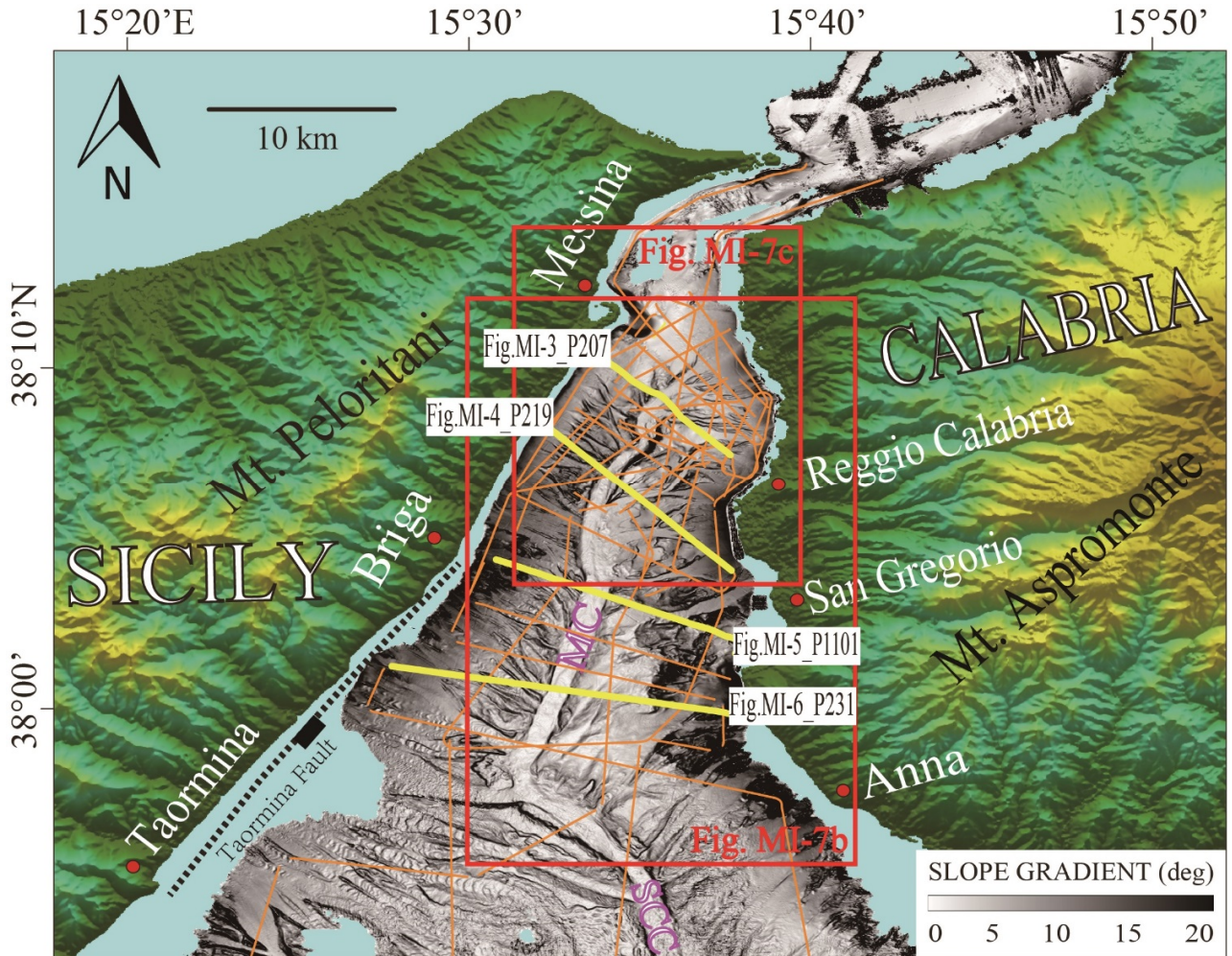


Figure MI- 2 Bathymetry (slope gradient) of the inner Messina Strait. MC, Messina Canyon [COLANTONI 1987]; SCC, South Calabria Canyon [RIDENTE *et al.* 2014]. Orange and yellow lines show the location of the seismic profiles. The profiles shown in this manuscript are marked in yellow. The red boxes show the ranges of Fig. MI-7b and Fig. MI-7c, respectively.

The inner Messina Strait is a fan-shaped narrow passage, broadening towards the south; the narrowest part of Messina bends to the northeast (Fig. MI-2). The Strait is ~40 km long, and ~3 km and ~16 km wide in the north and south, correspondingly. From north to south, its depth gradually increases. The seafloor of the Strait gradually tilts (~3°) from north to south (Fig. MI-2). The seafloor shows a pronounced relief throughout the Strait area.

The most prominent morphological feature is the Messina/South Calabria Canyon (MC and SCC in Fig. MI-2) in the centre of the inner Messina Strait [*COLANTONI 1987; RIDENTE et al. 2014*]. The northern part of this canyon (MC) runs roughly N-S. It is ~1500 m wide and ~50 m deep. The canyon bends to the southeast between Taormina and Anna and is called SCC from there on. The SCC is ~1700 m wide and ~110 m deep. This master canyon system is fed by several narrow gullies running across a very narrow continental shelf and slope [*RIDENTE et al. 2014*] (Fig. MI-2). These gullies/canyons stretch in the Strait like leaf veins.

4.2 High-resolution 2D multi-channel seismic data

4.2.1 Sedimentary architecture of the inner Messina Strait

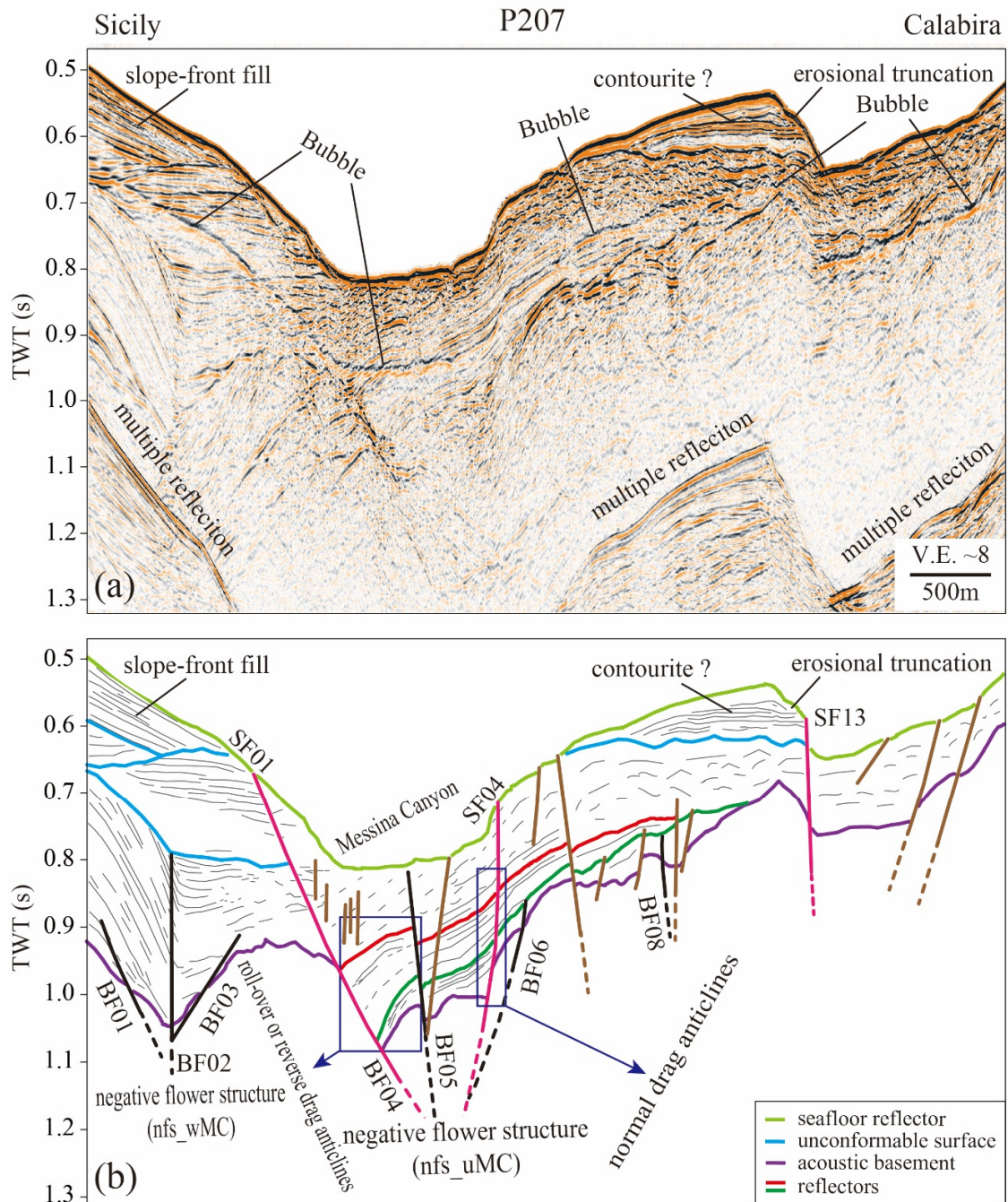


Figure MI- 3 (a) Seismic Profile P27 and (b) line drawing. Pink and black solid lines mark major surface faults and basement faults, respectively. Brown solid lines mark minor faults. Dashed lines show inferred continuations of faults. Vertical exaggeration is 8. See Fig. MI-2 and small inset map for location of profile. nfs_wMC, negative flower structure west of the Messina Canyon; nfs_uMC, negative flower structure under the Messina Canyon.

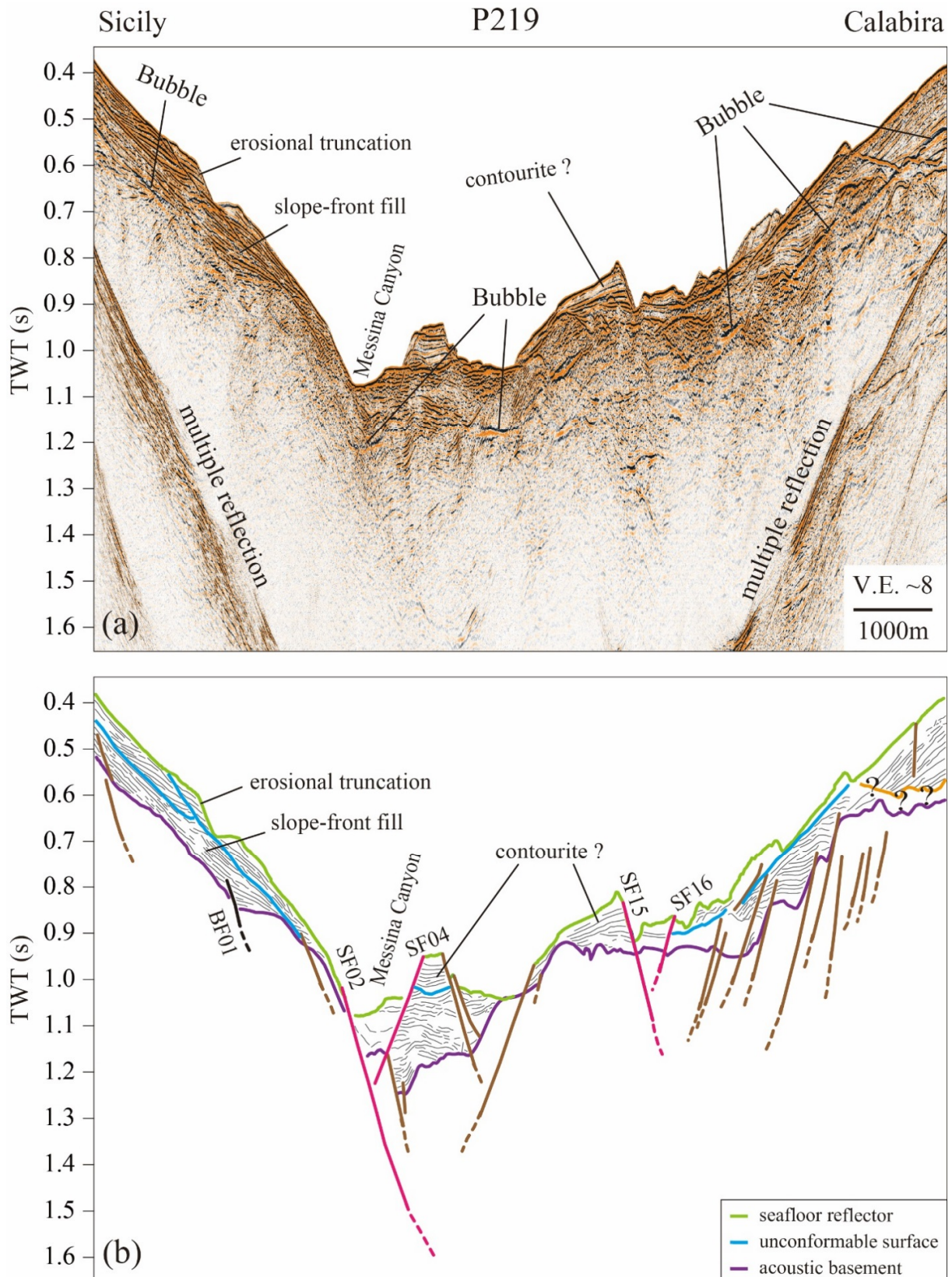


Figure MI- 4 (a) Seismic Profile P219 and (b) line drawing. Pink and black solid lines mark major surface faults and basement faults, respectively. Brown solid lines mark minor faults. Dashed lines show inferred continuations of faults. Vertical exaggeration is 8. See Fig. MI-2 and small inset map for location of profile.

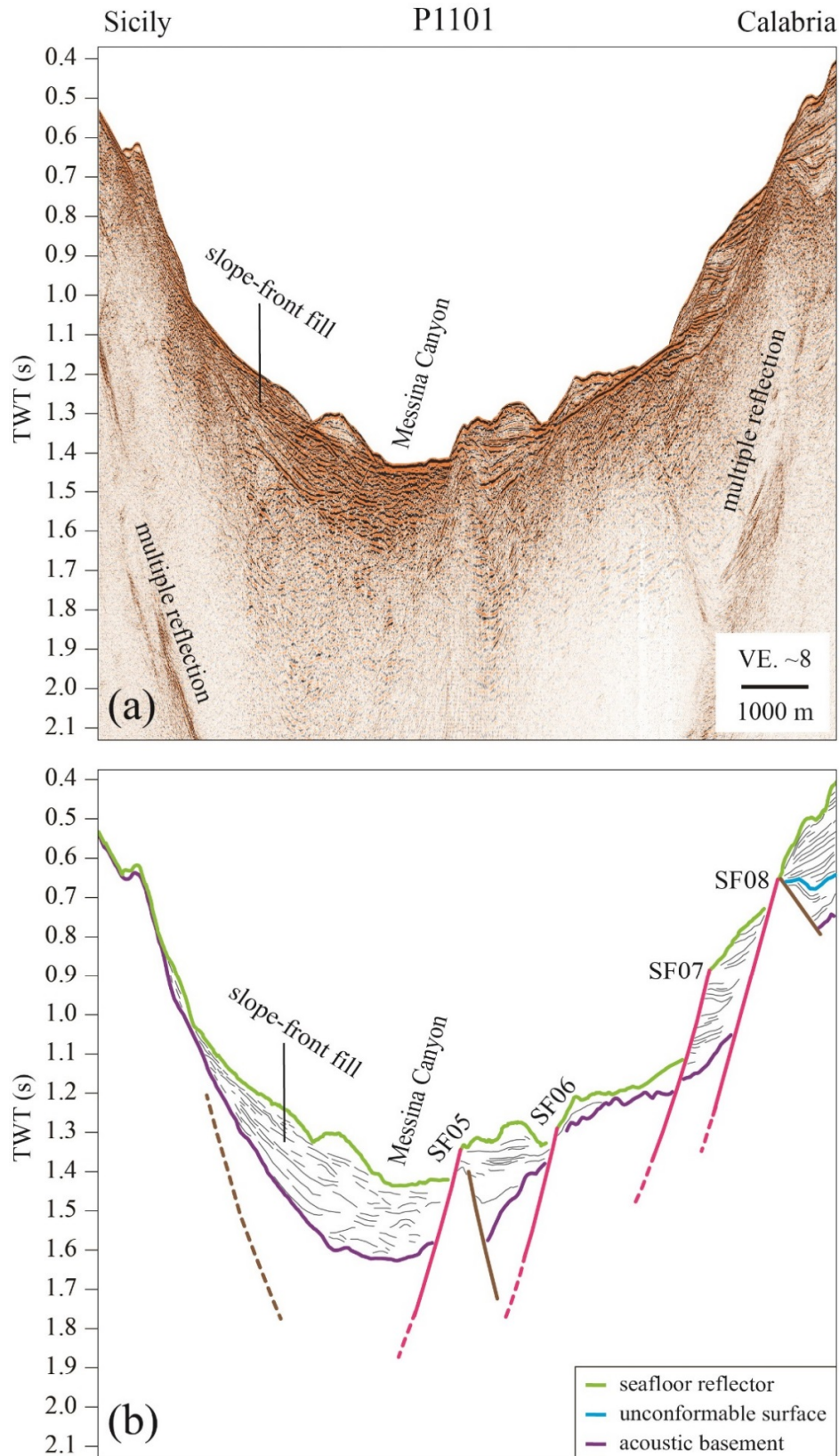


Figure MI- 5 (a) Seismic Profile P1101 and (b) line drawing. Pink and black solid lines mark major surface faults and basement faults, respectively. Brown solid lines mark minor faults. Dashed lines show inferred continuations of faults. Vertical exaggeration is 8. See Fig. MI-2 and small inset map for location of profile.

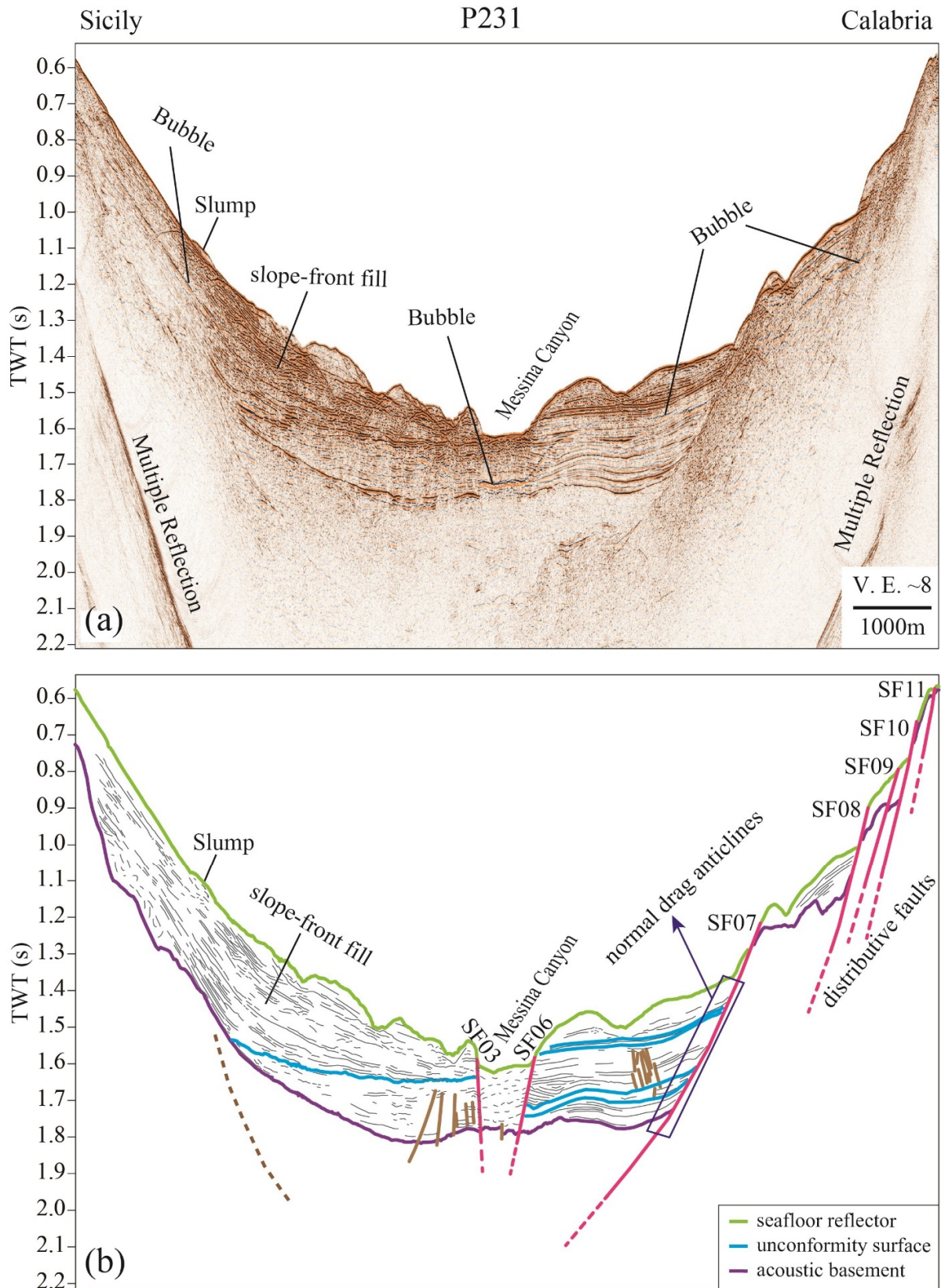


Figure MI- 6 (a) Seismic Profile P231 and (b) line drawing. Pink and black solid lines mark major surface faults and basement faults, respectively. Brown solid lines mark minor faults. Dashed lines show inferred continuations of faults. Vertical exaggeration is 8. See Fig. MI-2 and small inset map for location of profile.

In general, the sediment of the research area shows a complex architecture (Figs. MI-3, MI-4, MI-5, MI-6). The complexity of the sedimentary architecture increases from south to north in the inner Messina Strait.

The acoustic basement is imaged in relatively shallow sub-surface depth (Figs. MI-3, MI-4, MI-5, MI-6). The total thickness (in s TWT) of the overlying strata varies between 0 s TWT and 0.4 s TWT (corresponding to 0 – 320 m, assuming a sediment velocity of 1500 m/s). Some parts of the acoustic basement directly outcrop at the seafloor (Figs. MI-4, MI-5, MI-6). From north to south, the depth of the acoustic basement increases (Figs. MI-3, MI-4, MI-5, MI-6). The acoustic basement shows similar characteristics as the seafloor surface.

The sediments overlying the acoustic basement are heavily disturbed. Numerous faults are observed, which are described in the next chapter. Continuity of individual reflectors is poor. Several unconformities are observed on all profiles. The seismic facies of the southern inner Strait (the Strait area south of Briga and San Gregorio, Figs. MI-2, MI-5, MI-6) exhibits less disturbance than in the northern inner Strait (the Strait area north of Briga and San Gregorio, Figs. MI-2, MI-3, MI-4).

Furthermore, slope fills and a channel fills have been recognized on the Sicilian side and in the Messina Canyon (Figs. MI-3, MI-4, MI-5, MI-6), respectively. The slope fill may extend offshore along the entire coast of northeast Sicily (Figs. MI-2, MI-3, MI-4, MI-5, MI-6). Other sedimentary structures such as small slumps and contourites are widespread (Figs. MI-3, MI-4, MI-5, MI-6), but not described in detail, as this study focuses on the tectonics of the inner Messina Strait.

4.2.2 Distribution of faults in the inner Messina Strait

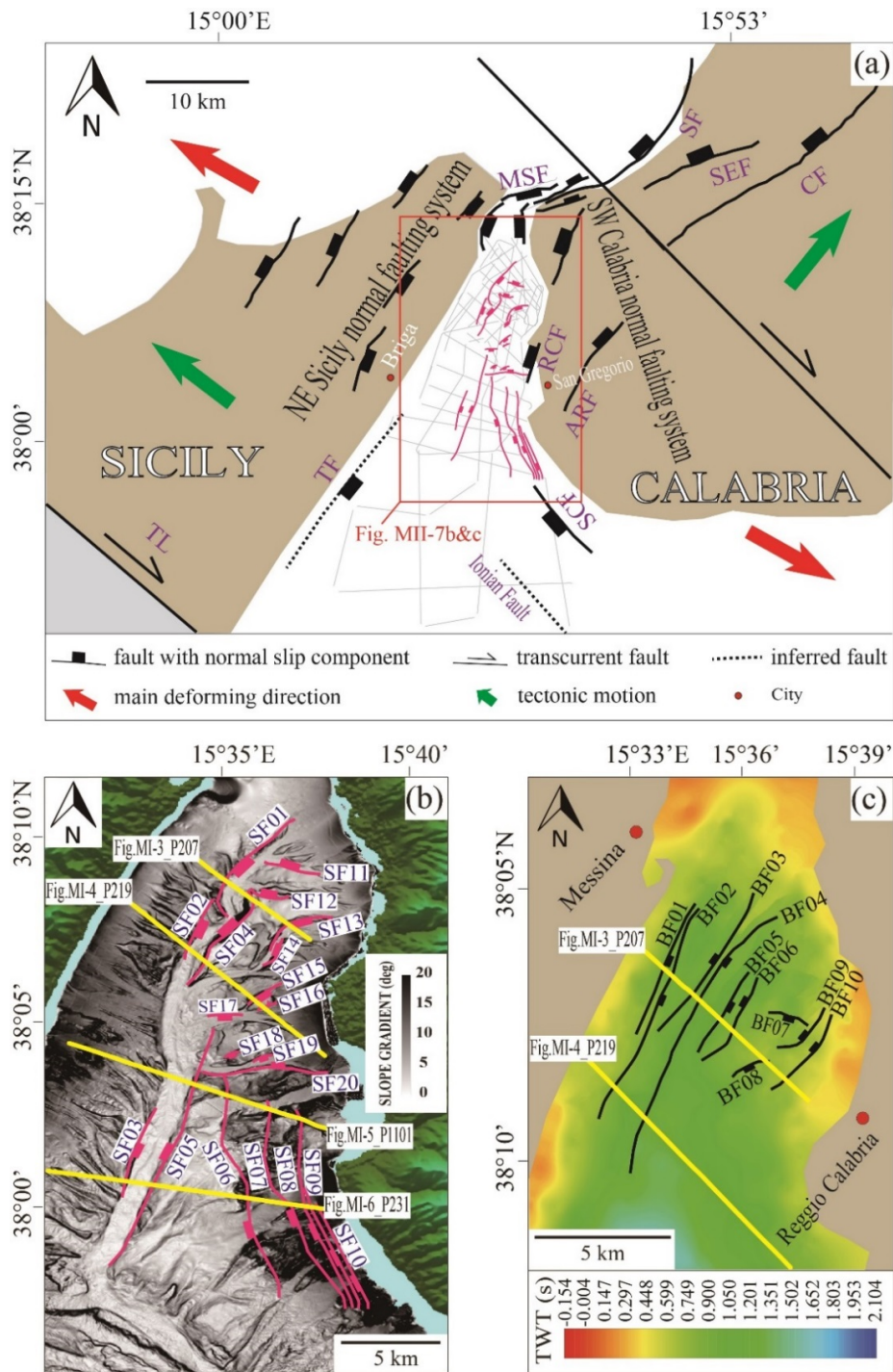


Figure MI- 7 (a) Newly-discovered near-surface faults (pink solid lines) in the tectonic framework of the inner Messina Strait. The location of faults previously described (in chapter 1.2.2) are shown in black: TL, Taormina Line; TF, Taormina Fault; RCF, Reggio Calabria Fault; ARF, Armo Fault; SF, Scilla Faults; SEF, S. Eufemia Fault; CF, Cittanova Fault; SCF, Southern Calabria Fault; MSF, Messina Straits Fault. Gray lines are seismic profiles. (b) Horizontal distributions of the newly-discovered near-surface faults (pink solid lines). (c) Horizontal distribution of the newly-discovered basement faults. See Fig. MI-2 for locations of maps shown on Fig. MI-7a and MI-7b.

Surface faults (SF01-20) can be traced across the entire Strait (Fig. MI-7b). Two general strike directions, N-S and E-W, can be identified. The N-S-trending faults are mainly located along the Messina Canyon (MC) (SF01-05) and in the southern inner Strait offshore Calabria (SF06-10), while the E-W-trending faults are situated in the northern inner Strait offshore Calabria (SF11-20). Basement faults (BF01-10) are clustered in the northern inner Strait. They mainly strike N-S (Fig. MI-7b). Table MI-1 summarizes the fault geometries of all major faults identified in the survey area.

Table MI- 1 Fault geometries in the inner Messina Strait. See locations in Fig. MI-7b. na, north azimuth; rhr, right hand rule; aada, average apparent dip angle; dd, dip direction; E. S. P., Equal-area stereo-graphic plots of the fault planes (strike, dip (rhr)).



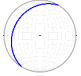
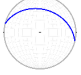
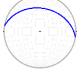

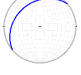
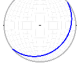
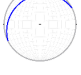

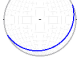

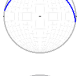
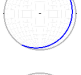
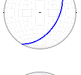



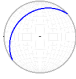



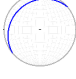

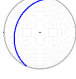
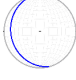
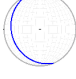
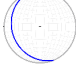
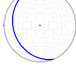
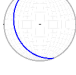
Fault name	Length (m)	Striking (°)(na) (rhr)	aada (°), dd (quad)	E. S. P.
northern inner Messina Strait				
SF01	6000	45	37 E	
SF02	3300	18	22 E	
SF04	5400	211	26 W	
SF11	2300	284	36 N	
SF12	1600	279	36 N	
SF13	3300	80	32 S	
SF14	1600	230	31 N	
SF15	1700	50	22 S	
SF16 (reverse fault)	900	243	21N	
SF17	1400	85	51 S	
SF18	700	65	17 S	
SF19	900	72	46 S	
SF20	2900	279	22 N	
BF01	4400	30	13 E	
BF02	7200	30	47 E	
BF03	4400	223	15 W	

Table MI-1 Continued

Fault name	Length (m)	Striking (°)(na) (rhr)	aada (°), dd (quad)	E. S. P.
BF04	9300	45	24 E	
BF05	3000	45	54 E	
BF06	3200	230	29 W	
BF07	1400	105	28 S	
BF08	1300	65	47 S	
BF09	2000	230	20 W	
BF10	3100	230	20 W	
nouthern inner Messina Strait				
SF03	4700	13	40 E	
SF05	12600	202	32 W	
SF06	12400	165	20 W	
SF07	11200	158	22 W	
SF08	10300	158	23 W	
SF09	6400	158	27 W	
SF10	5700	158	30 W	

In the northern inner Strait (Figs. MI-2, MI-7a), fourteen major surface faults (SF01, SF02, SF04 and SF11 to SF20) were identified (Fig. MI-7b; Table MI-1). SF01, SF02, and SF04 strike along the Messina Canyon in N-S direction and are characterized as channel boundary faults (Figs. MI-3b, MI-

4b, MI-7b). They dip toward the canyon at low to intermediate angles (Table MI-1). SF01 and SF04 are the longest faults in this northern inner Strait. Both can be traced for more than 5 km (Figs. MI-3b, MI-4b, MI-7b; Table MI-1) in the horizontal direction. Faults SF11-20 run offshore Calabria and reveal an E-W trend (Figs. MI-3b, MI-4b, MI-7b). These faults show the same strike direction as onshore mapped faults in southern Calabria. Most of them dip toward the south and host apparent dip angles of $\sim 30^\circ$ (Table MI-1). SF17 is the steepest fault (apparent dip angle $\approx 50^\circ$) in the inner Strait (Table MI-1). SF13 and SF14, as well as SF19 and SF20, exist in pairs as antithetic faults. Graben structure forms in-between the antithetic faults, with lengths of ~ 1 km, widths of ~ 500 m, and depths of ~ 50 m (Fig. MI-7b). SF16 is the only reverse fault in the research area (Fig. MI-7b).

Basement faults in the inner Messina Strait are only identified in the northern inner Strait (Fig. MI-7c). BF02, BF05, and BF08 reveal a higher dip angle (apparent dip angle $>45^\circ$) than the other basement faults (Figs. MI-3b, MI-4b, MI-7c; Table MI-1). Most of these faults dip toward the west. The most prominent basement fault is BF04 (Figs. MI-3b, MI-4b, MI-7c). It reveals the largest apparent displacement (~ 310 m) and its fault plane can be traced for ~ 9300 m (Table MI-1).

Two negative flower structures have been identified in the inner Messina Strait (Fig. MI-3b). The negative flower structure under the Messina Canyon (nfs_uMC) is mainly composed of SF01, SF04, BF05, and BF06 (Fig. MI-3b). SF01 and SF04 are two channel boundary faults (Fig. MI-3b). Their fault planes are slightly concave upwards with a dip decreasing with depth. Their hanging walls are thicker than the footwalls. A series of roll-over or reverse drag anticlines and normal drag anticlines appear in the hanging wall of SF01 and SF04, respectively. Particularly, SF01 and BF04 are so close to each other (Fig. MI-3b) that the lower fault plane of SF01 superimposes on the upper fault plane of BF04 in the central-northern segments of these two faults, where the structural high west of these two faults becomes lower and wider from north to south along its strike direction (Figs. MI-3b, MI-7b). SF02 and BF04 seems to be the same fault. The northern segment of BF04, however, has no surface expression, while its southern segment, SF02, crops out at the sea floor (Fig. MI-4b). The negative flower structure west of the Messina Canyon (nfs_wMC) is composed by BF01-03 (Fig. MI-3b).

In the southern inner Strait (Figs. MI-2, MI-7a), seven major surface faults (SF03 and SF05-10) were identified (Figs. MI-5b, MI-6b, MI-7a; Table MI-1). These faults strike N-S. SF03 and SF05 bound and dip toward the Messina Canyon at intermediate angles (Figs. MI-6b, MI-7b; Table MI-1). SF05 is the longest (~ 12.6 km) (Fig. MI-6b; Table MI-1) surface fault in the southern inner Strait. SF06-10 is a group of distributive/multiple/step faults, located on the slope offshore Calabria (Figs. MI-6b, MI-7b). They are arranged as stairs with subparallel westward dipping fault planes. The apparent dip angles

increase from SF06 to SF10 from 20 to 30 degree (Table MI-1; Figs. MI-5b, MI-6b). A series of normal drag anticlines appear in the hanging wall of SF06 (Fig. MI-6b).

Due to intensive erosion in the inner Messina Strait [*RIDENTE et al. 2014*], the tectonic contributions to the apparent displacements of these faults are difficult to judge. Therefore, no apparent displacements are analysed in this study.

5 Discussion

5.1 General seafloor morphology of the Messina Strait

5.1.1 *The formation of the canyons*

The bathymetric data show a feather-like submarine canyon system in the inner Messina Strait (Fig. MI-2). It incises the seafloor nearly along the axis of the entire inner Strait.

In general, a canyon may form (among others) due to steep slope gradients, faulting structures, mass failures, and turbidity currents. In the inner Messina Strait, the seafloor shows a slope gradient of $\sim 3^\circ$, which is steep enough for the generations of turbidity currents and mass failures. Turbidites have been identified in some cores in the Messina Strait [RYAN and HEEZEN 1965]. Frequent earthquakes in the Messina region are the most likely trigger for frequent turbidity currents. A large amount of sediments is transported to the Messina Strait by several streams and rivers onshore (Sicily and Calabria). Due to the absence of a shelf, canyons directly connect with onshore rivers in glacial and interglacial times. Hence, we expect the canyons to be active, i.e. sediment transport is ongoing through the canyons. This is supported by a single box corer taken during Cruise M86/2 in the axis of the Messina Canyon (MC), which contained major plastic pieces of waste products of civilization.

The seismic data suggest that the geomorphology of some canyons is controlled by normal faulting structures, e.g. MC is bounded by SF01-05; the canyon bounded by SF13-14 and the canyon between SF19 and SF20 (Fig. MI-7b) are located on the Calabrian side in the northern inner Strait. As these boundary faults are transtensional faults, these canyons can be judged as graben structures. These grabens may be preferred pathways for turbidity currents and prone for canyon erosion, as the boundary surface faults are potential zones of weakness. These faults could partly explain the recent locations of these canyons.

It is worth noting that the N-S-trending MC suddenly turns toward the southeast when it runs into the west Ionian Sea at the southern mouth of the inner Strait (Fig. MI-2). The seismic data, however, do not show any pronounced faulting structures close to this turn, which means that this sudden course change is not caused or coherent with major fault activity. We assume that MC might be forced to change its course by some joint canyons at the southern mouth of the inner Strait. These joint canyons

are located offshore northeast of Taormina (Fig. MI-2) and as wide as the MC. At their terminations, these canyons and the MC continue to extend southeastward as South Calabria Canyon (SCC) (Fig. MI-2).

5.1.2 Sedimentation in the Strait

In general, the thickness of the sediments on top of the acoustic basement in the inner Strait is thin (0 - 300 m) and decreases from the axis of the Strait toward the Calabrian and the Sicilian sides of the Strait. On one hand, strong tidal currents [BRANDT *et al.* 1997] and internal waves [ARTALE *et al.* 1990] have been observed in the inner Strait area. They may prevent sediment from depositing [CACCHIONE *et al.* 2002] on the slopes in the inner Strait. This may lead to insufficient sediment supply. On the other hand, turbidity currents [RYAN and HEEZEN 1965; SELLI *et al.* 1979] could contribute to the erosion of seafloor sediments. Deposition centres of these turbidity currents would be in the outer Messina Strait.

Along the Ionian coast off Sicily, a continuous, E-dipping slope-front-fill has been identified (Figs. MI-3, MI-4, MI-5, MI-6). The sediments of this slope-front-fill were probably brought from land by streams and rivers, which deposit their sediment freight along and perpendicular to the Ionian coast off Sicily (Fig. MI-2).

5.2 Characterization of tectonic features and their structural relevance to the tectonic framework of the Messina Strait

The negative flower structure has been identified in the inner Messina Strait (Fig. MI-3b), which may reflect that the inner Messina Strait is controlled by a transtensional regime. Faults in the Messina Strait are transtensional faults. The motions of these faults have both dip- and strike-slip components.

A transtensional regime fits well to the tectonic framework of the Messina Strait (Fig. MI-7a). It has been widely acknowledged that the Messina Strait is undergoing a relative uniform NW-SE extension [RIUSCETTI and SCHICK 1975; TORTORICI *et al.* 1995; MONTONE *et al.* 1997; D'AGOSTINO and SELVAGGI 2004; GOES *et al.* 2004; NERI *et al.* 2004; SERPELLONI *et al.* 2005; SERPELLONI *et al.* 2007; SERPELLONI *et al.* 2010]; the rates are ~3 mm/yr or ~65 nanostrains/yr [SERPELLONI *et al.* 2010]. This extension is controlled by an active stress regime: a minimum compressional stress (σ_3), horizontally trending ca.

N115°E, and a maximum compressional stress (σ_1), oriented subvertically [MONTONE *et al.* 2004; NERI *et al.* 2004]. This stress regime makes it possible to generate N-S- and E-W-trending transtensional faults. Subvertical σ_1 could contribute to the strike-slip components of the motions of these faults.

The relative motion between Sicily and Calabria may contribute to the formation and motion of these transtensional faults as well. GPS data [NERI *et al.* 2004; SERPELLONI *et al.* 2010] recorded that Sicily moves fast northward with respect to Calabria. Such motions may cause a regional right-lateral differential motion between Sicily and Calabria. Therefore, faults trending N-S are most likely right-lateral transtensional faults, while their E-W-striking conjugate faults may be left-lateral transtensional faults. Our data, however, do not allow distinguishing between right- and left-lateral fault displacements. These interpretations, however, are consistent with the fault models (Fig. A2 in appendix) proposed by D'AGOSTINO and SELVAGGI [2004] based on the GPS data.

In the southern inner Strait, a set of distributive/multiple/step faults are imaged offshore southern Calabria (Figs. MI-6b, MI-7a&b). We assume that the development of these faults may be a response to the extension and subsidence of the Strait area and the southeastward bending of the inner Calabrian Arc.

Since the 1908 Messina earthquake and tsunami, macroseismic, seismological, and geodetic data [BARATTA 1910; BOSCHI *et al.* 1989b] show that the Strait area close to the narrowest section of the Messina Strait (close to Messina, Fig. 1a) is beyond doubt the most suitable location for the causative fault of the 1908 Messina earthquake [BILLI *et al.* 2008]. Based on our new seismic data, several newly-discovered faults (Fig. MI-7) nicely fit to the suggested focal mechanisms of the 1908 Messina earthquake (Fig. 1a), but it is unlikely that one of them was really the master fault of this quake, as all faults are relatively small (<15 km). According to an empirical formula proposed by WELLS and COPPERSMITH [1994] ($M = 5.08 + 1.16 * \log(SRL)$). With M, moment magnitude; SRL, surface rupture length), the surface rupture length of the seismogenic fault should be at least 40 km for generating an earthquake of 7 Mw similar to the 1908 Messina earthquake. Therefore, our newly-discovered faults are too small to generate such a large earthquake.

5.3 The graben structure of the Messina Strait

When comprehensively considering our new data and previous models, we support the hypothesis that the inner Messina Strait is an angular graben [*MULARGIA et al. 1984a*].

The inner Messina Strait gradually broadens toward the south, showing a fan or triangular shape (Figs. MI-1a, MI-2, MI-7). The Messina Strait graben is bounded by two antithetic normal faulting systems: the northeastern Sicily normal faulting system and the southwestern Calabria normal faulting system (Fig. MI-7a). Both of the fault systems strike NE-SW and dip toward the Strait area [*SELLI et al. 1979*; *GHISETTI 1992a*; *TORTORICI et al. 1995*; *BOTTARI et al. 2005*]. This jigsaw-like boundary faulting systems give way to a downdropped graben-like basin. In the Strait, the newly-discovered N-S-trending near-surface faults contribute to the development of the master graben and form some secondary grabens, such as Messina Canyon (Figs. MI-3, MI-4, MI-5, MI-6, MI-7b).

According to the tectonic evolution of the central-western Mediterranean Sea [*GOES et al. 2004*], the Messina Strait was already opened before the inner Calabrian Arc (CA) docked at its present location (Fig. A1 in appendix). Therefore, it is difficult to infer how and when the Messina Strait originally formed. Nevertheless, the graben structure proves that the Messina Strait have experienced NW-SE extension (Chapter 4 2, Fig. MI-7a).

The angular shape of the Messina Strait graben is probably caused by the bending of the inner CA (Fig. MI-1a). The central part of the inner CA bends to the southeast with respect to its other part (Fig. MI-1a). Along this concave belt, a series of “horst and graben” structures have been recognized. All grabens are angular grabens [*MULARGIA et al. 1984a*]; the Messina Strait is largest one of them (Fig. MI-1a). This horst-graben structures may be an upper crustal response to a regime of different vertical movements between the uplifting thrust chain and the stretching Tyrrhenian Sea [*GHISETTI 1984b*] and to the extensional deformations both parallel and perpendicular to the inner CA [*SELVAGGI 1998*; *FREPOLI and AMATO 2000*].

5.4 The Taormina Fault

As previously mentioned, the Taormina Fault (TF) has not been directly documented so far [*ARGNANI et al. 2009a*]. The TF could not be identified on our new seismic data as well (Figs. MI-3, MI-4, MI-5,

MI-6), though we collected several profiles across or near the proposed area for the TF. There may be three possibilities: i) The TF does not exist; ii) The TF is buried too deep to be imaged by our new high-resolution seismic data; iii) The TF is mainly located in the data gap area between our new seismic profiles and the onshore Ionian coastal areas of Sicily.

We cannot exclude possibility ii but we consider it as unlikely that an active fault does not show any expression in the depth range of our seismic data. As for the third postulation, several faults have already been discovered onshore along the Ionian coastal area of Sicily (Figs. MI-1a, MI-7a), which implies that the data gap is as small as the distance between the coastline and our new data. If the dip angle of the TF is very high, it may be impossible to identify the TF on our new seismic data; the TF may be located in the data gap area between the seismic profiles and the Ionian coastline of Sicily. However, we consider it as unlikely that a fault is exactly located in the small data gap between the coastline and our profiles, as this gap is only ~2 km wide. Hence, we prefer the interpretation that the TF does not exist.

6 Conclusions

We constructed the fault pattern of the inner Messina Strait based on a dense net of new high-resolution 2D reflection seismic data. Our new data supports the hypothesis that the inner Messina Strait is an angular graben structure, which may have been shaped by the bending of the inner Calabrian Arc and the extension across the Messina Strait. In this graben, surface faults mainly strike N-S and W-E. N-S-trending faults distribute along the Messina Canyon and the coastline off southern Calabria, respectively. These faults dip toward the Messina Canyon at apparent dip angles of 20 to 40 degree. E-W-trending faults are situated in the northern inner Messina Strait off Calabria. The apparent dip angles of them vary between 20 and 50 degrees. Most of them dip toward the south. The appearance of the negative flower structure indicates that the newly-discovered surface faults are transtensional faults. We interpret the N-S- and the E-W- trending surface faults as right- and left- lateral transtensional faults, respectively.

The fault pattern of the inner Messina Strait fits well to the active stress field: a ca. N115°E horizontal trending minimum compressional stress (σ_3) and a subvertical maximum compressional stress (σ_1), which controls the Messina Strait area. The fault pattern also fits to the subsidence of the Strait area, the tectonic motions of Sicily and Calabria with respect to Eurasian plate, and the relative motion between Sicily and Calabria.

Despite the fact that several newly-discovered surface faults fit well to the suggested focal mechanisms of the 1908 Messina earthquake, we were not able to identify the master fault of this event. The lengths of the fault planes (< 15 km) are too small to generate an earthquake of 7 Mw. However, it may well be that the faults are only surface expressions of deeper and longer faults, which were not imaged due to the limited penetration of our new seismic data.

The inferred Taormina Fault (TF) was considered as one of the most hazardous and largest seismic gaps in Italy. However, this fault has not been imaged on any exist seismic data set, even not in our new seismic data. We consider it as unlikely that an active fault does not show any expression in the depth range of our seismic data and that a fault is exactly located in a ~2 km gap between the coastline and our profile. Hence, we doubt the existence of the TF.

5 MANUSCRIPT II

An active transtensional fault zone between two STEP faults in the outer Messina Strait, Southern Italy

Lili Fu¹, Sebastian Krastel¹, Felix Gross¹, Irena Schulten^{1, 2}, Jörg Bialas³, Francesco Chiocci⁴, Domenico Ridente⁵

¹Institute of Geosciences, University of Kiel, Kiel 24118, Germany

²Now at department of Oceanography, Dalhousie University, 1355 Oxford Street, Halifax, Nova Scotia, Canada B3H 4R2

³GEOMAR Helmholtz Centre for Ocean Research Kiel, Kiel 24148, Germany

⁴Department of Earth Sciences, Sapienza University of Rome, Rome 00185, Italy

⁵National Research Council, Roma, Italy

Abstract

New seismic data collected across a dominant scarp-like structure (DSS) in the outer Messina Strait led to the discovery of a prominent fault zone, which we named the Fiumefreddo - Melito di Porto Salvo Fault Zone (F-MPS_FZ). In this manuscript, we present a detailed analysis of this newly-discovered fault zone. It is located in the source area proposed for the 1908 Messina tsunami. The F-MPS_FZ is an E-W-trending left-lateral transtensional fault zone, which shows ongoing tectonic activity and supports a transtensional regime in the outer Messina Strait. Most of the faults in this zone dip toward the south at apparent dip angles around 60 degrees. The dominant scarp-like structure (DSS) represents the surface expression of the master fault of the F-MPS_FZ. The F-MPS_FZ may be a STEP-Connector Fault, linking the two postulated Subduction-Transform Edge Propagator (STEP) faults: the Ionian Fault and the Alfeo-Etna Fault. This STEP-Connector Fault may have formed in two ways: in a pull-apart basin style or in a fault-termination basin style. Based on our data, we prefer the pull-apart basin style model for this new fault zone.

1 Introduction

The 1908 Messina earthquake and tsunami was the deadliest event in Europe since then, causing 80,000 to 100,000 casualties. Since the tsunami was assumed to have been triggered by the earthquake, several numerical models were built up based on available field data (e.g., seismological data and tsunami run-up heights), but none of them could explain both the earthquake and the tsunami [*TINTI et al. 1999b*; *GERARDI et al. 2008*].

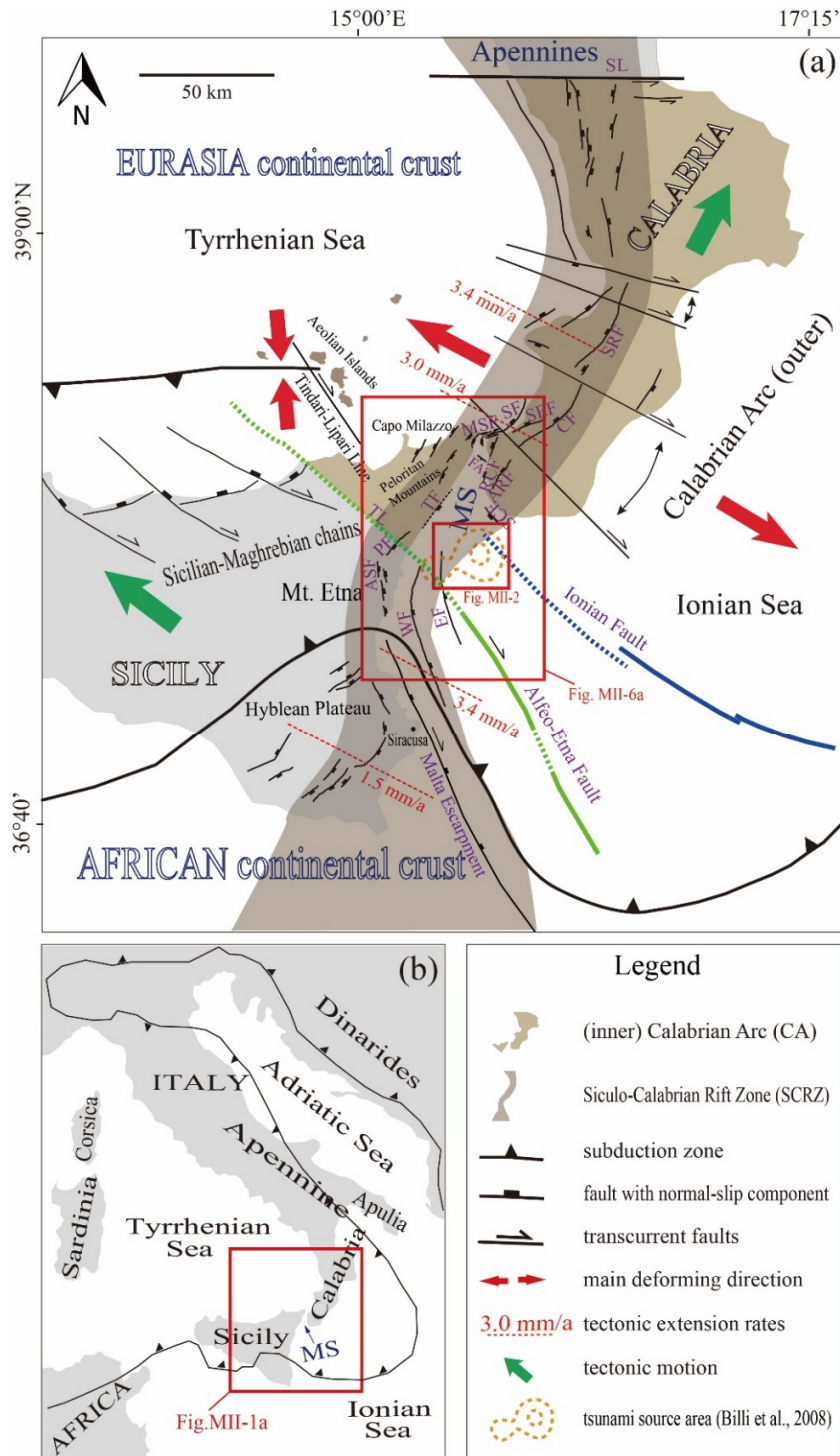


Figure MII- 1 (a) Overall tectonic framework of Southern Italy. Modified from *GOVERS and WORTEL [2005]; ARGNANI and BONAZZI [2005]; GUARNIERI [2006]; CATALANO et al. [2008]; ARGNANI et al. [2009a]; POLONIA et al. [2011b]; POLONIA et al. [2014]; VITI et al. [2011b]; DOGLIONI et al. [2012]; GALLAIS et al. [2013]*. The green and blue lines show the location of Subduction-Transform Edge Propagator (STEP) faults. Dashed lines are inferred fault locations. MS, Messina Strait. SL, Sangineto line; TL, Taormina Line. RIF, Rosolini–Ispica faults; AF, Avola fault; WF, Western Ionian Fault; EF, Eastern Ionian Fault; ASF, Acireale–S. Alfio faults; PF, Piedimonte fault; TF, Taormina fault; RCF, Reggio Calabria fault; ARF, Armo fault; SF, Scilla faults; SEF, S. Eufemia fault; CF, Cittanova fault; SRF, Serre fault; VF, Vibo fault; CVF, Capo Vaticano fault; SCF, Southern Calabria fault; FA, fault identified by *ARGNANI et al. [2009a]*; MSF, Messina Straits fault. (b) General map of central Mediterranean Sea.

Hence, *BILLI et al. [2008]* postulated that the 1908 Messina tsunami might be caused by a submarine landslide. The most likely source area is in the outer Messina Strait offshore southwest of the southwestern tip of Calabria and east of Giardini Naxos city (Sicily) (see suggested tsunami source area (orange dashed lines) in Fig. MII-1a). A landslide in this region, however, was strongly doubted by several authors, because new high-resolution seismic and bathymetric data did not image a young landslide in this area [*ARGNANI et al. 2009b; GROSS et al. 2014*]. Instead, an almost 15 km-long dominant scarp-like structure (DSS) of unknown origin was imaged by bathymetric data. This feature is just located in the source area proposed by *BILLI et al. [2008]* (Fig. MII-1a) and between two postulated Subduction-Transform Edge Propagator (STEP) faults: the Ionian Fault and the Alfeo-Etna Fault (Fig. MII-1a). Hence, we collected a dense grid of seismic lines mainly across the DSS. The main objectives of this manuscript are to i) characterize the internal architecture of the DSS and its surroundings and ii) to analyse the relationship between the DSS and the regional tectonic framework of the outer Messina Strait.

2 Tectonic settings

2.1 The inner Calabrian Arc and the Siculo-Calabrian Rift Zone

The Messina Strait crosscuts the southern part of the inner Calabrian Arc (CA) and is situated in the Siculo-Calabrian Rift Zone (SCRZ) (Fig. MII-1a).

The inner CA (Fig. MII-1a) connects the Apennines with the Sicilian-Maghrebian chains. It developed during the Neogene-Quaternary Africa-Europe collision, when the African Plate subducted northwestward beneath the Eurasian Plate [BARBERI *et al.* 1973; MALINVERNO and RYAN 1986; BOCCALETTI *et al.* 1990; PATACCA *et al.* 1990; DEMETS *et al.* 2010]. Since the Pliocene, the inner CA was dominated by extension, both longitudinal and transversal, causing the development of structural highs and marine sedimentary basins [GHISETTI and VEZZANI 1982]. Due to the roll-back of the subducting Ionian slab and the corresponding back-arc extension of the Tyrrhenian Basin, the CA moved (5 - 6 cm/yr) toward the east or southeast [MALINVERNO and RYAN 1986; GUEGUEN *et al.* 1998; FACCENNA *et al.* 2004]. During the Middle-Late Pleistocene, a tectonic reorganization [FACCENNA *et al.* 2001] slowed down (1 - 2 cm/yr) the slab roll-back.

The SCRZ (Fig. MII-1a) is a ~370 km long, N-S trending normal fault zone. It runs along the inner side of the inner CA, through the Messina Strait, and along the Ionian coast of Sicily [TORTORICI *et al.* 1995; MONACO and TORTORICI 2000b; CATALANO *et al.* 2008] (Fig. MII-1b). A variety of data suggest a ~N115°E extension for the SCRZ (Fig. MII-1a), with rates of 3.6 ± 0.6 mm/yr [D'AGOSTINO and SELVAGGI 2004; CATALANO *et al.* 2008]. This extension is still ongoing, and normal faults developed in southern Calabria and northeastern Sicily are in response to this extension [BIANCA *et al.* 1999; MONACO and TORTORICI 2000b]. The extension may be caused by one or more of the following tectonic motions: (1) the back-arc stretching in the Tyrrhenian Sea; (2) the counter clockwise rotation of the Adriatic microplate which has generated an intensive stress field at its western margin [D'AGOSTINO and SELVAGGI 2004; D'AGOSTINO *et al.* 2008]; (3) the Hellenic slab dragging eastward the entire Ionian-Calabrian domain [GOES *et al.* 2004].

2.2 The STEP faults

Continual tearing of the lithosphere occurs near most of the horizontal terminations of subduction trenches. This tearing transform fragment is called “Subduction-Transform Edge Propagator (STEP)” fault [GOVERS and WORTEL 2005]. Two main STEP faults, the Ionian Fault [POLONIA *et al.* 2014] and the Alfeo-Etna Fault [GALLAIS *et al.* 2013; POLONIA *et al.* 2014], have been inferred in the outer Messina Strait (Fig. MII-1a).

2.2.1 The Alfeo-Etna Fault

The Alfeo-Etna Fault (Fig. MII-1a) is located at the southwest edge of the Ionian Basin, ~50 km east of the Malta Escarpment (ME) [GALLAIS *et al.* 2013] (Fig. MII-1a). It is a ~N150° trending fault, cutting more than 200 km into the Ionian Basin [GALLAIS *et al.* 2013]. The southernmost termination of this fault cannot be traced further south than latitude 36.4°N [GALLAIS *et al.* 2013]. Its vertical throw decreases toward the south [GALLAIS *et al.* 2013]. A set of data obtained from geodetic, tomographic, geochemical, structural, and seismic studies support that the vertical movement observed along this fault is the surface expression of a STEP fault [GALLAIS *et al.* 2013].

The Alfeo-Etna Fault accompanies (a) the advance of the inner CA toward the southeast and (b) the southeastward roll-back of the Ionian slab [GALLAIS *et al.* 2013] (Fig. MII-1a) with (1) crustal dextral strike-slip movement in northeast Sicily between Hyblean Plateau and the Peloritani–Calabria block, as confirmed by earthquake focal mechanisms [GALLAIS *et al.* 2013] and (2) lithospheric vertical movement beneath western Ionian Sea, which propagates upward through a ~N150° trending crustal scale fault [GALLAIS *et al.* 2013], respectively. GALLAIS *et al.* [2013] further suggest that the Alfeo-Etna Fault propagates in the Ionian Basin during the late Neogene through the inherited Continent–Ocean Boundary which was acquired during the formation of the Mesozoic passive margin of the basin.

ARGNANI [2014] pointed out that the Tindari-Lipari and/or Taormina lines (Fig. MII-1a) may represent possible extending of the Alfeo-Etna Fault into the Tyrrhenian Sea. Although quite popular in the literature [GALLAIS *et al.* 2013], none of these faults has a clear surface expression. No convincing data, supporting active structures along the trend of the Tindari-Lipari and the Taormina lines, have been presented onshore and are lacking offshore. Instead, active deformation in this sector appears to be located between Capo Milazzo and the central Aeolian Islands [ARGNANI *et al.* 2007] (Fig. MII-1a).

2.2.2 The Ionian Fault

The Ionian Fault is located ~70 km east of the toe of the Malta Escarpment (ME) [POLONIA *et al.* 2011b; POLONIA *et al.* 2014] (Fig. MII-1a). It strikes MW-SE and connects the plate boundary of northern Sicily to the subduction thrust of the Ionian Sea.

The Ionian Fault is a major lithospheric structure with a shallow expression of a STEP fault [POLONIA *et al.* 2011b]. It segments the Calabrian accretionary wedge and accommodates different rates of the slab roll-back [POLONIA *et al.* 2011b]. This differential motion may result in substantial deformation, rotation, and the formation of sedimentary basins [POLONIA *et al.* 2011b]. According to ARGNANI [2014], the Ionian Fault is a right-lateral transtensional fault, younger than the Alfeo-Etna Fault, and therefore very recent. Its present activity is documented by sedimentary basins and seafloor displacements imaged by shallow subsurface CHIRP data [POLONIA *et al.* 2011b].

The Ionian Fault plays an important role in controlling subduction processes and margin segmentation, and may represent a seismogenic feature likely to have generated major earthquakes in the past, such as the 1908 Messina earthquake and 1963 Catania earthquake [POLONIA *et al.* 2011b].

The structural features observed by ARGNANI and BONAZZI [2005] support the occurrence of a lithospheric tear between the Ionian Basin and the Hyblean Plateau [POLONIA *et al.* 2011b]. ARGNANI [2014], however, pointed out that the structures in the two areas separated by the southern segment of the Ionian Fault, are post Messinian but likely much older than Quaternary. This casts some doubt on the occurrence of two STEP faults (the Ionian Fault and the Alfeo-Etna Fault) cutting through the Ionian lithosphere, also considering that the Ionian Fault has not been completely documented.

3 Data and Method

From December 27th, 2011 to January 17th, 2012, a new dataset was collected during RV Meteor Cruise M86/2 off Southern Italy, by means of a bathymetric multi-beam echo sounder, a parametric sediment echo sounder, and a high-resolution 2D reflection seismic system. Additional high-resolution bathymetric data collected in the frame of the MAGIC project (Marine Geohazards along the Italian Coasts, *CHIOCCI and RIDENTE [2011]*) were assessed for this study as well.

A Kongsberg-Simrad EM122 deep-water bathymetric multi-beam echo sounder was used to acquire new bathymetric data. Bathymetric data were processed with Multi-Beam System[®] (version 5.2) and displayed by Generic Mapping Tool[®] (version 4.9) and Global Mapper (version 12).

A parametric Atlas PARASOUND P70 system was used for collecting sediment echo sounder data. The system was operated with 4 kHz. Kingdom Suite[®] (version 8.6) was used to display and interpret the data.

High-resolution 2D reflection seismic data were collected using a 162.5 m-long, 104-channel digital Geometrics GeoEel streamer. The seismic signal was generated using a 1.7 l GI gun, operated in harmonic mode and a shot interval of 4 s. Sub-bottom penetration was up to 1 s TWT (Two-Way-Travel-Time). The processing steps include geometry setup, binning, band-pass filtering (10/20/600/1000 Hz, assumed for low truncation frequency, low cut frequency, high cut frequency, and high truncation frequency, respectively), Normal Move-Out (NMO) corrections, despiking, stacking and time-migration. The lateral bin size was set to 2 m, which results in an average fold of 14. Due to the relative short length of streamer system, no velocity analysis was carried out; a constant sound velocity of 1500 m/s was applied during NMO corrections and data migration. Gedco Vista Seismic Processing[®] (Schlumberger, version 11) and IHS Kingdom Suite[®] (version 8.6) were used for processing and interpretation.

Fault interpretations were based on the following criteria: i) abrupt offset of steeply dipping strata reflections; ii) tracking of fault plane reflections; iii) sudden vertical changes of the number and shape of the reflectors. Identified surface faults (fault planes intersect with the seafloor) were divided into major faults and minor faults. Major faults are those that could be traced on at least two parallel or subparallel profiles, while those usually only recognized on one single profile are minor faults. Major surface faults have been marked as 'SFxx'.

4 Results

4.1 Seafloor morphology

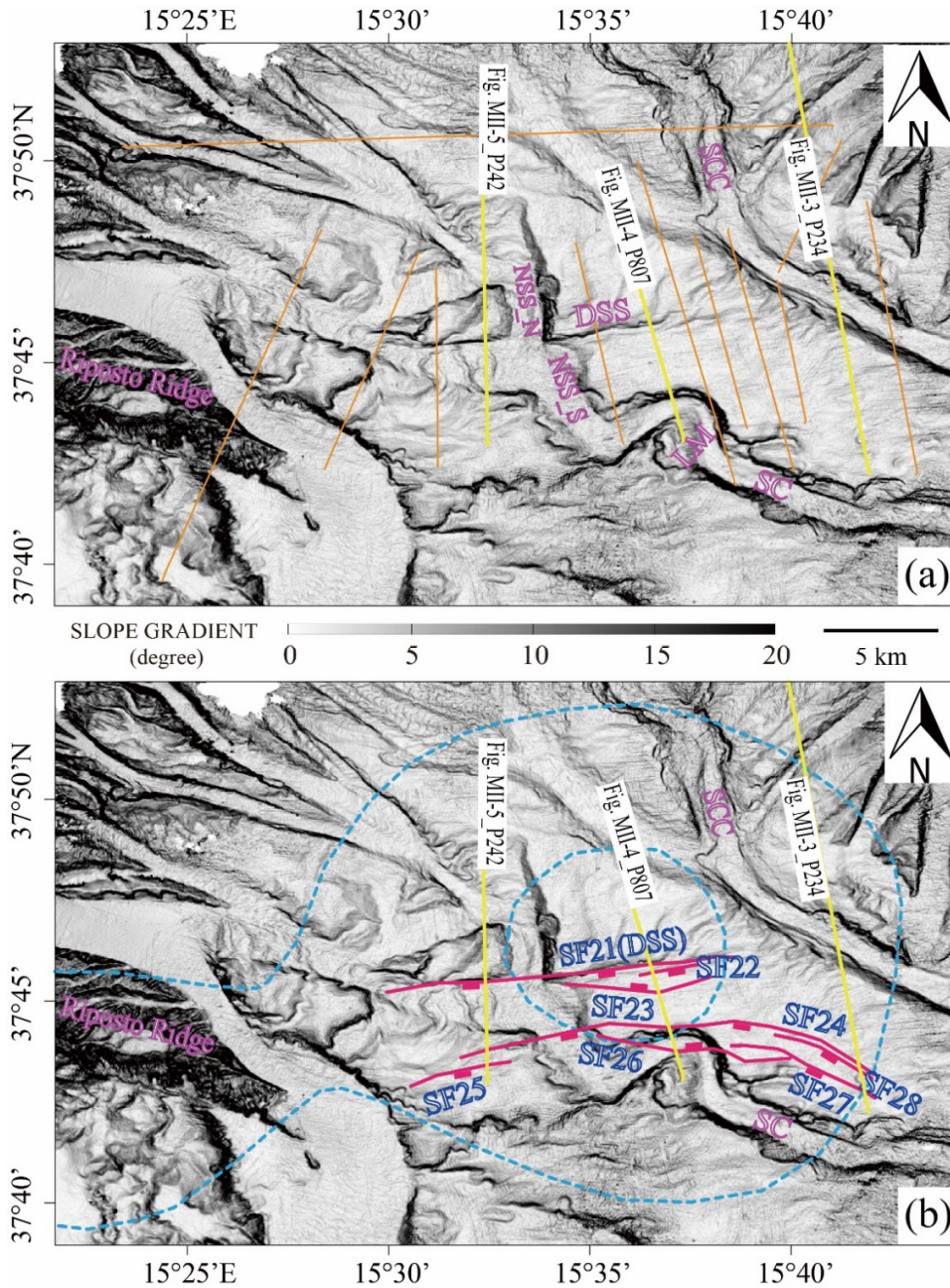


Figure MII- 2 (a) Bathymetry of the outer Messina Strait with 2D seismic profiles. Location of map is shown on Fig. MII-1. DSS, dominant scarp-like structure; NSS_N, northern N-S trending scarp-like structure; NSS_S, southern N-S trending scarp-like structure; SCC, South Calabria Canyon [RIDENTE *et al.* 2014]; SC, South Canyon; LM: large meander. Orange and yellow solid lines are 2D seismic survey lines. (b) Fault pattern of the outer Messina Strait reconstructed based on the selected seismic profiles. The DSS is the surface expression of fault SF21. Light blue dashed curves circle out the source area proposed by BILLI *et al.* [2008] for the 1908 Messina tsunami. See text for details.

The most remarkable features observable at the seafloor in the outer Messina Strait are canyons, which are incised up to 160 m into their surrounding material (Fig. MII-2a). The South Calabria Canyon (SCC) [RIDENTE *et al.* 2014] (Depth:Width \approx 90m:1950m), and the canyon which we refer to as South Canyon (SC) (Depth:Width \approx 90m:1700m) are two major canyons in this area. Both extend toward the southeast.

Another most eye-catching feature is a scarp-like structure which we named as dominant scarp-like structure (DSS) (Fig. MII-2a). It is located in the centre of the outer Messina Strait, corresponding to the source area proposed by BILLI *et al.* [2008] for the 1908 Messina tsunami. The DSS strikes E-W, terminating to the east at the SCC and cutting across the SC with its western segment. The DSS is \sim 13 km long and on average \sim 60 m height. An N-S trending scarp-like structure (NSS) runs across the DSS. This NSS is cut into two segments, NSS_N and NSS_S. The NSS_N is located further west with respect to the NSS_S.

4.2 Fault pattern in the outer Messina Strait

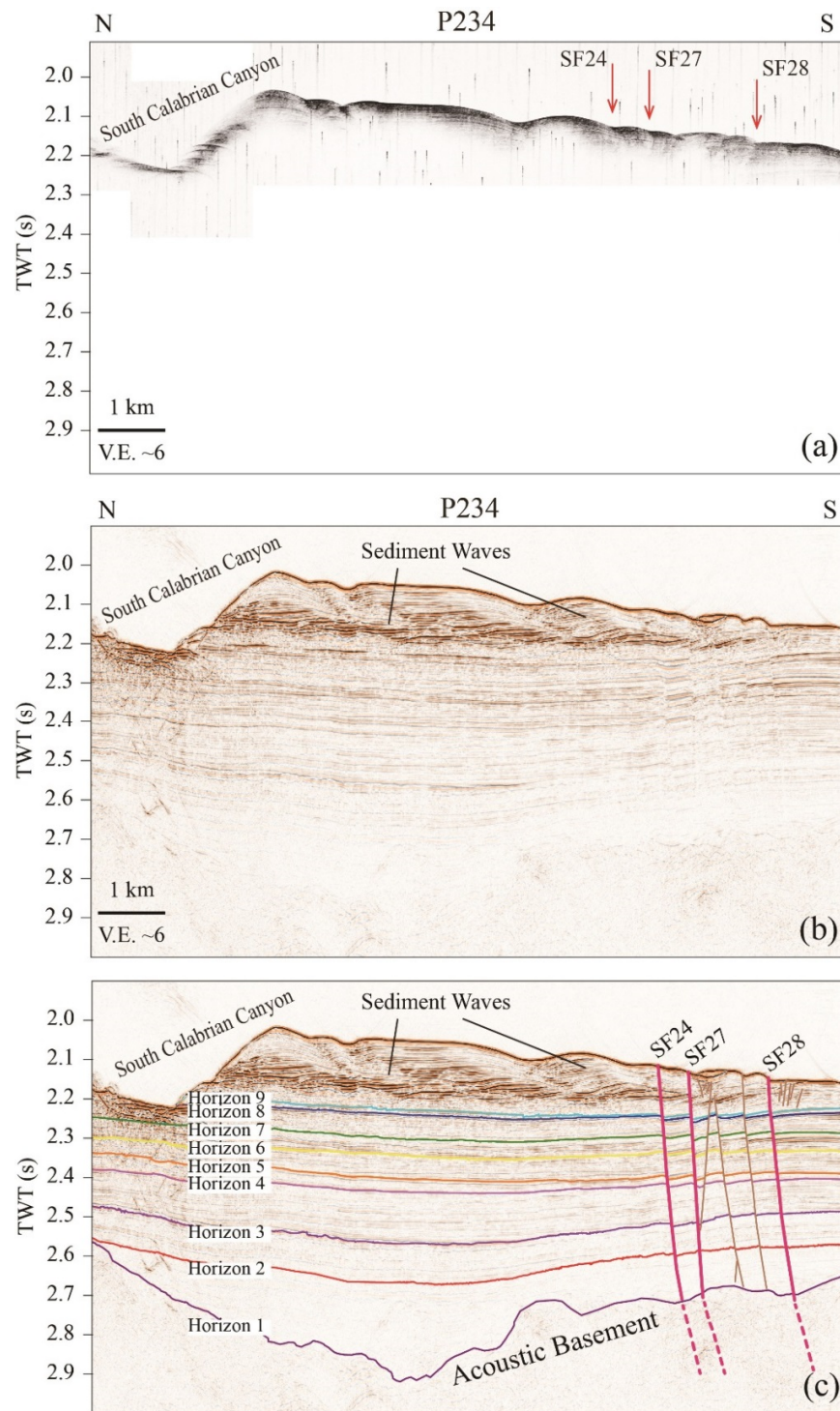


Figure MII-3 (a) Sediment echo sounder data interpretation of profile P234. Red arrows indicate the surface expressions of major faults. Vertical exaggeration is 6. (b) Uninterpreted and (c) interpreted seismic sections of P234. Faults in pink are major surface faults. Faults in brown are minor surface faults. The dashed lines show the uncertain lower parts of the major surface faults. Colored solid lines show the picked horizons. TWT, Two-Way-Travel-Time. Vertical exaggeration is 6. See Fig. MII-2 for location of profile.

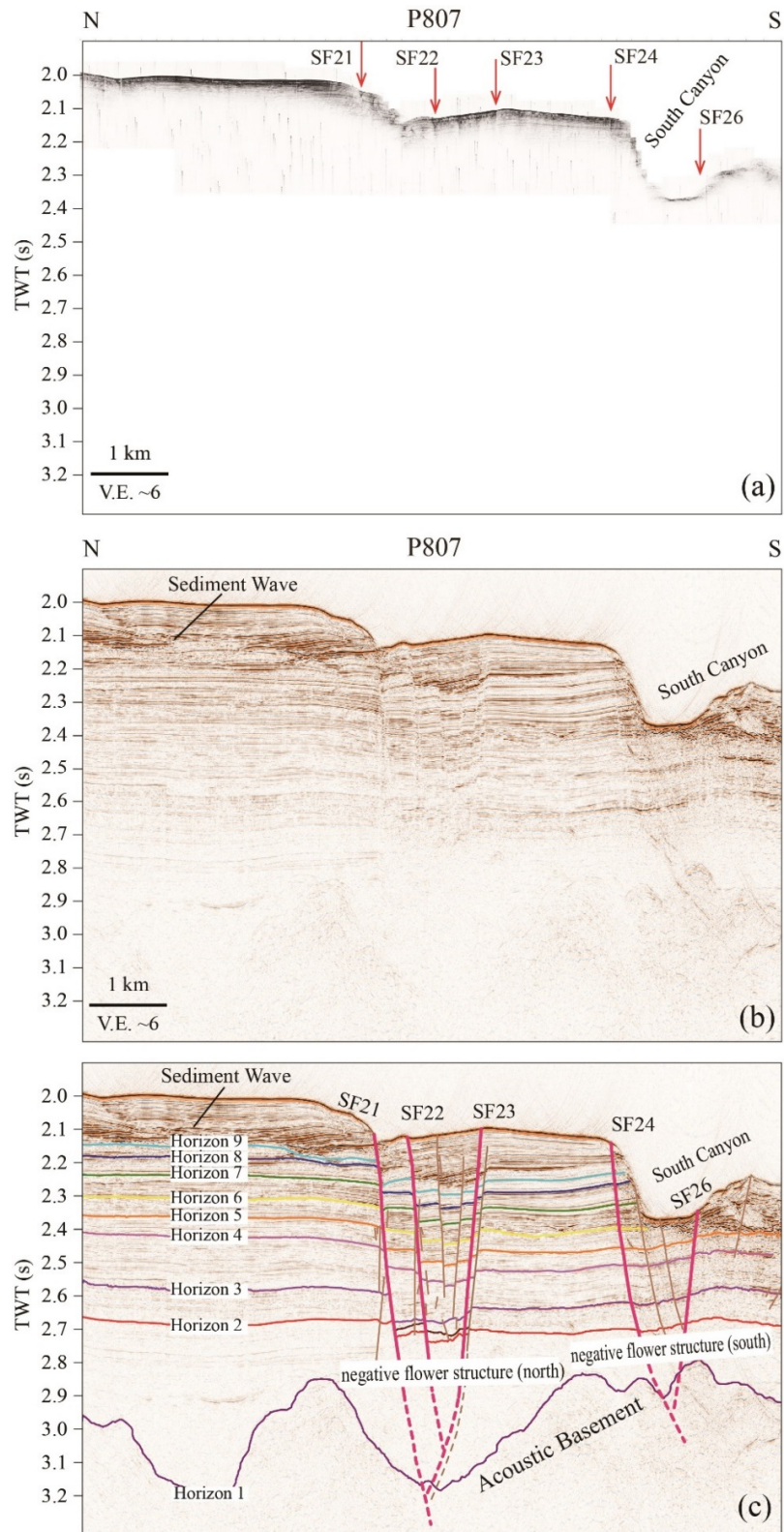


Figure MII- 4 (a) Sediment echo sounder data interpretation of profile P807. Red arrows indicate the surface expressions of major faults. Vertical exaggeration is 6. (b) Uninterpreted and (c) interpreted seismic sections of P807. Faults in pink are major surface faults. Faults in brown are minor surface faults. The dashed lines show the uncertain lower parts of the major surface faults. Colored solid lines show the picked horizons. TWT, Two-Way-Travel-Time. Vertical exaggeration is 6. See Fig. MII-2 for location of profile.

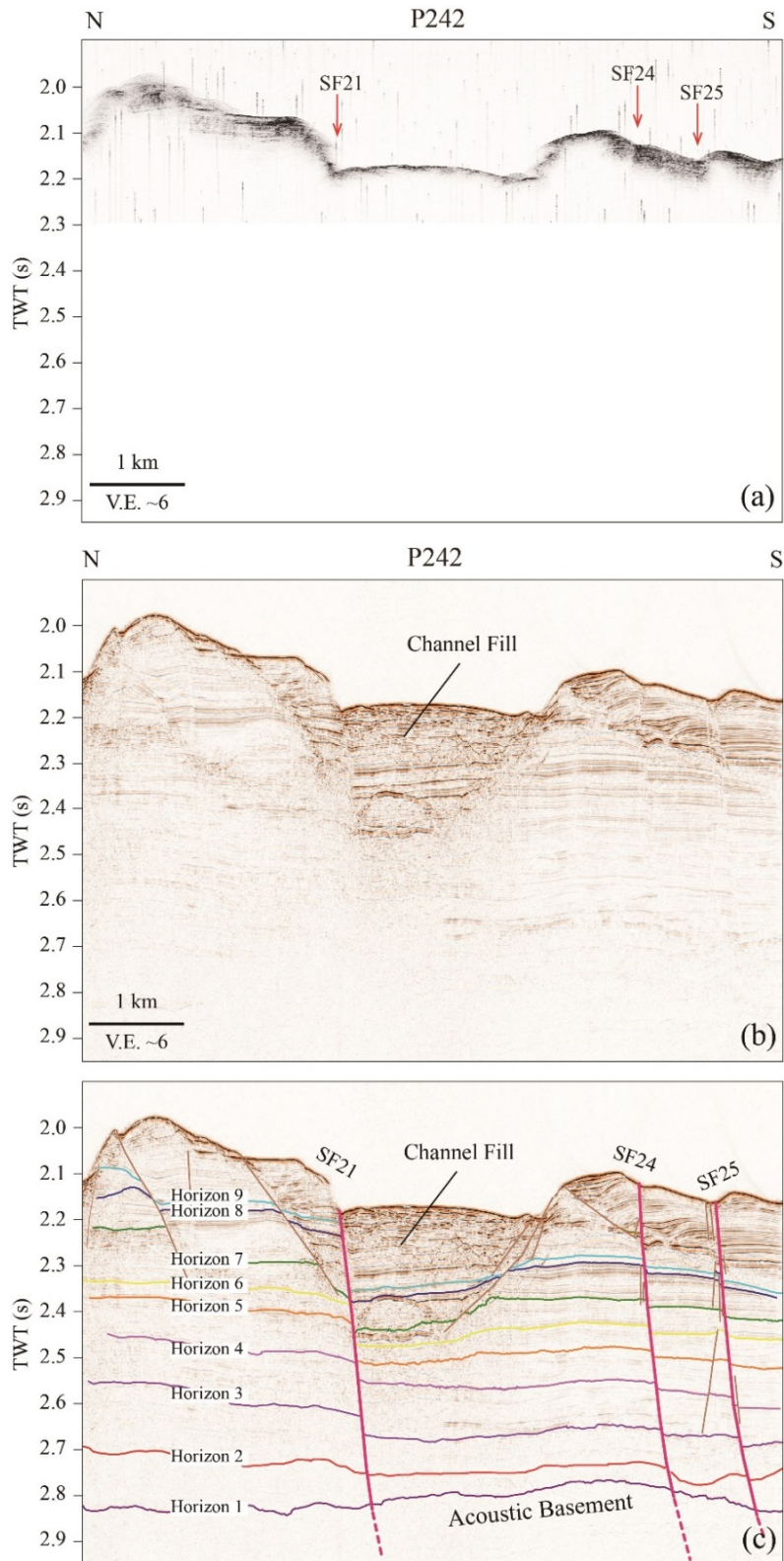


Figure MII- 5 (a) Sediment echo sounder data interpretation of profile P242. Red arrows indicate the surface expressions of major faults. Vertical exaggeration is 6. (b) Uninterpreted and (c) interpreted seismic sections of P242. Faults in pink are major surface faults. Faults in brown are minor surface faults. The dashed lines show the uncertain lower parts of the major surface faults. Colored solid lines show the picked horizons. TWT, Two-Way-Travel-Time. Vertical exaggeration is 6. See Fig. MII-2 for location of profile.

Seismic profiles P234, P807 and P242 were selected as representative sections in the working area (Figs. MII-3, MII-4, MII-5). In general, the subsurface of the outer Messina Strait shows well stratified sedimentary formations (Horizon 2 to Horizon 9) above the acoustic basement (Horizon 1) (Figs. MII-3, MII-4, MII-5). The average thickness of the sediment above the acoustic basement is ~ 0.6 s TWT (~ 450 m). A series of sediment waves is imaged between seafloor and Horizon 9. These sediment waves only appear in the northeastern part of the outer Messina Strait (Figs. MII-2, MII-3b&c, MII-4b&c).

All profiles (Figs. MII-3, MII-4, MII-5) show several major surface faults, which can be traced between the profiles (the distance between the profiles is about 1 to 5 km). In addition, abundant minor faults are imaged on the profiles as well. Profile P234 (Fig. MII-3) is located east of the DSS (Fig. MII-2), while profiles P807 (Fig. MII-4) and P242 (Fig. MII-5) cross the DSS (Fig. MII-2). As Fig. MII-4 and MII-5 show, the DSS is the surface expression of a fault (SF21).

Table MII- 1 Fault geometries in the outer Messina Strait.

Fault Name		SF21	SF22	SF23	SF24	SF25	SF26	SF27	SF28
Length (m)		13200	2100	5500	16000	3800	7300	5900	4300
¹ ADA (°)	² SP P234				60				70
	P810				54				66
	P238				67		58	61	
	P809	58		52	69		60	58	64
	P240	53	58	63	51		62	49	
	P807	59	61	64	47		57	41	
	P805	73		63	55		57		
	P242	59			58	55			
	P803	47				56			
	Average		58	60	61	58	56	59	52
		S	S	N	S	S	N	S	S
³ SD (°)		83	80	252	90	80	285	125	125
E. S. P.									

¹ADA, Apparent Dip Angle;

²SP, Seismic Profile;

³SD, Strike Direction (North Azimuth);

⁴E. S. P., Equal-area stereo-graphic plots of the fault planes (strike, dip (rhr)).

In total, we identified eight major surface faults, SF21-28 (Figs. MII-2, MII-3, MII-4, MII-5). They are located east of Riposto Ridge, southwest of the SCC, and in the source area proposed by *BILLI et al. [2008]* for the 1908 Messina tsunami (Fig. MII-2). These newly-discovered faults in fact form a fault zone which we refer to as Fiumefreddo - Melito di Porto Salvo Fault Zone (F-MPS_FZ).

The F-MPS_FZ is made out of two major sets of faults. SF21-23 builds the first set which is in the core part of area. The surface expression of SF21 is exactly the DSS (Figs. MII-2, MII-4, MII-5). All the other faults are situated to south of SF21 (Fig. MII-2). SF24-28 builds the second main set of faults, extending further west in comparison to the first set of faults. Parameters for all faults are given in Table MII-1.

In general, these major surface faults strike E-W (Fig. MII-2). SF24 bends toward the southeast in its eastern segment. SF27-28 are parallel to the bending eastern segment of SF24 and trend NW-SE. SF24 with ~16 km is the longest fault observable in the working area (Table MII-1). The second longest fault is SF21 (~13.2 km), whereas SF22 (~2.1 km) is the shortest fault in the research area.

Most of the observable faults are dipping toward south (Figs. MII-3c, MII-4c, MII-5c). Only two faults (SF23 and SF26) (Fig. MII-4c) are dipping towards north. The apparent dip angles of all faults are ~60° (Table MII-1). The seismic sections (Figs. MII-3, MII-4, MII-5) clearly show dominant normal components for all faults. Two well-developed negative flower structures have been recognized on the central Profile P807 (Fig. MII-4c). The northern negative flower structure is mainly made up of the first set of faults (SF21-23, Fig. MII-4c) and located in the core part of the tsunamigenic source area proposed by *BILLI et al. [2008]* (Fig. MII-2). The horizontal width across the northern negative flower structure is ~2 km. The southern negative flower structure mainly involves in SF24 and SF26 (Fig. MII-4c). The horizontal width across the southern negative flower structure is ~1 km. SF21 and SF24 are master faults of the northern and the southern negative flower structures, respectively. Moreover, in the southeastern part of the research area, SF24, SF27-28, and some minor faults form a tilted structure (Fig. MII-3). The horizontal width across this structure is ~1.5 km. Faults in the F-MPS_FZ arrange in a right-stepping style (Fig. MII-2b).

5 Discussion

5.1 The characteristics of the Fiumefreddo - Melito di Porto Salvo Fault Zone (F-MPS_FZ) in the outer Messina Strait

A new fault system – the Fiumefreddo - Melito di Porto Salvo Fault Zone (F-MPS_FZ) – was identified by means of high-resolution bathymetry and seismic sections in the outer Messina Strait. This fault zone can be considered as an active fault system, as most of the observed fault planes show clear surface expressions at the seafloor. The largest vertical displacement (~60 m) at the seafloor is found at SF21 (Fig. MII-2). This implies a high grade of tectonic activity in the outer Messina Strait. We consider the F-MPS_FZ as the shallow expression of a deeply rooted transtensional fault zone. It is expressed by a prominent negative flower structure within the upper 750 m of the sedimentary strata (Fig. MII-3). It has both normal-slip and strike-slip components.

The morphology and the regional tectonic setting suggest that the F-MPS_FZ is a left-lateral transtensional fault zone. The morphology shows that the DSS cut the NSS into NSS_N and NSS_S (Fig. MII-2a). The NSS_N is located further west with respect to the NSS_S (Fig. MII-2a), suggesting a left-lateral strike-slip component for the F-MPS_FZ. However, we cannot exclude that erosive processes might form both parts of the NSS as this area is shaped by a complex pattern of canyons. Hence, we can only speculate that we have a left lateral strike-slip component.

A left-lateral transtensional fault system, however, would fit to the regional tectonic framework. The Messina Strait has undergone a ~N115°E extension (chapter 5 2.1) and a clockwise rotation (Fig. A3 in appendix). Such a setting would likely result in left-lateral strike-slip components for faults in the survey area. Moreover, the E-W-trending faults which have been identified in the inner Messina Strait also have left-lateral strike-slip components. This results would support the left-lateral strike-slip of the F-MPS_FZ.

5.2 How do the newly-discovered Fiumefreddo - Melito di Porto Salvo Fault Zone (F-MPS_FZ) in the outer Messina Strait fit to the regional tectonic framework?

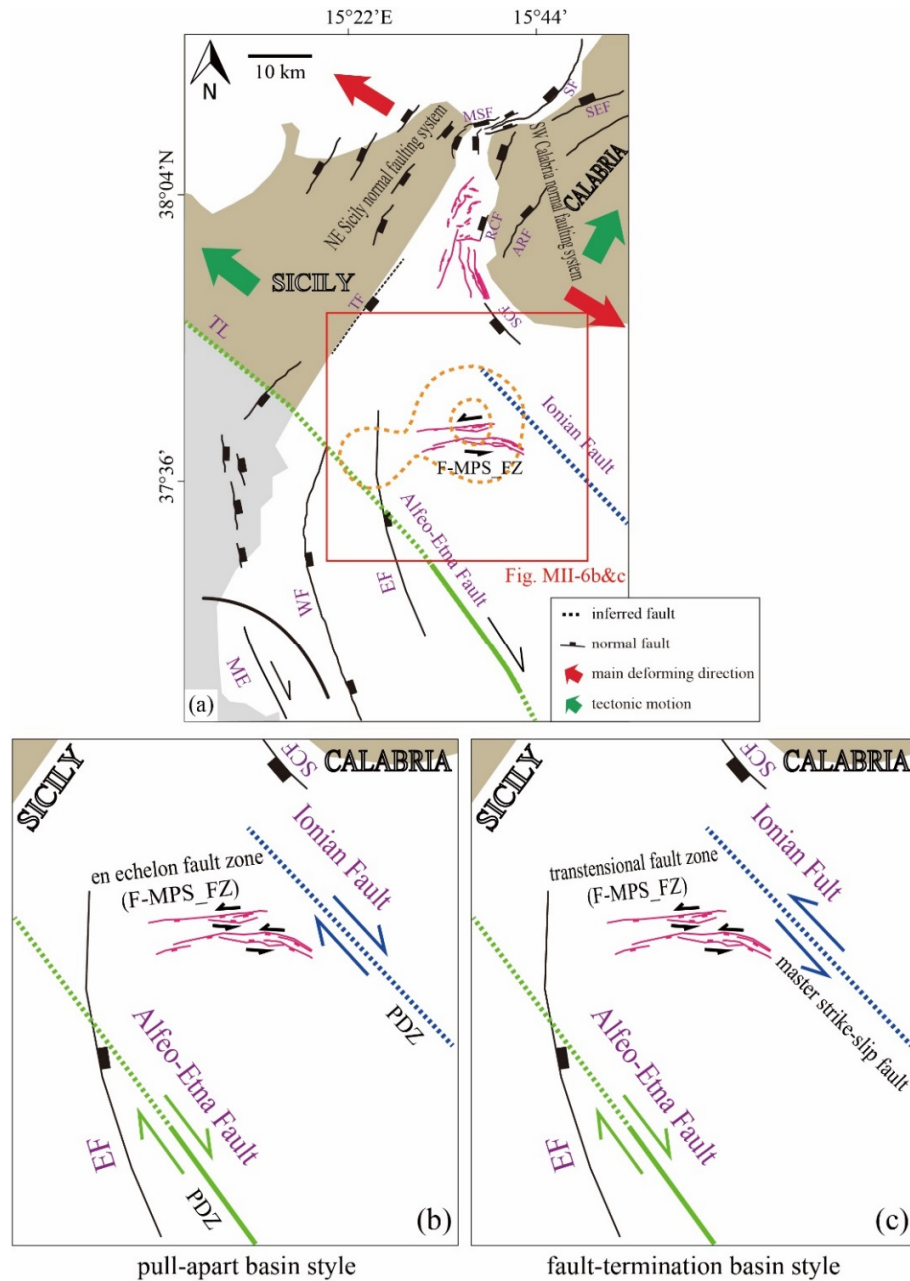


Figure MII- 6 Fiumefreddo - Melito di Porto Salvo Fault Zone (F-MPS_FZ) in the regional tectonic framework of the outer Messina Strait. See figure 1a for location of map. Modified from *GOVERS and WORTEL [2005]; ARGNANI and BONAZZI [2005]; GUARNIERI [2006]; CATALANO et al. [2008]; ARGNANI et al. [2009a]; [POLONIA et al. 2011b; POLONIA et al. 2014]; VITI et al. [2011b]; DOGLIONI et al. [2012]; GALLAIS et al. [2013]*. TL, Taormina Line; WF, Western Ionian Fault; EF, Eastern Ionian Fault; TF, Taormina fault; RCF, Reggio Calabria fault; SF, Scilla faults; SEF, S. Eufemia fault; ARF, Armo fault; SCF, Southern Calabria fault; FA, fault identified by Argnani; MSF, Messina Straits fault; ME, Malta Escarpment. The green and blue lines show the location of Subduction-Transform Edge Propagator (STEP) faults. Dashed lines are inferred fault locations. (b) Pull-apart basin and (c) fault-termination basin style models for the patterns of the “H” faulting system in the outer Messina Strait. PDZ, principle displacement zone. See text for details.

The F-MPS_FZ in the outer Messina Strait is located between the Ionian Fault and the Alfeo-Etna Fault (Fig. MII-6). The Ionian Fault and the Alfeo-Etna Fault are described as Subduction-Transform Edge Propagation (STEP) Faults [POLONIA *et al.* 2011b; GALLAIS *et al.* 2013; POLONIA *et al.* 2014]. The Ionian Fault terminates northwestward at an area pretty near the easternmost of the F-MPS_FZ. It may transfer to the Alfeo-Etna Fault through the F-MPS_FZ. Therefore, the F-MPS_FZ may work as a connector, linking the two STEP faults (Fig. MII-6). Thus, the F-MPS_FZ, the Ionian Fault, and the Alfeo-Etna Fault constitute a faulting system. We call this system “H” faulting system. As the direction of the movement of the Ionian Fault is still unclear (left lateral or right lateral), we suggest two possible models for the pattern of this “H” faulting system: the pull-apart basin style model (Fig. MII-6b) and the fault-termination basin style model (Fig. MII-6c).

5.2.1 The pull-apart basin style model

The Alfeo-Etna Fault is described as a right-lateral fault [GALLAIS *et al.* 2013]. If the Ionian Fault is a right-lateral fault, the “H” faulting system may be a pull-apart basin style system (Fig. MII-6b). In this system, the Ionian Fault and the Alfeo-Etna Fault are the principle displacement zones (PDZs). The F-MPS_FZ is the en echelon fault zone generated by the relative motions between the PDZs -- the Ionian Fault and the Alfeo-Etna Fault. The right-lateral motions of the Ionian Fault and the Alfeo-Etna Fault could generate a left-lateral F-MPS_FZ. Our suggested left-lateral movement of the F-MPS_FZ fits well to this model.

There are some additional implications supporting such a model. i) According to ARGNANI [2014], the occurrence of the lithospheric tear at the Ionian Fault is based on the identifications of two lobes with a different structural style in the frontal part of the Calabrian accretionary prism. This lithospheric tear may be caused by differential roll-back of the Ionian slab located under central Calabria. This part of the Ionian slab has been interpreted as continuous and recently decoupled from the remainder of the Ionian slab that is instead broken off. From this point of view, the Ionian Fault would be a right-lateral fault. ii) The clockwise rotation in the outer Messina Strait (Fig. MII-6b, Fig. A3 in appendix) supports a right-lateral Ionian Fault. iii) The regional tectonic setting (Fig. MII-1a) shows that in Southern Italy, almost all the MW-SE trending faults with strike-slip components are right-lateral faults. This observation supports a right-lateral motion of the Ionian Fault.

However, there are also facts, doubting the pull-apart basin style model. i) In literature [ATMAOUI *et al.* 2006], a pull-apart basin style faulting system is a product of Riedel shear mechanism. If the PDZs are right-lateral faults, the en echelon faults in-between would be arranged in a left-stepping style, but the faults in the F-MPS_FZ are in a right-stepping style. ii) There is a step-over area between the Ionian Fault and the Alfeo-Etna Fault (Fig. MII-1a). The slip rates of both STEP faults are still unknown. If the Ionian Fault is more active, this step-over area would be controlled by a compressional regime; if the Alfeo-Etna Fault is faster, we have an extensional regime.

According to the discussed issues, it seems that the pull-apart basin style model could explain major parts of the “H” faulting system.

5.2.2 *The fault-termination basin style model*

Transtensional stress domains, if a part of a crustal block undergoes translation within the block, will result in shortening/uplift at one end and extension/subsidence at the other [MIALL 2000; UMHOEFER *et al.* 2007]. Basins formed by such extension/subsidence are referred to as fault-termination basins or transtensional fault-termination basins. Normally, fault-termination basins are developed at the ends of strike-slip faults where normal or oblique slip faults diffuse or splay off to terminate the deformation field.

In our case, the transtensional F-MPS_FZ indicates that the outer Messina Strait is an area controlled by a transtensional regime. The Ionian Fault terminates in the north at the F-MPS_FZ. If the Ionian Fault is a left-lateral fault, the Ionian Fault and the F-MPS_FZ constitute a fault-termination basin style faulting system (Fig. MII-6c). In this system, the Ionian Fault is the master strike-slip fault. The F-MPS_FZ is the transtensional fault zone diffusing or splaying off to terminate the deformation field. The southward bending of the eastern segments of SF24 and SF27-28 (Fig. MII-2b) is an indication for this effect. It is worth noting that the Alfeo-Etna Fault does not terminate at the F-MPS_FZ but extends far north of it. This would suggest that the Alfeo-Etna Fault is not a member of this fault-termination basin style faulting system. As most of the faults in the F-MPS_FZ dip toward the south which indicating that the working area may be dominated by a southeastward extension, the right-lateral Alfeo-Etna Fault may be a contributor to this extension.

However, we see some serious problems for such a model. i) If the Ionian Fault is suggested to be likely a left-lateral fault, faults in the F-MPS_FZ should be right-lateral faults. We suggest that the F-MPS_FZ contains left-lateral faults but we do not have a final proof for this statement. Hence, we cannot exclude that we have a right-lateral movement. ii) The clockwise rotation of the outer Messina Strait (see “geodetic strain rate field” in Fig. A3 in appendix) and the existences of the other right-lateral faults in Southern Italy (Fig. MII-1a) would be in conflict to a left-lateral Ionian Fault.

5.2.3 The pull-apart basin style model versus the fault-termination basin style model: some additional thoughts

There are several facts which are worth to be considered. Both models assume that two STEP faults are present in the working area. However, the northern segments of the Ionian Fault and the Alfeo-Etna Fault are inferred segments of these two faults. They are not clearly imaged on any seismic data including our data. Our new seismic data are of high resolution but very limited penetration. The STEP faults and their fault planes are buried too deeply to be identified on our new data and most likely on other existing seismic data [ARGNANI *et al.* 2009a]. In addition, according to Argnani *et al.*, 2014, the Ionian Fault is relatively recent and younger than the Alfeo-Etna Fault. However, the structures in the two areas separated by the Ionian Fault are post Messinian, and likely much older than Quaternary [ARGNANI 2014]. This casts some doubt on the occurrence of two STEP faults cutting through the Ionian lithosphere, also considering that the Ionian Fault has not been completely documented [ARGNANI 2014]. Moreover, the distribution of the geodetic strain rates and rotations in the marine area off Southern Italy is the interpolated data based on the GPS data acquired on land. There may be deviations between the interpolated results and true motions.

However, assuming that both STEP faults do exist, the F-MPS_FZ may be classified as a new type of fault – a STEP-Connector Fault. We consider the pull-apart basin style model as more plausible for the pattern of the “H” faulting system in the outer Messina Strait, although many questions remain open. More surveys including deep reaching seismic data are need for further investigations of this area.

6 Conclusions

In this manuscript, we present a detailed analysis of the newly-discovered, E-W-trending Fiumefreddo - Melito di Porto Salvo Fault Zone (F-MPS_FZ) in the outer Messina Strait.

The F-MPS_FZ is a left-lateral transtensional fault zone, which shows ongoing tectonic activity. This is indicated by the appearance of the negative flower structure. A prominent dominant scarp-like structure (DSS) with heights of up to 60 m represents the surface expression of the master fault of the F-MPS_FZ.

The transtensional F-MPS_FZ supports a transtensional regime in the outer Messina Strait. Such a regime fits well to the observed northwest and southeast movements of Calabria and Sicily with respect to the Eurasian plate, respectively.

The F-MPS_FZ builds an “H” faulting system with two postulated STEP faults: the Ionian Fault and the Alfeo-Etna Fault. The F-MPS_FZ may be a STEP-Connector Fault, linking the Ionian Fault and the Alfeo-Etna Fault. Two possible models have been put forward for this system: the pull-apart basin style model and the fault-termination basin style model. The pull-apart basin style model is more reasonable based on all available data.

6 MANUSCRIPT III

Tsunami potential for Southern Italy related to a newly-discovered active fault zone in the outer Messina Strait, based on fault activity reconstructions and tsunami modelling

Lili Fu¹, Mohammad Heidarzadeh^{1, 2}, Deniz Cukur^{3, 4}, Sebastian Krastel¹, Francesco Chiocci⁵, Domenico Ridente⁶, Felix Gross¹, Jörg Balas³

¹Institute of Geosciences, University of Kiel, Kiel 24118, Germany

²Earthquake Research Institute, University of Tokyo, 1-1-1 Yayoi, Bunkyo-ku, Tokyo, 113-0032, JAPAN

³GEOMAR Helmholtz Centre for Ocean Research Kiel, Kiel 24148, Germany

⁴now at Korea Institute of Geoscience and Mineral Resources, Daejeon 305-350, Korea

⁵Department of Earth Sciences, Sapienza University of Rome, Rome 00185, Italy

⁶National Research Council, Roma, Italy

Abstract

The 1908 Messina tsunami was the most catastrophic tsunami hitting the coastlines of Southern Italy in the younger past. The source of this tsunami, however, is still heavily debated, and both, rupture along a fault and a slope failure, have been postulated as origin for the tsunami. The newly-discovered Fiumefreddo - Melito di Porto Salvo Fault Zone (F-MPS_FZ) in the outer Messina Strait is located in an area which was suggested to be the source area of the 1908 Messina tsunami. In this manuscript, we reconstructed the activity of the F-MPS_FZ and ran tsunami models based on fault parameters of this fault zone derived from seismic data. The F-MPS_FZ is an E-W-trending fault zone reaching down to the acoustic basement. It has been active during the entire regional tectonic evolution of the outer Messina Strait. During its evolution, the fault activity alternated between tranpressional and transtensional with varying apparent displacements. Currently, the F-MPS_FZ is an active transtensional fault zone. Based on the results of the tsunami modelling, the F-MPS_FZ could generate tsunamis, and an assumed slip of up to 15 m could generate a tsunami comparable to the 1908 Messina tsunami, but we do not consider the F-MPS_FZ as a source for the 1908 Messina tsunami, because an E-W-trending fault is not in agreement with seismological data of the 1908 Messina earthquake, and a 15 m slip event is highly unlikely. However, we still consider this fault as a highly potential hazard source in Southern Italy, because it shows the most obvious vertical displacement in the entire Messina Strait and seems to be active.

1 Introduction

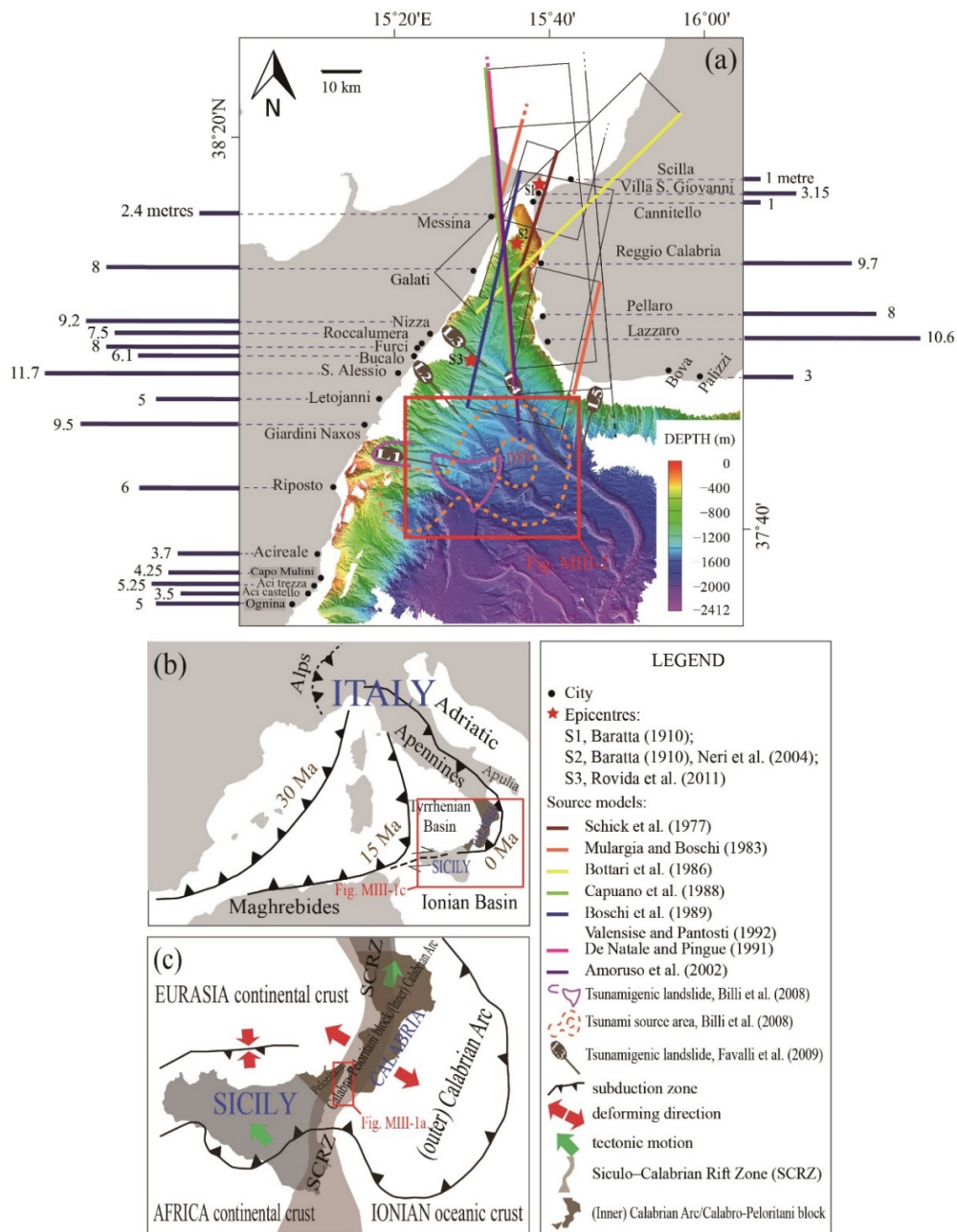


Figure MIII- 1 (a) Bathymetry of the Messina Strait and proposed source models for the 1988 Messina earthquake and tsunamis. Modified after *BILLI et al. [2008]*; *FAVALLI et al. [2009a]*; *PINO et al. [2009b]*; *POLONIA et al. [2011b]*; *GALLAIS et al. [2013]*. The coloured straight lines together with the black rectangles show the possible seismogenic faults of the 1988 Messina earthquake. The coloured straight lines indicate the intersections of the proposed fault planes and the earth surface (cut-off lines). The black rectangular represent the surface projections of the fault planes. The dashed segments of the fault planes show the uncertain parts of those faults. The straight lines connected to the ellipses indicate the moving directions of landslides. The blue bars perpendicular to the frame of the figure represent the observed run-up heights of the 1988 Messina tsunamis in some cities. The numbers beside these bars are the values of the run-up heights in metres. The red box marks the research area of this study and the range of Fig. MIII-2. DSS, dominate scarp-like structure. (b) Overall tectonic evolution of the central Mediterranean Sea (Southern Italy). Modified after *NERI et al. [2009]*. (c) Present tectonic setting of Southern Italy. Please see the LEGEND to know the meanings of the symbols used in the figure.

The 1908 Messina tsunami was the most destructive tsunami in Europe since then, in terms of run-up height (>10 m) [PLATANIA 1909] (Fig. MIII-1a) and impacted area [SOLOV'EV *et al.* 2000]. It hits the entire coasts of the Messina Strait (Fig. MIII-1a). The southern inner Messina Strait was hit by higher tsunami run-ups (5 - 10 m) than the northern part (1 - 3 m) (Fig. MIII-1a). The highest run-up heights were reported south of Galati and Reggio Calabria (up to 12 m) (Fig. MIII-1a).

As the tsunami was assumed to be triggered by the coseismic seafloor displacement during the earthquake [TINTI and ARMIGLIATO 2003b], several tsunami models have been built up based on some most common fault solutions [TINTI and ARMIGLIATO 2003b; FAVALLI *et al.* 2009b] (Fig. MIII-1a). However, no one meets all observations [TINTI *et al.* 1999b; GERARDI *et al.* 2008]. Hence, BILLI *et al.* [2008] postulated that the 1908 Messina tsunami may have been triggered by submarine landslide that was caused by the earthquake. The source area is located in the outer Messina Strait off Giardini Naxos and Lazzaro (Fig. MIII-1a). It was constructed based on observed arrival times of the tsunami and identified morphological features in this area, which were interpreted as landslide by the authors. This scenario, however, was strongly doubted by some authors [ARGNANI *et al.* 2009b; GROSS *et al.* 2014] as new high-resolution bathymetric and seismic data do not show indications for a recent landslide in this area. In addition, modelling results presented by GERARDI *et al.* [2008] shows that the tsunami characteristics is compatible with a seismic dislocation source, because landslide sources concentrate large run-ups over relatively limited stretches of coastline, whereas seismic dislocations can affect much longer stretches of the coast.

As the location of BILLI *et al.* [2008]'s newly proposed source area was calculated based on the travel times of the 1908 tsunami, it is to some extent reliable that this area might be a potential source area for tsunamis. Therefore, new high-resolution hydro-acoustic and 2D seismic data were collected in this area and show a prominent fault zone (Fu *et al.*, this thesis, chapter 5). The objectives of this study are to reconstruct the activities of this fault zone and to run tsunami models based on derived fault parameters, in order i) to assess the activity of the fault zone over time, especially in modern times and ii) to assess the potential of this fault zone for generating tsunamis.

2 Tectonic settings

The outer Messina Strait is a highly complex tectonic area [*FACCENNA et al. 2003; GOES et al. 2004; PONDRELLI et al. 2006*], as is situated both in the Siculo-Calabrian Rift Zone (SCRZ) (Fig. MIII-1c) and the inner Calabrian Arc (Fig. MIII-1b). This complex tectonic framework is the result of the long-term evolution of the converging African- and Eurasian plate boundary zone (Fig. MIII-1b).

Between ~80 and ~30 Ma, the African and the Eurasian plates converged slowly [*FACCENNA et al. 2001; FACCENNA et al. 2003*]. The African plate subducted underneath the Eurasian plate. Since ~30 Ma (Fig. MIII-1b), a trench retreat had occurred leading to a progressively opening and southeast extension of the western Mediterranean Sea [*GUEGUEN et al. 1998; GOES et al. 2004*]. 0.8 – 0.5 My ago (Fig. MIII-1b&c), when the Calabro-Peloritani block docked between Apulia and Sicily, the trench retreat seemed to have slowed down to a minimum. The accompanying Tyrrhenian back-arc extension has almost ceased as well [*D'AGOSTINO and SELVAGGI 2004; GOES et al. 2004*]. The Ionian section of the African plate moved northeastward away from the remaining plate, controlling the current eastward motion of Calabria and Apulia with respect to Africa. As plate boundaries have been readjusted, very strong deformations have been recorded at the area between Europe, Africa, and Calabria (Fig. MIII-1c). These young tectonics may be associated with strong and sometimes devastating seismicity.

3 Data and Method

From December 27th, 2011 to January 17th, 2012, a new high-resolution seismo- and hydro-acoustic dataset was acquired during RV Meteor Cruise M86/2 off Southern Italy. Data were collected by means of a bathymetric multi-beam echo sounder, a sediment echo sounder, and a high-resolution 2D reflection seismic system. Additional high-resolution bathymetric data collected in the frame of the MAGIC project (Marine Geohazards along the Italian Coasts, *CHIOCCI and RIDENTE [2011]*) were assessed for this study as well.

High-resolution 2D reflection seismic data were collected using a 162.5 m-long, 104-channel digital Geometrics GeoEeL streamer. The seismic signal was generated by means of a 1.7 l GI gun, operated in harmonic mode and a shot interval of 4 s. A Sub-bottom penetration of up to 1 s TWT (Two-Way-Travel-Time) was achieved. The processing steps include geometry setup, binning, band-pass filtering (10/20/600/1000 Hz, assumed for low truncation frequency, low cut frequency, high cut frequency, and high truncation frequency, respectively), Normal Move-Out (NMO) corrections, despiking, stacking and time-migration. The lateral bin size was set to 2 m. A constant sound velocity of 1500 m/s was applied during NMO corrections and data migration because the short length of the streamer does not allow a reliable velocity analysis. Gedco Vista Seismic Processing[®] (Schlumberger, version 11) and IHS Kingdom Suite[®] (version 8.6) were used for processing and interpretation.

Fault activity reconstructions have been done by the software Move 2014.2[®], in order to investigate the activity of the newly-discovered fault zone in the outer Messina Strait. Seismic profiles P807 and P242 (Figs. MIII-2, MIII-3, MIII-4) were selected as representative examples. These profiles run across the central and the western parts of the newly-discovered fault zone, respectively. Prominent reflectors, which can be securely traced across the entire working area, were picked. Unfortunately, no age control is available for any of the picked reflectors. The selected horizons were converted to depth sections using a constant sound velocity of 1500 m/s.

The restoring steps include backstripping and decompacting sedimentary layers (decompaction), restoring faults (move on fault), and unfolding. “Decompaction” is to remove the loading effect of the top sequence. For different lithology, the amount of decompaction depends on the relationship between solidity (solidity = 1 - porosity) and depth. Here, we used the default parameters (50% shale, 50% sand, porosity = 0.56 fraction, depth coefficient = 0.39/km, sound velocity = 2200 m/s, density = 2680 kg/m³, Young Modulus = 23750 MPa, Poisson Ratio = 0.3) as there are no valid rock properties for horizons

within the model due to the lack of the core data in the outer Messina Strait. “Move on fault” is to restore the paleo-topography or depositional surface to be a continuous layer with topography. In this step, a simple-shear algorithm was used, assuming that the hanging wall deforms by simple shear and the footwall remained undeformed through the extension [WHITE *et al.* 1986]. Then, a flexural-slip “unfolding” algorithm was used to merge the top surface and the paleo-depositional surface, assuming concentric folds with constant bed thickness [KEETLEY and HILL 2000]. Afterwards, a new top sedimentary layer was decompacted. Then, the same procedure was repeated, until only the deepest sediment layer is left.

Tsunami modelling was performed using the nonlinear shallow water code TUNAMI-N2, developed at the Tohoku University, Japan [GOTO *et al.* 1997]. TUNAMI-N2, which solves governing equations of water motions using the leap-frog scheme of Finite Differences on a Cartesian Coordinate system, has been validated using experimental and field data [SYNOLAKIS and BERNARD 2006] and has been applied to several tsunamigenic zones worldwide [YALÇINER *et al.* 2004; HEIDARZADEH *et al.* 2009; SUPPASRI *et al.* 2011]. We applied a 30 m bathymetric grid, which was generated by us based on available multi-beam data. Simulations were conducted using a time step of 2 s and for a total simulation time of 12 h to account for possible reflected waves as the region is geographically narrow and several reflections are expected. Coseismic seafloor deformation were calculated by using the analytical formula by OKADA [1985], which solves the dislocation problem on a half space. Fault parameters used for coseismic seafloor calculations are: Strike, dip, rake angles, top depth of the fault, length and width of the fault as well as the slip amount (Table MIII-1). Parts of these parameters were taken from the seismic data (e.g. fault length, strike and dip); several test were run for the parameters, which could not be determined by the seismic data (e.g., slip amount).

4 Results

4.1 Fault pattern in the outer Messina Strait

Seismic profiles P807 and P242 were selected as representative sections (Figs. MIII-2, MIII-3, MIII-4). These profiles show clear subsurface expressions and cover the major surface faults and abundant minor faults (Figs. MIII-3, MIII-4).

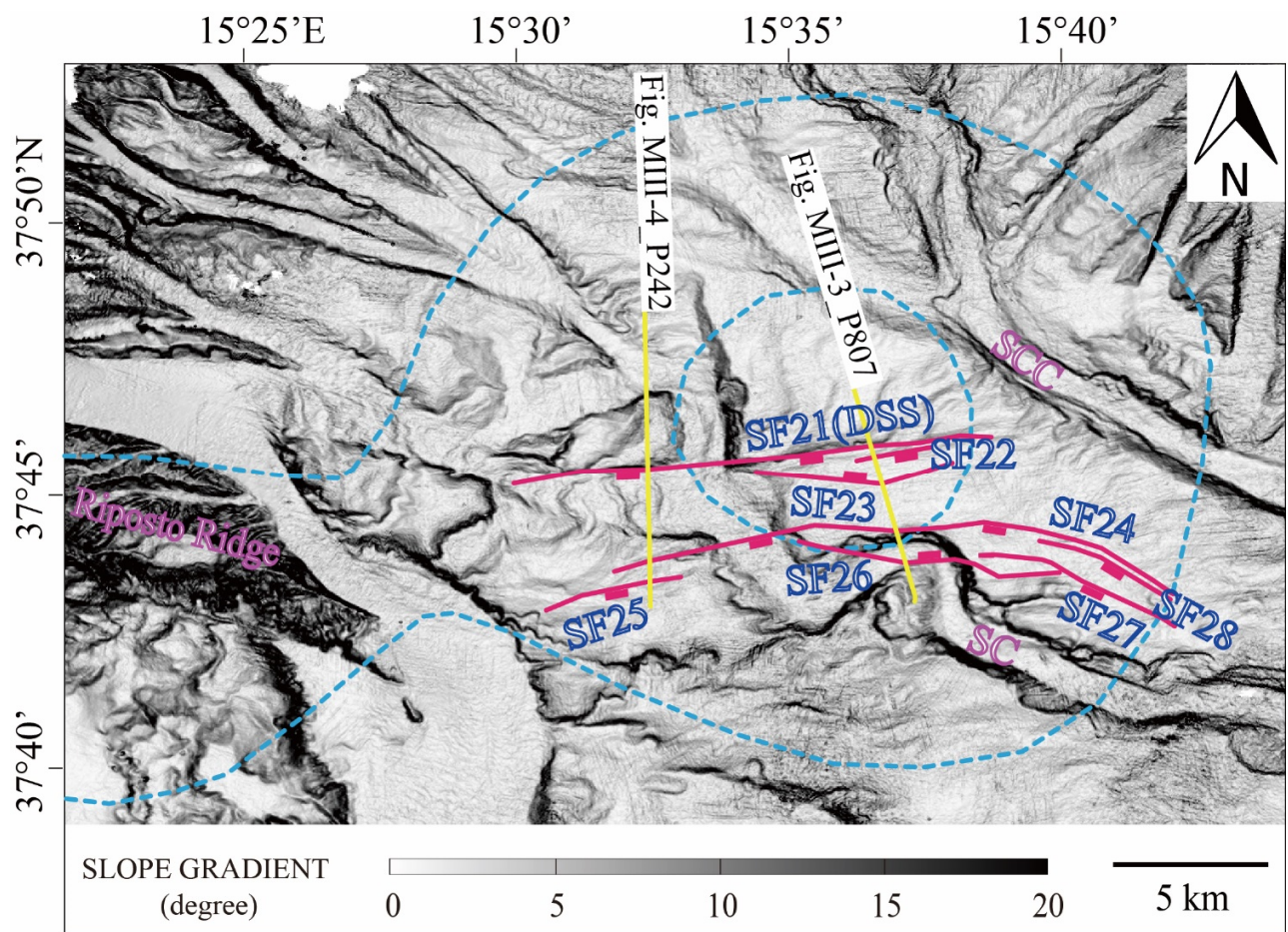


Figure MIII- 2 Horizontal distributions of the newly-discovered Fiumefreddo - Melito di Porto Salvo Fault Zone in the outer Messina Strait. SCC, South Calabria Canyon [RIDENTE *et al.* 2014]; SC, South Canyon. Pink lines show the faults. Light blue dashed closed curves show the source area proposed by BILLI *et al.* [2008] for the 1908 Messina tsunami. Yellow lines mark the locations of the selected seismic profiles, P807 and P242. See Fig. MIII-1 a for location of map.

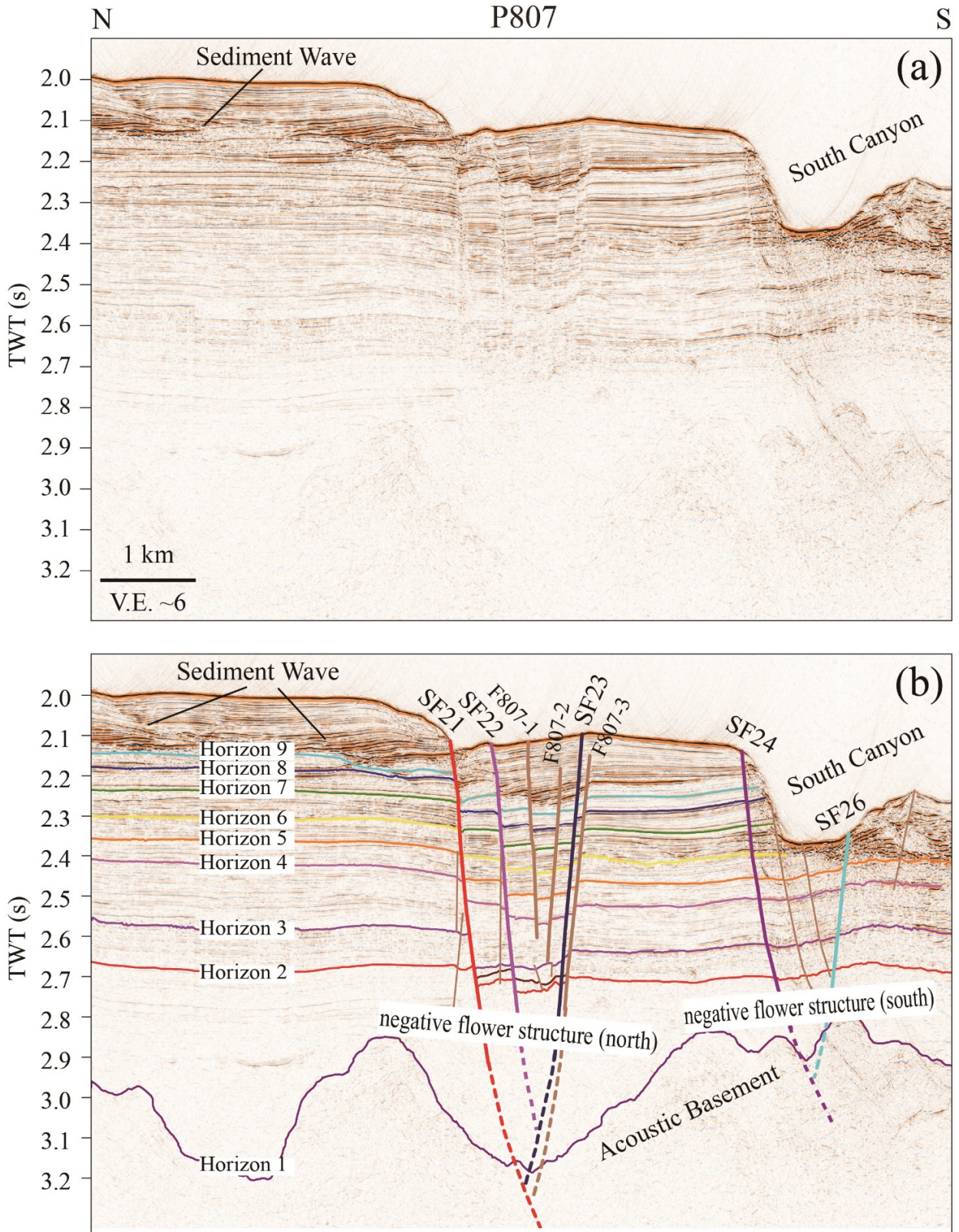


Figure MIII- 3 (a) Uninterpreted and (b) interpreted seismic sections of profile P807. Faults in brown are minor surface faults; faults in other colours are the major surface faults. The dashed lines show the uncertain lower parts of the faults. Solid coloured horizontal lines show the picked horizons. TWT, Two-Way Travel Time. The vertical exaggeration is 6. See Fig. MIII-2 for location of the profile.

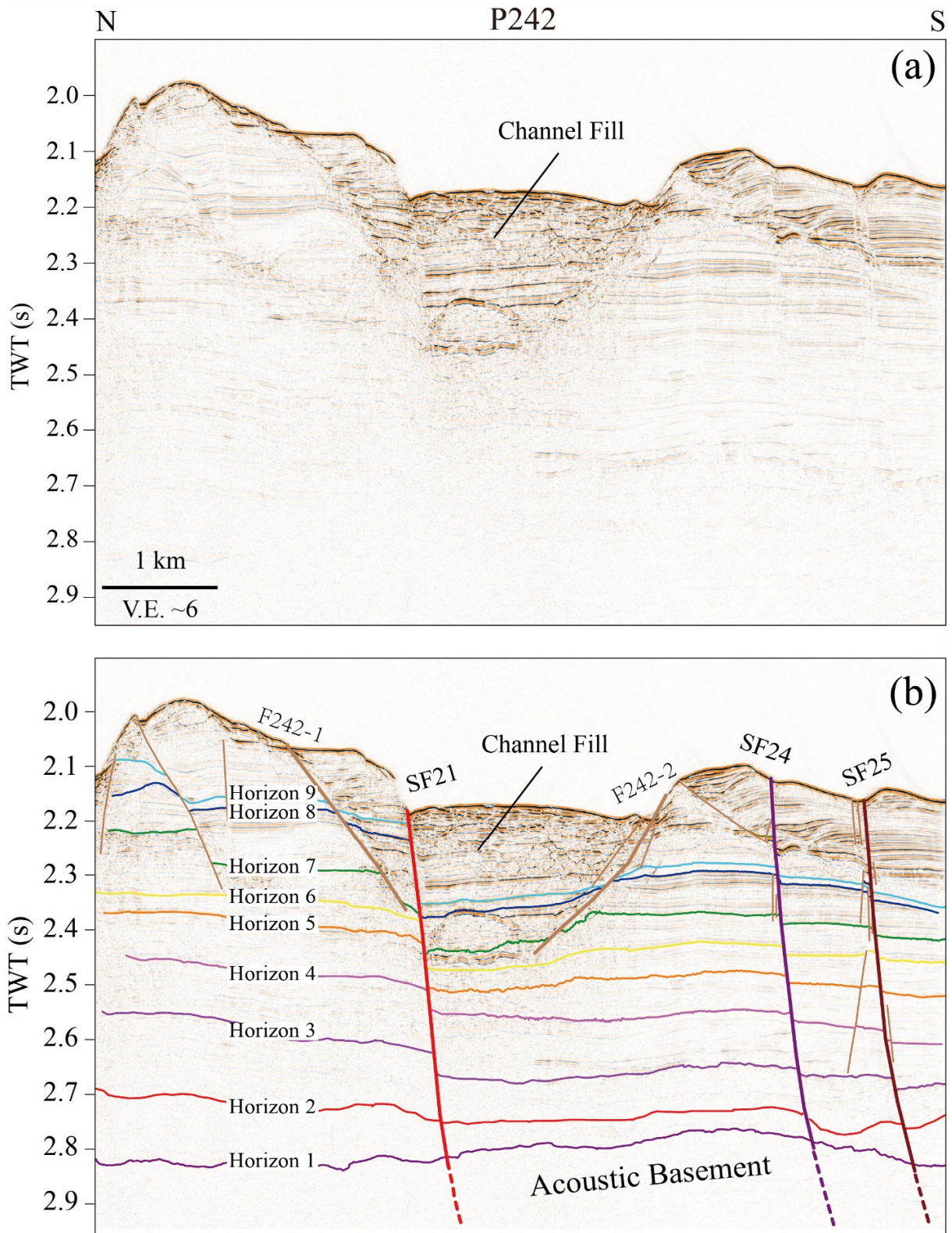
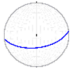
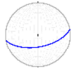
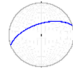
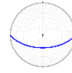
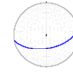
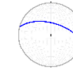
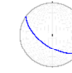
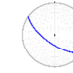


Figure MIII- 4 (a) Uninterpreted and (b) interpreted seismic sections of profile P242. Faults in brown are minor surface faults; faults in other colours are the major surface faults. The dashed lines show the uncertain lower parts of the faults. Solid coloured horizontal lines show the picked horizons. TWT, Two-Way Travel Time. The vertical exaggeration is 6. See Fig. MIII-2 for location of the profile.

Table MIII- 1 Fault geometries of the major surface faults in the newly-discovered Fiumefreddo - Melito di Porto Salvo Fault Zone in the outer Messina Strait. Details are given in Fu et al. (this thesis) (chapter 5 4.2).

Fault Name	SF21	SF22	SF23	SF24	SF25	SF26	SF27	SF28
Length (m)	14000	2100	5500	16000	3800	7300	5900	4300
¹ ADA (°)	58	60	61	58	56	59	52	67
	S	S	N	S	S	N	S	S
³ SD (°)	83	80	252	90	80	285	125	125
⁴ E. S. P.								
⁵ AD_H9 (m)	61	16	11	9	14	9	4	6

¹ADA, Apparent Dip Angle;

²SP, Seismic Profile;

³SD, Strike Direction (North Azimuth);

⁴E. S. P., Equal-area stereo-graphic plots of the fault planes (strike, dip (rhr));

⁵AD_H9, Apparent Displacement on Horizon 9.

Eight major surface faults, SF21-28, and some minor faults have been identified in the outer Messina Strait (Fig. MIII-2). Major faults can be traced on at least two profiles, while minor faults are only imaged on one single profile. They constitute a fault zone, the Fiumefreddo - Melito di Porto Salvo Fault Zone (F-MPS_FZ), which is located exactly in the source area proposed by *BILLI et al. [2008]* for the 1908 Messina tsunami. SF21-23, especially SF21, are in the core part of this area. The surface expression of SF21 is exactly the dominant scarp-like structure (DSS) (Figs. MIII-2, MIII-3, MIII-4). All other major surface faults are located south of SF21 (Fig. MIII-2).

In general, all major surface faults strike E-W (Fig. MIII-2) and show apparent dip angles of $\sim 60^\circ$. All faults, except for SF23 and SF26 dip toward south. The length of individual fault is up to ~ 16 km. Important fault parameters are summarized in Table MIII-1. A detailed description of the fault zone is given in chapter 5 4.2.

4.2 Reconstructions of fault activities in the outer Messina Strait

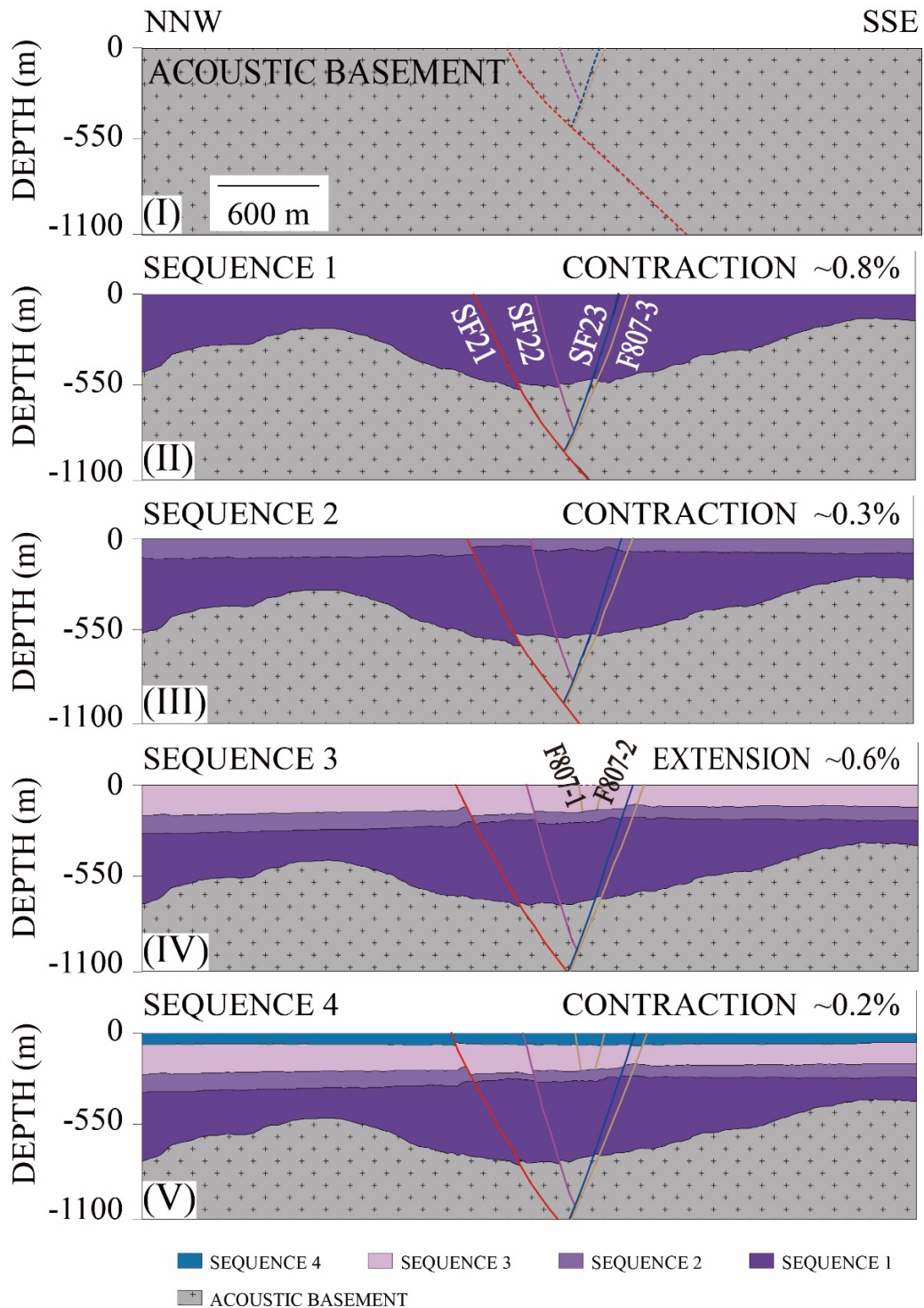


Figure MIII- 5 Reconstructions of fault activities of the F-MPS_FZ, based on profile P807 that runs across the central part of the F-MPS_FZ. Stage 1. See Fig. MIII-2 for the location of the profile. F807-1, F807-2, and F807-3 are minor surface faults on the section P807. From the acoustic basement to sequence 9, no water column is included, as the water column has already been decompacted when reconstructing the sequence 9 from the present phase. We set the depth to 0, as we do not have any evidences for the paleo-water depths at the time of the sequences' deposition.

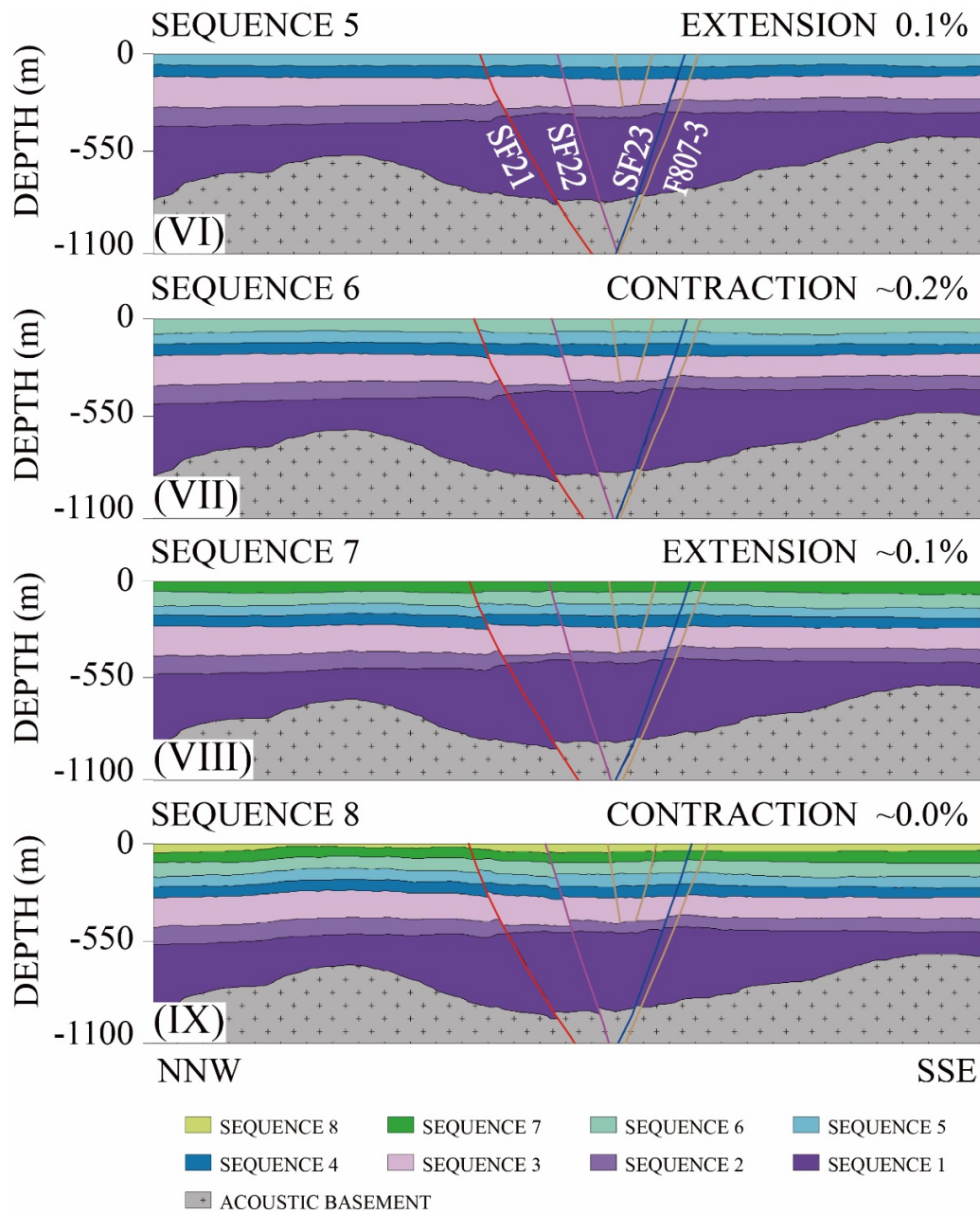


Fig. MIII-5 Continued: Reconstructions of fault activities of the F-MPS_FZ, based on profile P807 that runs across the central part of the F-MPS_FZ. Stage 2.

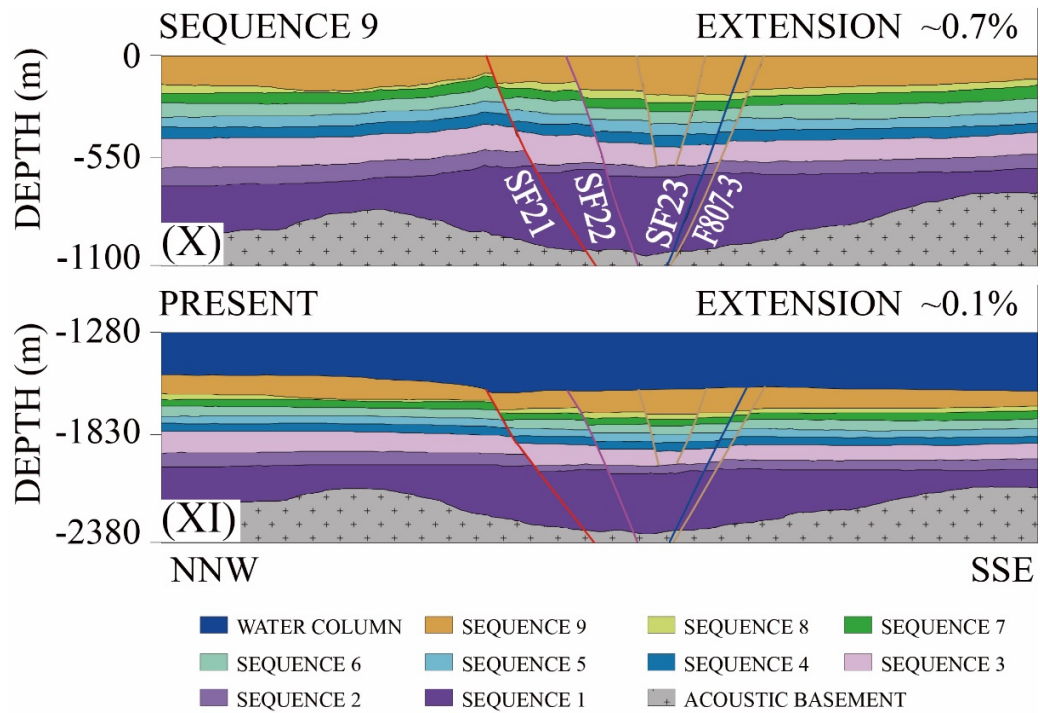


Fig. MIII-5 Continued: Reconstructions of fault activities of the F-MPS_FZ, based on profile P807 that runs across the central part of the F-MPS_FZ. Stage 3.

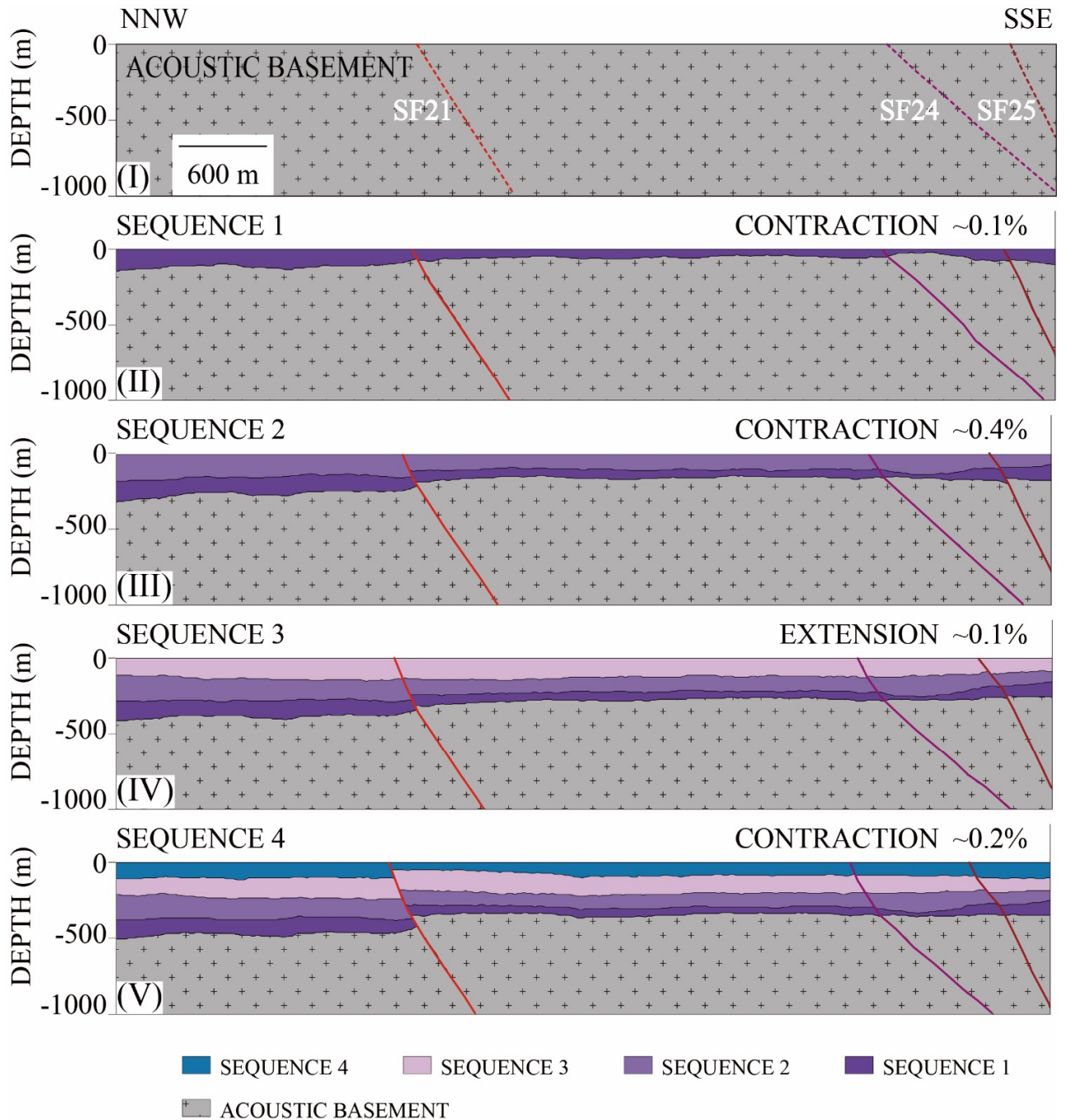


Figure MIII- 6 Reconstructions of fault activities of the F-MPS_FZ, based on profile P242 that runs across the western part of the F-MPS_FZ. Stage 1. See Fig. MIII-2 for the location of the profile. F242-1 and F242-2 are minor surface faults on the section P242. From the acoustic basement to sequence 9, no water column is included, as the water column has already been decompacted when reconstructing the sequence 9 from the present phase. We set the depth to 0, as do not have any evidence for the paleo-water depths at the time of the sequences' deposition.

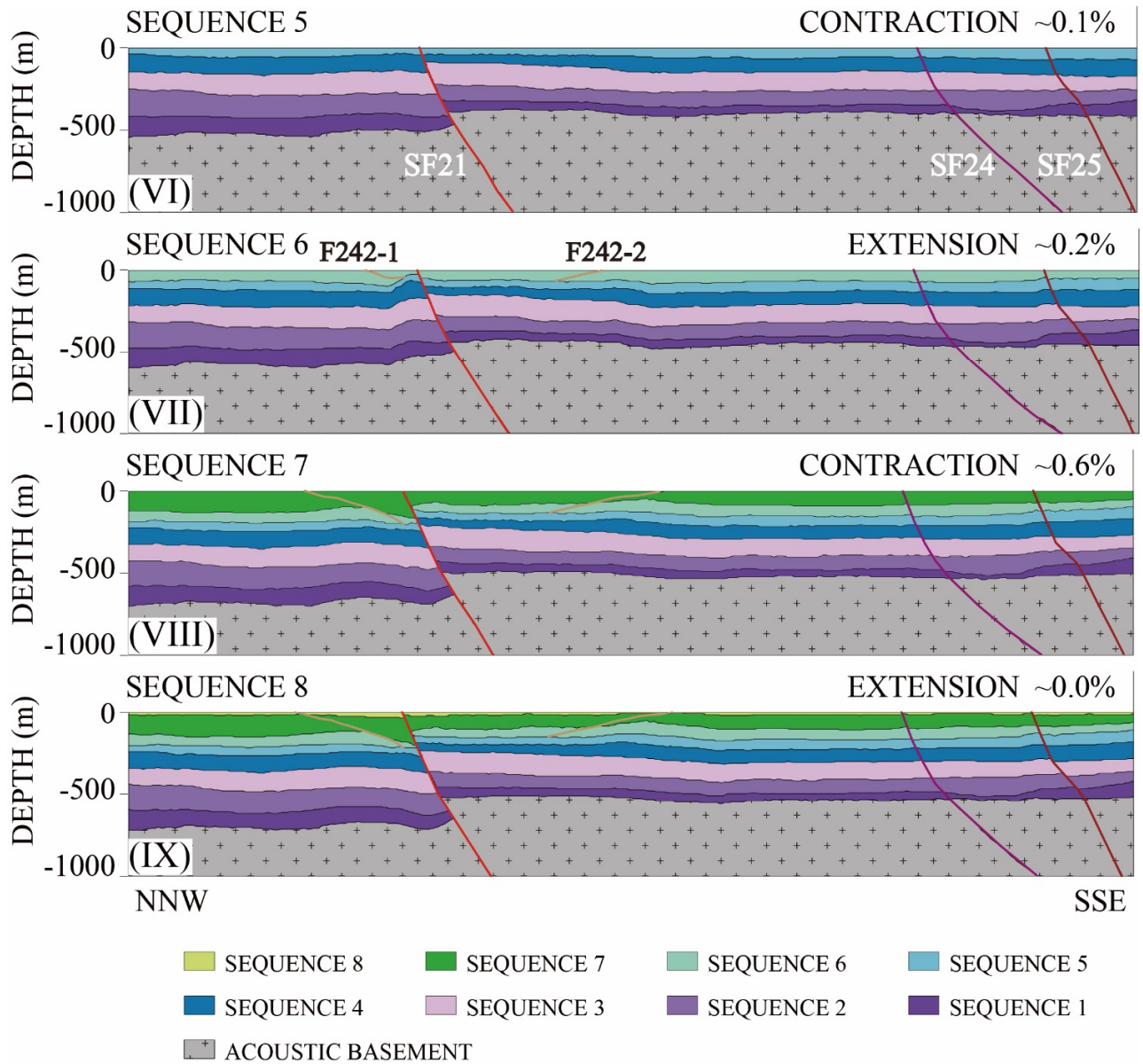


Fig. MIII-6 Continued: Reconstructions of fault activities of the F-MPS_FZ, based on profile P242 that runs across the western part of the F-MPS_FZ. Stage 2.

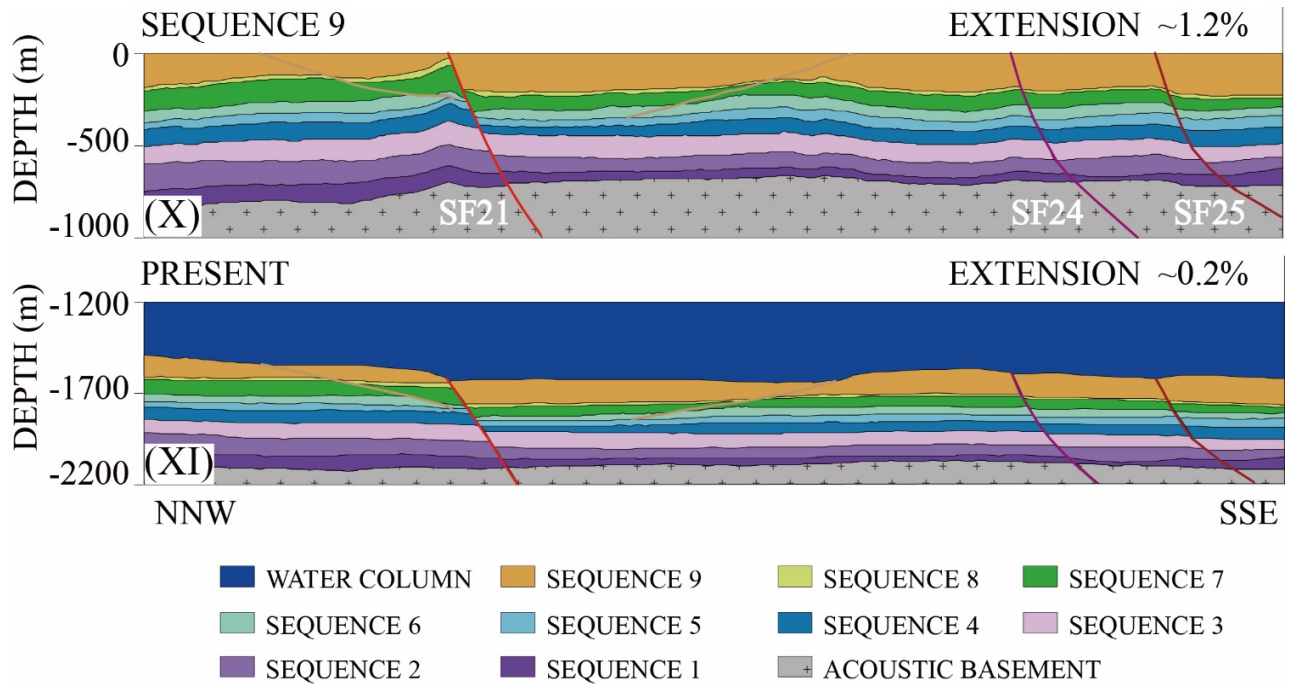


Fig. MIII-6 Continued: Reconstructions of fault activities of the F-MPS_FZ, based on profile P242 that runs across the western part of the F-MPS_FZ. Stage 3.

Table MIII- 2 Reconstructed amounts of the apparent displacements of the faults in the outer Messina Strait at the end of the formation of each sequence. Negative and positive signs indicate the normal and the reverse slip components, respectively.

Stratigraphic Sequences	West (P242)				Tectonic Activities	%	Centre (P807)						Tectonic Activities	%
	FT & AD		Tectonic Activities				FT & AD		Tectonic Activities					
	F242-1	SF21	F242-2	SF24	SF25		SF21	SF22	F807-1	F807-2	SF23	F807-3		
² A. BASEMENT														
SEQUENCE 1		-5		9	14	CONTRACTION	0,1	52	31		1	12	CONTRACTION	0,8
SEQUENCE 2		45		-1	24	CONTRACTION	0,4	43	-29		4	-5	CONTRACTION	0,3
SEQUENCE 3		0		6	-18	EXTENSION	-0,1	-65	9	0	0	-15	EXTENSION	-0,6
SEQUENCE 4		67		-9	-13	CONTRACTION	0,2	18	12	1	3	3	CONTRACTION	0,2
SEQUENCE 5		6		6	6	CONTRACTION	0,1	-3	-15	4	-2	0	EXTENSION	-0,1
SEQUENCE 6		0	27	0	3	EXTENSION	-0,2	18	18	2	-5	6	CONTRACTION	0,2
SEQUENCE 7		116	78	27	11	CONTRACTION	0,6	3	-13	-2	3	-3	EXTENSION	-0,1
SEQUENCE 8		-33	4	2	7	EXTENSION	0,0	-4	18	0	0	-3	CONTRACTION	0,0
SEQUENCE 9		-5	-87	25	16	EXTENSION	-1,2	-57	-40	-16	-10	-12	EXTENSION	-0,7
PRESENT		-34	18	-87	-3	EXTENSION	-0,2	-16	0	0	0	0	EXTENSION	-0,1

¹FT & AD, Fault Type & Apparent Displacement (m)

²A. BASEMENT, Acoustic Basement

The seismic sections P807 (~4600 m long) and P242 (~ 6200 m long) traverse the central and the western parts of the Fiumefreddo - Melito di Porto Salvo Fault Zone (F-MPS_FZ), respectively (Fig. MIII-2). The nine picked horizons separate each section into ten sequences (Figs. MIII-3b, MIII-4b). According to the results of the reconstructions of the fault activities (Figs. MIII-5, MIII-6; Table MIII-2), the evolution of the F-MPS_FZ can be divided into three stages (Stage 1 to 3). SF21 showing the

most prominent surface expression on the seafloor (Fig. MIII-2) is the most important fault and will be described in detail in the following section.

4.2.1 Stage 1

Stage 1 includes the deposition of the sequences 1 - 4 (Figs. MIII-5I–V, MIII-6I–V). The dominant tectonic process during this stage was contraction, though the entire area experienced some extension during the deposition of sequence 3 (Figs. MIII-5, MIII-6). During the formation of sequence 1, the central part of the area underwent stronger contraction than the western part (Figs. MIII-5II, MIII-6II). The amounts of contraction were similar for the remaining periods, except for period 3, where the behaviour changed to extension. This overall behaviour is well documented by the activity along fault SF 21 (Table MIII-2). During the deposition of sequence 1, SF21 formed as major reverse fault in the central part of the section (Figs. MIII-5, MIII-6; Table MIII-2). This behaviour continued during the deposition of sequence 2 but changed to reverse slip during the deposition of sequence 3 before it changed again to normal slip during the deposition of sequence 4. The amounts of the apparent displacements of SF21 in the central area are larger than those in the western area (Table MIII-2). Overall, SF21 and SF22 have accommodated the largest extension and contraction throughout this stage.

4.2.2 Stage 2

Stage 2 spans the period of deposition of sequence 5 to sequence 8 (Figs. MIII-5VI–IX, MIII-6VI–IX). During this stage, extension and contraction occurred alternately in the entire area but the amounts were less than 0.2% (~15 m) and therefore very minor. The only exception is the sequence 7 where a relatively larger contraction (0.6%, ~40 m) occurred in the western part of the area (Fig. MIII-6; Table MIII-2). The fault behaviour of SF21 changed as well. The apparent displacements of SF21 in the central area are smaller than those in the western area (Table MIII-2). SF21 and SF22 show larger apparent displacements than the other faults in the entire working area, but the amount of displacement is small compared to the first and third stage (Table MIII-2).

4.2.3 Stage 3

The recent stage, Stage 3, includes sequence 9 and the present (Figs. MIII-5X-XI, MIII-6X-XI). The entire area has experienced significant amounts of continuous extension. The western area (e.g. $\sim 1.2\%$, ~ 70 m) has extended more than the central area (e.g. $\sim 0.7\%$, ~ 30 m) (Table MIII-2). During the deposition of sequence 9 (Figs. MIII-5X, MIII-6X), the western region (Fig. MIII-5X) shows an extension of 1.2% (~ 80 m), which is larger than the total amount of extension during the entire remaining period of fault activity (Figs. MIII-5, MIII-6). Throughout this period, extension continued, though mild, when compared with the previous phases (Figs. MIII-5X–XI, MIII-6X-XI). The respective faults had normal slip components at this stage (Figs. MIII-5X-XI, MIII-6X-XI; Table MIII-2); SF21, SF22, and F242-2 show the largest apparent displacements.

4.2.4 Interim Summary

The tectonic activity of the outer Messina Strait can be subdivided into three stages. During Stage 1 and Stage 3, the area mainly underwent contraction and extension, respectively. In Stage 2, both extension and contraction occurred at low rates. We consider this stage as a period with minor tectonic activity. SF21 has been the most active fault and shows the largest apparent displacements.

4.3 Numerical modelling of tsunami

We modelled possible tsunamis from the newly-discovered faults in the outer Messina Strait and compared the simulated coastal wave heights and arrival times with those observed during the 1908 Messina tsunami.

The fault parameters and extensions outlined in Table MIII-2 and Fig. MIII-2 were used as input parameters for tsunami sources. Four tsunamis scenarios have been modelled, using the following fault parameters: Strike: 83° , dip: 58° , rake: -90° ($=270^\circ$), length: 30 km, width: 15 km, top depth (corresponding to water depth): 1.5 km, and slip: 2, 5, 10, and 15 m. Among these parameters, the dip and the top depth were taken from seismic data. The strike, the length, and the width of the fault zone were estimated by combining seismic and bathymetric data (Fig. MIII-2). The slip is varied, based on a “trial-and-error method”.

Normal fault (rake = -90°) mechanisms were considered for all scenarios as the fault reconstruction (Figs. MIII-5, MIII-6) suggest dominant normal faulting mechanisms in recent times. In our scenarios, the slip amount is ranging from 2 to 15 m (Fig. MIII-7). According to empirical relationships between fault length and slip [WELLS and COPPERSMITH 1994], the maximum predicated slip from a fault with length of 30 km is only ~ 2 m. However, large overall slips of up to 60 m (Table MIII-2) are indicated by the seismic profiles although it is unlikely that such large slips occurred during one or only a few events. However, the seismic profiles (Fig. MIII-3, MIII-4) may suggest that the F-MPS_FZ is susceptible to large slips. This may justify applications of slip values of up to 15 m for fault parameters (Fig. MIII-7c&d).

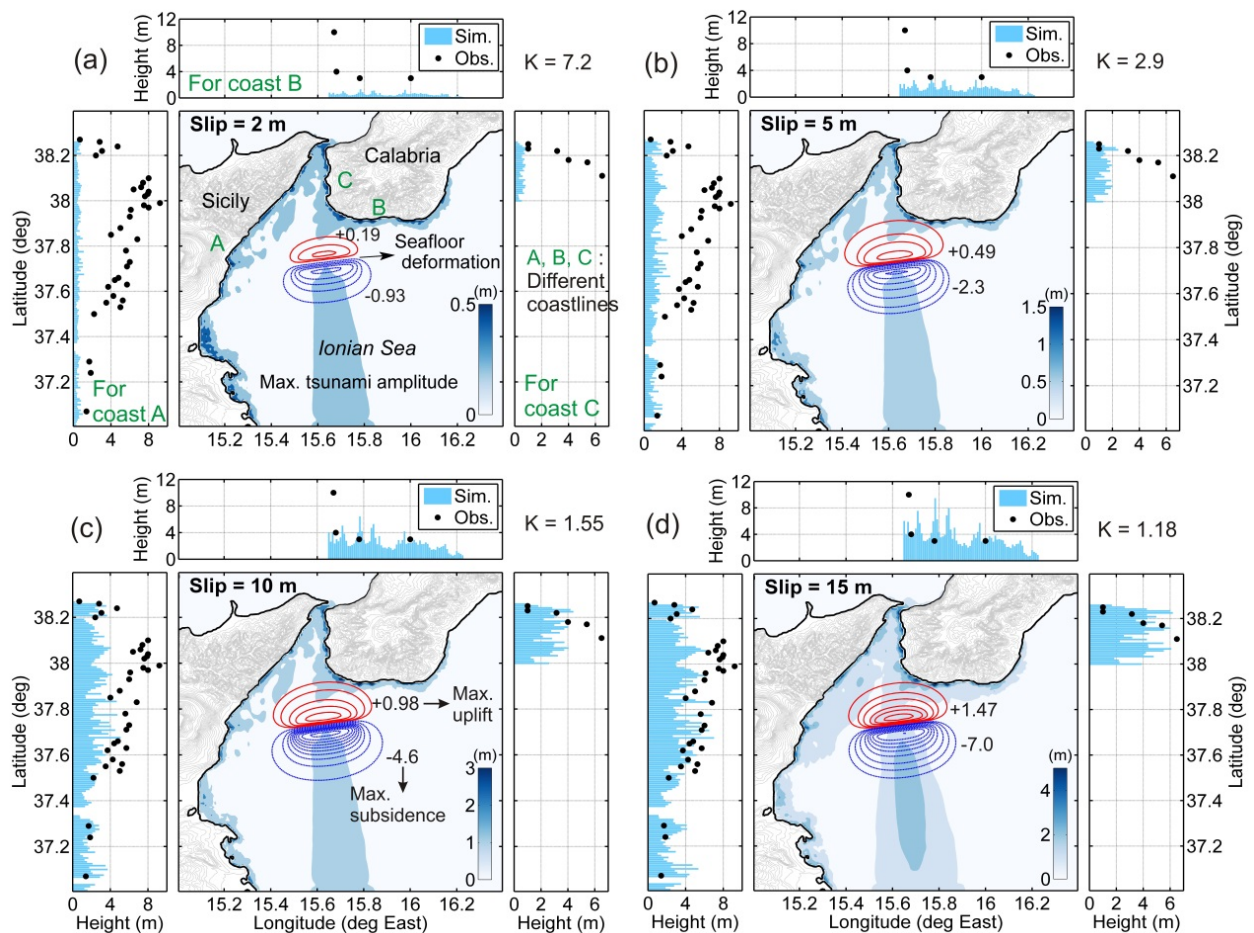


Figure MIII- 7 Results of tsunami simulations for four scenarios with slips of 2 m (a), 5 m (b), 10 m (c) and 15 m (d) and comparisons with observed wave heights. The red and blue contours represent the uplift and subsidence due to the tectonic source, respectively. The colour maps show the distribution of maximum tsunami amplitudes due to each source scenario. The parameter K shows the quality of fit between observations and simulations according to Equ. (1).

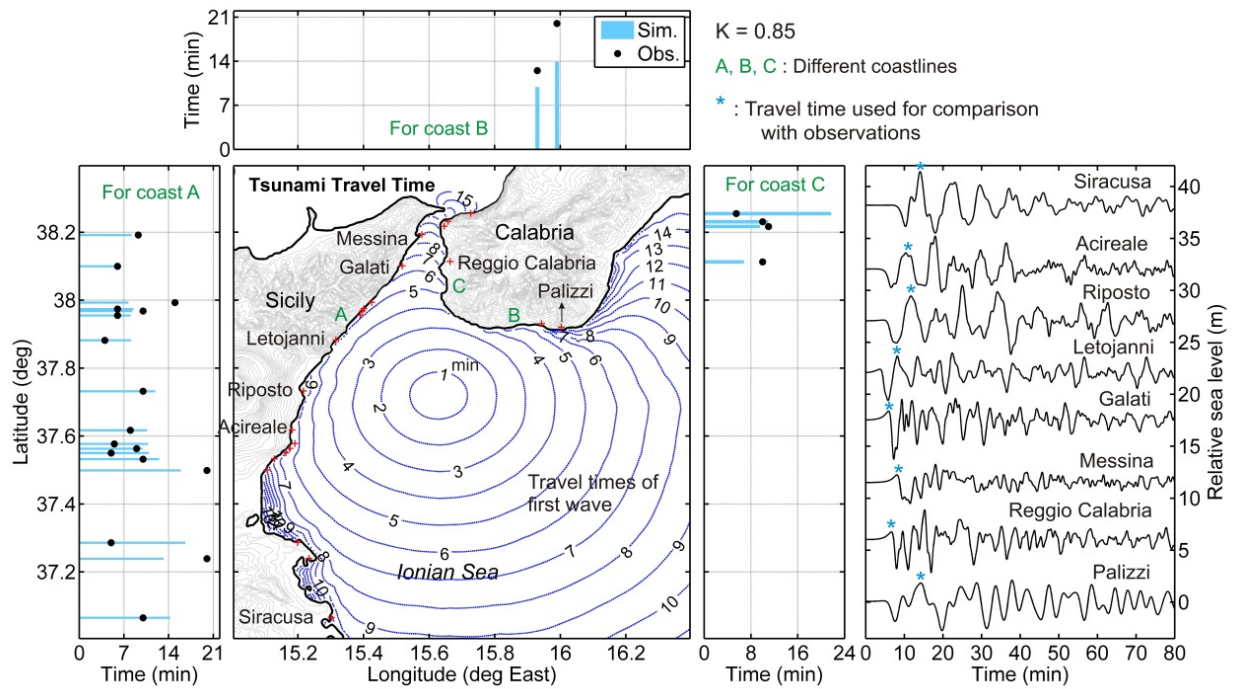


Figure MIII- 8 Tsunami travel times in minutes for scenario (d) shown in Fig. MIII-7. The contours are in minutes and show the arrivals of first tsunami waves. The side plots compare the observed arrival times with the first noticeable peak (with amplitude > 0.5 m) in simulations. The right panel shows some of the simulated waveforms. The parameter K shows the quality of fit between observations and simulations according to Equ. (1).

Figs. MIII-7 and MIII-8 present the results of tsunami simulations, which are compared with both coastal run-up data (Fig. MIII-7) and tsunami arrival times (Fig. MIII-8) observed during the 1908 Messina tsunami as reported by *BARATTA [1910]*. Fig. MIII-7 shows that a fault with a slip of < 5 m would not cause a significant tsunami. According to Figs. MIII-7d and MIII-8, a fault with a slip of 15 m is able to fairly reproduce the run-up heights and arrival times observed during the 1908 Messina tsunami.

5 Discussion

5.1 Quality of the fault reconstruction

Independent reconstructions of the fault activities show comparable results for both profiles presented in this study, i.e. contraction during stage 1, only minor activity during stage 2, and extension during stage 3. Details, however, vary significantly between the profiles. We would like to point out that the reconstruction includes several uncertainties. Depth conversion were done with a constant velocity, and standard parameters were used for the decompaction. Better velocity models and core data would help to overcome these uncertainties.

The calculated amounts of extension/contraction are relatively small. Hence, picking errors will have a significant effect on the calculated amounts. The high-quality seismic data allow tracing reflectors across the faults with high reliability. We picked the same phase for all reflectors but small picking errors will remain. Hence, we consider the small amount of extension/contraction during stage 2 as not relevant. Stage 2 was most likely a transitional period between contraction during stage 1 and extension during stage 3.

5.2 Evolution of the newly-discovered Fiumefreddo - Melito di Porto Salvo Fault Zone in the outer Messina Strait

Unfortunately, no age control is available for any of the picked reflectors. Hence, we cannot link the reconstructed fault history to the overall tectonic evolution of the Messina region. However, in the following we briefly discuss the temporal evolution of the Fiumefreddo - Melito di Porto Salvo Fault Zone (F-MPS_FZ).

The activity of the F-MPS_FZ started latest with formation of the acoustic basement. The fault zone may have been active even longer but older sediments are not imaged by our seismic system. During stage 1, the outer Messina Strait was mainly affected by contraction. Correspondingly, faults in the F-MPS_FZ showed reverse-slip components most of the time. The local tectonic activity in the central part of the outer Strait might be stronger than that in the western part, because SF21 showed larger apparent displacements in its central segment than in its western segment. The relatively steep apparent

dip angles ($>55^\circ$) may indicate that faults in the F-MPS_FZ also had strike-slip components. Hence, the F-MPS_FZ was a transpressional fault zone, indicating that the outer Messina Strait was locally controlled by a transpressional regime during the first stage. We consider stage 2 as a transitional or an adjusting period between early contraction stage and later extension stage. The amounts of the reconstructed contraction or extension are too small to be relevant (see chapter 6 5.1). During stage 3, the outer Messina Strait has been continuously extending. Correspondingly, nearly all faults in the F-MPS_FZ showed normal slip components. SF21 exhibits larger apparent displacements than all other faults.

During the entire reconstruction period, the variations of the fault types and apparent displacements of SF21 were generally consistent with the overall result of the reconstruction. This consistency demonstrates that the activity of SF21 reflects the activity of the F-MPS_FZ. SF21 is the primary fault of and the most important contributor to the F-MPS_FZ in the outer Messina Strait.

5.3 Implications from tsunami modelling

The newly-discovered Fiumefreddo - Melito di Porto Salvo Fault Zone (F-MPS_FZ) was active and characterized by ongoing transtension in recent time. The vertical movements (most of them >10 m, Table MIII-1) of the faults in the F-MPS_FZ seem to be large enough for generating tsunamis.

The largest unknowns are the slip rate of individual faults and how many earthquakes had contributed to the slips of faults. To test different slip values, we applied a trial-and-error method. We examined whether these slip values could generate tsunamis or not. The observed run-up heights and arrival times of the 1908 Messina tsunami were taken as references to test the simulated results. In each case, the slip is assumed to occur in one event.

To examine how much our simulated data fit to the observed data, we applied the parameter K according to the following equation [*SATAKE and TANIOKA 2003*]:

$$\log K = \frac{1}{N} \sum_{i=1}^N \log \left(\frac{Obs_i}{Sim_i} \right) \quad (1)$$

in which, N is the total number of data, Obs_i and Sim_i are the observed and simulated values, respectively. If the observed and simulated values are the same, K will be 1. If K is less than 1, the simulations are understating the observations and vice versa.

The K parameters for the scenario d (Fig. MIII-7d, MIII-8) are 1.18 and 0.85 for the run-up heights and arrival times, respectively, which are closer to 1 when compared with the K values of other scenarios, indicating that the scenario d is more acceptable than other scenarios. One of the main difficulties of other source models proposed for the 1908 Messina tsunami was the lack of match between observations and simulations along the coast of Sicily (coast A in Fig. 7) [PIATANESI *et al.* 1999]. Our scenario gives acceptable results along the coast of Sicily (coast A in Fig. MIII-7d).

Despite the fact that our tsunami models match well with the observed data of the 1908 Messina tsunami and that the location corresponds well with the source area suggested by BILLI *et al.* [2008], we doubt that the F-MPS_FZ was the source of the 1908 Messina tsunami, because the strike of the fault zone contradicts all seismological observations which suggest a N-S-striking fault in the inner Messina Strait [AMORUSO *et al.* 2002b; TINTI and ARMIGLIATO 2003b; ARGNANI *et al.* 2009a]. A slip of 15 m along a relatively short fault (<16 km) is also highly unlikely.

However, we still consider the F-MPS_FZ as a potential hazard, because it is the most obvious tectonic feature in the entire Messina Strait with an escarpment height at the seafloor of up to 60 m. The tsunami modelling suggests that a slip rate of ~2 m would not trigger a significant tsunami but slip rates of ~5 m would result in local run-up heights of more than 2 m. An even higher slip rate increases the estimated tsunami height significantly. The newly-discovered F-MPS_FZ adds a new source candidate for tsunamis in the Messina Strait in Southern Italy.

5.4 Do submarine landslides tsunami triggers exist in the outer Messina Strait?

Since the 1908 Messina earthquake and tsunami, the northern inner Messina Strait was considered to be an area in which the epicentre and the causative fault of the earthquake may be located [TINTI and ARMIGLIATO 2003b]. The run-up heights of the tsunami, however, can be better explained by a source south of this area [BOSCHI *et al.* 1989b]. [OMORI 1911] and TINTI and ARMIGLIATO [2003b] pointed out that the earthquake caused the surface depression but not necessarily the tsunami. Hence, by using the simple backward ray-tracing method, BILLI *et al.* [2008] located the source area of the 1908 Messina tsunami in the outer Messina Strait (Fig. MIII-1a) where we identified the F-MPS_FZ, and postulated that the trigger candidate for the tsunami is a submarine landslide located off Giardini (Fig. MIII-1a).

However, based on our new seismic data, no evidence of slide scarps or slide deposits support the existences of such a large potentially tsunamigenic landslides in this area. The undulations of the uppermost sediment layers of some parts of the area are interpreted as sediment waves/bedforms (Figs. MIII-3b, MIII-4b). The slide crown and body identified by *BILLI et al. [2008]* is a landscape typical for long-term erosion within a canyon environment rather than a very recent and large failure event [*ARGNANI et al. 2009b*] (Figs. MIII-1, MIII-2). Therefore, landslide source for the 1908 tsunami is highly unlikely.

6 Conclusions

Tsunamis are a major threat for the coastlines of Southern Italy as demonstrated by the devastating tsunami following the 1908 Messina earthquake.

In this study, we discovered an E-W-trending fault zone, the Fiumefreddo - Melito di Porto Salvo Fault Zone (F-MPS_FZ), in the outer Messina Strait. It is located in an area proposed as a source area for the 1908 Messina tsunami by Billi et al. (2008) and shows an up to 60 m-high escarpment as prominent surface expression.

Fault activity reconstructions for the F-MPS_FZ suggest an initial tranpressional stage followed by an adjusting period. The recent stage is characterized by ongoing transtension.

The F-MPS_FZ may be a candidate for generating tsunamis. Tsunami modelling results show that a slip rate around 5 m would already generate tsunamis with local run-up heights exceeding 2 m. A fault with a slip of up to 15 m could even generate a tsunami comparable to the 1908 Messina tsunami, though such a scenario is highly unlikely, due to the unrealistically high slip.

We did not find any indications for a tsunamigenic landslide, as suggested by Billi et al. (2008). Although an E-W-trending fault zone contradicts all suggested focal mechanisms for the 1908 Messina tsunami, we still consider the F-MPS_FZ as a potential source for tsunamis in the Messina Strait, Southern Italy, as it is the most obvious tectonic feature in the entire Messina Strait.

7 FINAL CONCLUSIONS AND OUTLOOK

7.1 Conclusions

The analysis of new seismic and hydro-acoustic data allowed i) to characterize the near-surface fault pattern of the inner Messina Strait and to link this fault pattern to the overall geodynamic framework, and ii) to assess the graben structure of the inner Messina Strait, iii) to falsify the proposed submarine Taormina Fault, iv) to analyze the type of faulting and activity of the newly-discovered Fiumefreddo - Melito di Porto Salvo Fault Zone (F-MPS_FZ) in the outer Messina Strait, and v) to assess the tsunami potential of the F-MPS_FZ based on modelled scenarios. The main conclusions of this thesis can be summarized as follows:

i) Near-surface fault pattern of the Messina Strait and its link to the overall geodynamic framework

Several near-surface faults have been identified in the inner Messina Strait. They mainly strike N-S and E-W. N-S-trending near-surface faults are right-lateral transtensional faults distributed along the Messina Canyon and the coastline off southern Calabria. E-W-trending near-surface faults are left-lateral transtensional faults situated in the northern inner Messina Strait off Calabria. This fault pattern fits well to the active stress field: a ca. N115°E horizontal trending minimum compressional stress (σ_3) and a subvertical maximum compressional stress (σ_1), which controls the extension across the Messina Strait, mainly caused by northwestward and northeastward movements of Sicily and Calabria with respect to the Eurasian plate, respectively. The N-S-trending near-surface faults that are located along the coastline off southern Calabria form a group of distributive faults, which could reflect the subsidence of the Strait area.

The N-S trending right-lateral transtensional faults in the central part of the inner Messina Strait fit well to the suggested focal mechanisms of the 1908 Messina earthquake. However, all of these faults show relatively small fault offsets and relatively short/small fault planes (< 15 km in length). Hence, it is unlikely that one of these faults was the master fault of the 1908 Messina Earthquake but they may represent shallow subsurface expressions of deeper and longer faults, which were not imaged due to the limited penetration of the new seismic data

ii) Graben structure of the inner Messina Strait

The new seismic data support the hypothesis that the inner Messina Strait is an angular graben structure as proposed by [MULARGIA *et al.* 1984a]. The Messina Strait graben is bounded by two antithetic normal faulting systems: the northeastern Sicily normal faulting system and the southwestern Calabria normal faulting system. In the graben, the newly-discovered N-S-trending near-surface faults contribute to the development of the master graben and form some secondary grabens, such as Messina Canyon. The formation of the graben structure of the Strait supports that the Messina Strait has experienced extension, which was directly caused by northwestward and northeastward movements of Sicily and Calabria with respect to the Eurasian plate, respectively. The angular shape of the graben is probably generated by the southeastward bending of the inner Calabrian Arc.

iii) Existence of the inferred Taormina Fault

The inferred Taormina Fault (TF) was considered as one of the most hazardous and largest seismic gaps in Italy. However, it has not been imaged on any exist seismic data set, even not in our new seismic data. Hence, the TF may not exist or could not be imaged by means of the new data because i) it is deeply buried without a surface expression on the seafloor or ii) it steeply dips in the area between offshore seismic profiles coverage and the Ionian coastal area of Sicily, which is not covered by the new data. We consider it as unlikely that an active fault does not show any expression in the depth range of our seismic data and that a fault is exactly located in a ~2000 m gap between the coastline and our profile. Hence, we doubt the existence of the TF.

iv) Activity of the newly-discovered Fiumefreddo - Melito di Porto Salvo Fault Zone (F-MPS_FZ) in the outer Messina Strait

A newly-discovered E-W-trending fault zone in the outer Messina Strait is named Fiumefreddo - Melito di Porto Salvo Fault Zone (F-MPS_FZ). It is located in an area identified by *BILLI et al.* [2008] as most likely source area for the 1908 Messina tsunami based on analysing arrival times of the tsunami.

The F-MPS_FZ is interpreted as left-lateral transtensional fault zone. A prominent dominant scarp-like structure (DSS) with heights of up to 60 m represents the surface expression of the master fault of the F-MPS_FZ. The DSS documents the ongoing activity of this fault zone. Based on the reconstruction of the fault activity, the F-MPS_FZ is currently in an extensional phase. The F-MPS_FZ builds an “H” faulting system with two postulated Subduction-Transform Edge Propagator (STEP) faults: the Ionian Fault and the Alfeo-Etna Fault. It may work as a STEP-Connector Fault between the Ionian Fault and the Alfeo-Etna Fault. Two possible models have been put forward for this “H” faulting system: the pull-

apart basin style model and the fault-termination basin style model. The pull-apart basin style model is more reasonable based on all available data.

v) Tsunami potential of the F-MPS_FZ

The F-MPS_FZ in the outer Messina Strait might be a candidate for generating tsunamis. Slip rates around 5 m would generate tsunamis with local run-up heights exceeding 2 m. A slip of up to 15 m could even generate a tsunami comparable to the 1908 Messina tsunami in terms of run-up heights and arrival times. Despite the fact, that such high slip rates are not reasonable, the 60m-high DSS clearly indicates strong vertical movements. It is, however, unlikely that this fault generated the 1908 tsunami because it contradicts all seismological observations, which suggest an N-S-trending fault.

Furthermore, a tsunamigenic submarine landslide proposed by *BILLI et al. [2008]* in the area of the F-MPS_FZ is not imaged on the new seismic data. Tsunamis originating in the outer Messina Strait might be caused by faulting structures such as the F-MPS_FZ, and the F-MPS_FZ needs to be considered as a potential source for tsunamis hitting the coastlines of the Messina Strait.

7.2 Outlook

This thesis contributes to many heavily debated questions related to the tectonics of the Messina Strait. The near surface fault pattern of the Messina Strait was mapped in detail for the first time. The most exciting result of this thesis is probably the discovery and the analysis of the F-MPS_FZ, which shows the most obvious surface expression of any fault in the Messina Strait; it may represent the most active fault zone in the working area. The location of this fault between two STEP faults makes this fault even more interesting as it is interpreted to be a connector between the STEP faults. The new seismic data, however, only allow to scratch the upper most parts of the lithosphere. Many secrets are still hidden in deeper layers, which are not imaged by the new seismic data. Hence, deep penetrating reflection seismic data in combination with the analyzed high-resolution seismic data would allow to characterize the tectonic setting and the exact location and character of deep reaching faults much better. Most interesting features to be discovered include the still unknown location of the seismogenic fault of the 1908 earthquake and the exact structure of the two STEP faults. However, such deep-penetrating reflection data are very complicated to collect in the working area. The small width of the Messina Strait makes it almost impossible to collect long-streamer data crossing major N-S-striking fault. Heavy ship traffic would further complicate data acquisition. In addition, deep penetration is very difficult to access even with large sources. The acoustic basement of the analyzed seismic data is in a pretty shallow depth and characterized by a diffuse zone with no coherent reflections. This zone may be described as substrate, which is very difficult to image due to energy scattering and attenuation. Hence, it may be difficult to image the deeper structure even with large sources.

Another critical knowledge gap is the missing age information of key horizons on the seismic section. Fault reconstruction was done in this thesis, but it is difficult to link the constructed fault behaviour to the overall tectonics due to the missing age information.

APPENDIXES

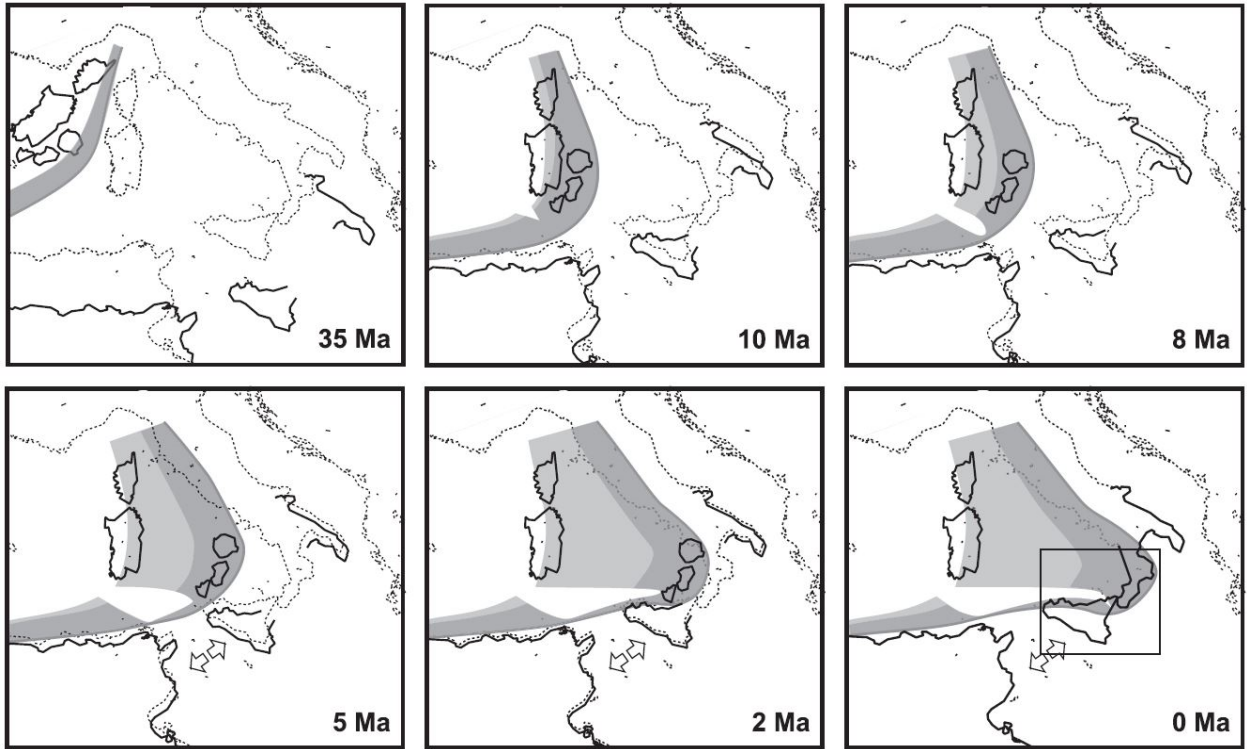


Figure A1 Sketch of the tectonic evolution of the central-western Mediterranean, based on *GOES et al. [2004]*, with the reconstruction of subducted plate geometry. Bold lines mark the reconstructed paleogeography from 35 Ma to present, relative to a fixed Europe. For reference, dotted lines show present-day geography in all panels. The dipping part of the slab is shaded in dark gray, the part that lies flat above 660 km in light gray. A gap (in white) develops in this slab after 15–10 Ma, starting just south of Sardinia. The bold gray line indicates the approximate location of the trench axis (not the deformation front). Extension in the Sicily Channel started around 5–6 Ma.

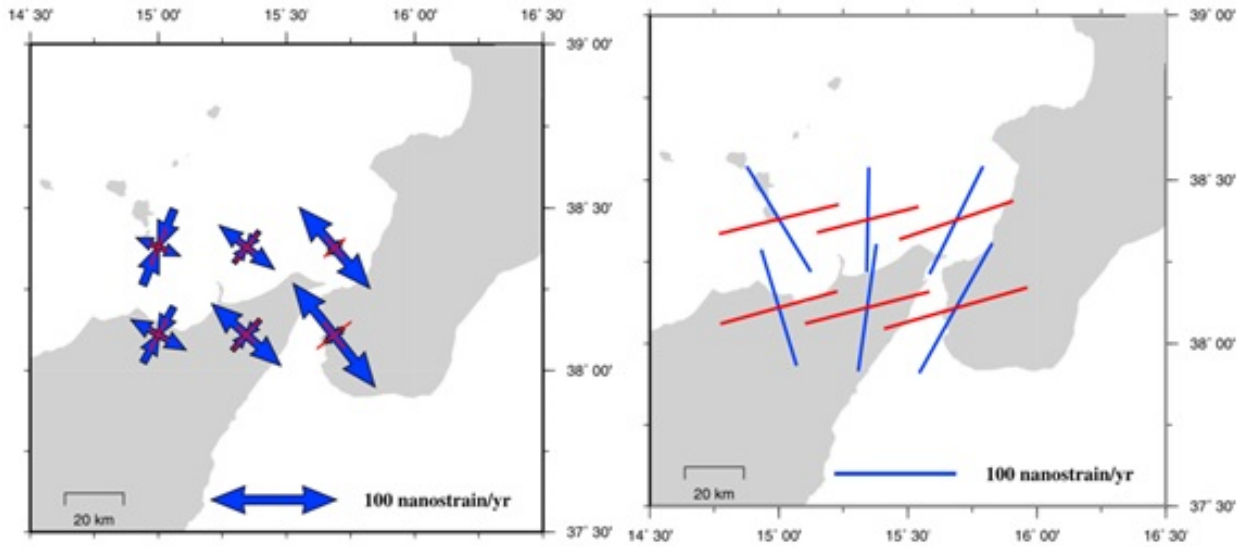


Figure A2 [Left] Principal axes of the horizontal strain rate tensor (in blue) and associated 1 sigma errors (red bars). [Right] The orientation of uniform faulting that can accommodate the strain rate field shown in the left figure. Red lines are faults with a left-lateral component; blue lines are faults with a right-lateral component. Line lengths are equal to the magnitude of the difference between the principal strain rates. Taken from *D'AGOSTINO and SELVAGGI [2004]*.

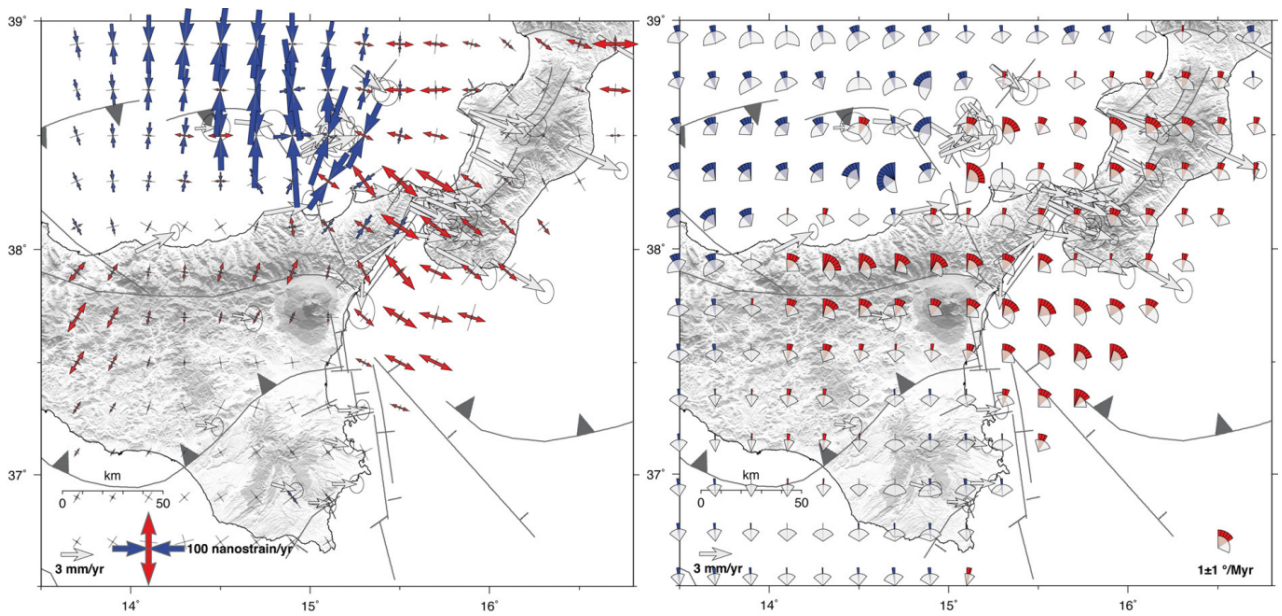


Figure A3 Geodetic strain rate field of Southern Italy computed over a regular $0.2^\circ \times 0.2^\circ$ grid. Taken from *SERPELLONI et al. [2010]*. [Left] Red and blue arrows show extensional and compressional strain rates, respectively. Grey crosses display 1σ uncertainties. [Right] Rotation rates and 1σ uncertainties (grey wedges). Red wedges show clockwise rotations, whereas blue wedges show counter-clockwise rotations. Grey arrows in both panels show GPS velocities with respect to the Nubian plate.

BIBLIOGRAPHY

- ALOISI, M., V. BRUNO, F. CANNAVO, L. FERRANTI, M. MATTIA *et al.*, 2013 Are the source models of the M 7.1 1908 Messina Straits earthquake reliable? Insights from a novel inversion and a sensitivity analysis of levelling data. *Geophysical Journal International* **192**: 1025-1041.
- ALPERS, W., and E. SALUSTI, 1983 Scylla and Charybdis Observed from Space. *Journal of Geophysical Research-Oceans and Atmospheres* **88**: 1800-1808.
- AMORUSO, A., L. CRESCENTINI and R. SCARPA, 2002a Source parameters of the 1908 Messina Straits, Italy, earthquake from geodetic and seismic data. *Journal of Geophysical Research-Solid Earth* **107**.
- AMORUSO, A., L. CRESCENTINI and R. SCARPA, 2002b Source parameters of the 1908 Messina Straits, Italy, earthquake from geodetic and seismic data. *Journal of Geophysical Research: Solid Earth (1978–2012)* **107**: ESE 4-1-ESE 4-11.
- ANTONIOLI, F., L. FERRANTI, K. LAMBECK, S. KERSHAW, V. VERRUBBI *et al.*, 2006a Late Pleistocene to Holocene record of changing uplift rates in southern Calabria and northeastern Sicily (Southern Italy, Central Mediterranean Sea). *Tectonophysics* **422**: 23-40.
- ANTONIOLI, F., S. KERSHAW, P. RENDA, D. RUST, G. BELLUOMINI *et al.*, 2006b Elevation of the last interglacial highstand in Sicily (Italy): a benchmark of coastal tectonics. *Quaternary international* **145**: 3-18.
- ANTONIOLI, F., S. KERSHAW, D. RUST and V. VERRUBBI, 2003 Holocene sea-level change in Sicily and its implications for tectonic models: new data from the Taormina area, northeast Sicily. *Marine Geology* **196**: 53-71.
- ANZIDEI, M., P. BALDI, C. BONINI, G. CASULA, S. GANDOLFI *et al.*, 1998 Geodetic surveys across the Messina Straits (Southern Italy) seismogenetic area. *Journal of Geodynamics* **25**: 85-97.
- ARGNANI, A., 2014 Comment on the article "Propagation of a lithospheric tear fault (STEP) through the western boundary of the Calabrian accretionary wedge offshore eastern Sicily (Southern Italy)" by Gallais *et al.*, 2013 *Tectonophysics*. *Tectonophysics* **610**: 195-199.
- ARGNANI, A., and C. BONAZZI, 2005 Malta Escarpment fault zone offshore eastern Sicily: Pliocene-Quaternary tectonic evolution based on new multichannel seismic data. *Tectonics* **24**.
- ARGNANI, A., G. BRANCOLINI, C. BONAZZI, M. ROVERE, F. ACCAINO *et al.*, 2009a The results of the Taormina 2006 seismic survey: Possible implications for active tectonics in the Messina Straits. *Tectonophysics* **476**: 159-169.
- ARGNANI, A., F. L. CHIOCCI, S. TINTI, A. BOSMAN, M. V. LODI *et al.*, 2009b Comment on "On the cause of the 1908 Messina tsunamis, Southern Italy" by Andrea Billi *et al.* *Geophysical Research Letters* **36**.
- ARGNANI, A., E. SERPELLONI and C. BONAZZI, 2007 Pattern of deformation around the central Aeolian Islands: evidence from multichannel seismics and GPS data. *Terra Nova* **19**: 317-323.
- ARTALE, V., D. LEVI, S. MARULLO and R. SANTOLERI, 1990 Analysis of nonlinear internal waves observed by Landsat thematic mapper. *Journal of Geophysical Research: Oceans (1978–2012)* **95**: 16065-16073.
- ASCIONE, A., S. CIARCIA, V. DI DONATO, S. MAZZOLI and S. VITALE, 2012 The Pliocene-Quaternary wedge-top basins of Southern Italy: an expression of propagating lateral slab tear beneath the Apennines. *Basin Research* **24**: 456-474.
- ATMAOUI, N., N. KUKOWSKI, B. STOCKHERT and D. KONIG, 2006 Initiation and development of pull-apart basins with Riedel shear mechanism: insights from scaled clay experiments. *International Journal of Earth Sciences* **95**: 225-238.

- AZZARO, R., and M. S. BARBANO, 2000 Analysis of the seismicity of Southeastern Sicily: a proposed tectonic interpretation. *Annali Di Geofisica* **43**: 171-188.
- AZZARO, R., and M. S. BARBANO, 2006 The attenuation of seismic intensity in the Etna region and comparison with other Italian volcanic districts.
- AZZARO, R., F. BERNARDINI, R. CAMASSI and V. CASTELLI, 2007 The 1780 seismic sequence in NE Sicily (Italy): shifting an underestimated and mislocated earthquake to a seismically low rate zone. *Natural Hazards* **42**: 149-167.
- BARATTA, M., 1910... *La catastrofe sismica Calabro messinese (28 dicembre 1908)*. Presso la Società geografica italiana.
- BARBERI, F., GASPARI, P., INNOCENT, F. and L. VILLARI, 1973 Volcanism of Southern Tyrrhenian-Sea and Its Geodynamic Implications. *Journal of Geophysical Research* **78**: 5221-5232.
- BASILI, R., G. VALENSISE, P. VANNOLI, P. BURRATO, U. FRACASSI *et al.*, 2008 The Database of Individual Seismogenic Sources (DISS), version 3: Summarizing 20 years of research on Italy's earthquake geology. *Tectonophysics* **453**: 20-43.
- BIANCA, M., C. MONACO, L. TORTORICI and L. CERNOBORI, 1999 Quaternary normal faulting in southeastern Sicily (Italy): A seismic source for the 1693 large earthquake. *Geophysical Journal International* **139**: 370-394.
- BILLI, A., C. FACCENNA, O. BELLIER, L. MINELLI, G. NERI *et al.*, 2011 Recent tectonic reorganization of the Nubia-Eurasia convergent boundary heading for the closure of the western Mediterranean. *Bulletin De La Societe Geologique De France* **182**: 279-303.
- BILLI, A., R. FUNICIELLO, L. MINELLI, C. FACCENNA, G. NERI *et al.*, 2008 On the cause of the 1908 Messina tsunami, Southern Italy. *Geophysical Research Letters* **35**.
- BLUMETTI, A., E. BRUSTIA, V. COMERCI, P. DI MANNA, D. FIORENZA *et al.*, 2008 THE ENVIRONMENTAL EFFECTS OF THE 1908 SOUTHERN CALABRIA-MESSINA EARTHQUAKE (SOUTHERN ITALY). *Annali di geofisica* **15**: 1371-1382.
- BOCCALETTI, M., N. CIARANFI, D. COSENTINO, G. DEIANA, R. GELATI *et al.*, 1990 Palinspastic Restoration and Paleogeographic Reconstruction of the Peri-Tyrrhenian Area during the Neogene. *Palaeogeography Palaeoclimatology Palaeoecology* **77**: 41-&.
- BONARDI, G., W. CAVAZZA, V. PERRONE and S. ROSSI, 2001 Calabria-Peloritani terrane and northern Ionian sea, pp. 287-306 in *Anatomy of an Orogen: The apennines and adjacent mediterranean basins*. Springer.
- BONFIGLIO, L., 1981 Terrazzi marini e depositi continentali quaternari di Taormina (Sicilia). *Quaternaria. Storia Naturale e Culturale del Quaternario Roma* **23**: 81-98.
- BONINI, M., F. SANI, G. MORATTI and M. G. BENVENUTI, 2011 Quaternary evolution of the Lucania Apennine thrust front area (Southern Italy), and its relations with the kinematics of the Adria Plate boundaries. *Journal of Geodynamics* **51**: 125-140.
- BOSCHI, E., D. PANTOSTI and G. VALENSISE, 1989a Modello di sorgente per il terremoto di Messina del 1908 ed evoluzione recente dell'area dello Stretto. *Atti VIII Convegno GNGTS, Roma* **1989**: 245-258.
- BOSCHI, E., D. PANTOSTI and G. VALENSISE, 1989b Modello di sorgente per il terremoto di Messina del 1908 ed evoluzione recente dell'area dello Stretto. *Atti VIII Convegno GNGTS, Roma* **1989**: 245-258.
- BOTTARI, A., C. BOTTARI, P. CARVENI, S. GIACOBBE and N. SPANÒ, 2005 Genesis and geomorphologic and ecological evolution of the Ganzirri salt marsh (Messina, Italy). *Quaternary international* **140**: 150-158.
- BOTTARI, A., P. CAPUANO, G. DE NATALE, P. GASPARI, G. NERI *et al.*, 1989a Source parameters of earthquakes in the Strait of Messina, Italy, during this century. *Tectonophysics* **166**: 221-234.
- BOTTARI, A., P. CAPUANO, G. DENATALE, P. GASPARI, G. NERI *et al.*, 1989b Source Parameters of Earthquakes in the Strait of Messina, Italy, during This Century. *Tectonophysics* **166**: 221-234.

- BOTTARI, A., E. CARAPEZZA, M. CARAPEZZA, P. CARVENI, F. CEFALI *et al.*, 1986 The 1908 Messina Strait Earthquake in the Regional Geostructural Framework. *Journal of Geodynamics* **5**: 275-302.
- BOTTARI, C., A. BOTTARI, P. CARVENI, C. SACCA, U. SPIGO *et al.*, 2008 Evidence of seismic deformation of the paved floor of the decumanus at Tindari (NE, Sicily). *Geophysical Journal International* **174**: 213-222.
- BRANDT, P., A. RUBINO, W. ALPERS and J. O. BACKHAUS, 1997 Internal waves in the Strait of Messina studied by a numerical model and synthetic aperture radar images from the ERS 1/2 satellites. *Journal of Physical Oceanography* **27**: 648-663.
- BUTLER, R. W., and M. GRASSOT, 1993 Tectonic controls on base-level variations and depositional sequences within thrust-top and foredeep basins: examples from the Neogene thrust belt of central Sicily. *Basin Research* **5**: 137-151.
- CACCHIONE, D., L. PRATSON and A. OGDON, 2002 The shaping of continental slopes by internal tides. *Science* **296**: 724-727.
- CAPUANO, P., G. DE NATALE, P. GASPARINI, F. PINGUE and R. SCARPA, 1988 A model for the 1908 Messina Straits (Italy) earthquake by inversion of levelling data. *Bulletin of the Seismological Society of America* **78**: 1930-1947.
- CAPUTO, M., 1979 Seismicity in the Straits of Messina. L'attraversamento dello Stretto di Messina e la sua fattibilità: 101-117.
- CAPUTO, M., L. PIERI, M. BARBARELLA, A. GUBELLINI, P. RUSSO *et al.*, 1981 Geophysical and Geodetic Observations in the Messina Straits. *Tectonophysics* **74**: 147-154.
- CARMINATI, E., M. LUSTRINO and C. DOGLIONI, 2012 Geodynamic evolution of the central and western Mediterranean: Tectonics vs. igneous petrology constraints. *Tectonophysics* **579**: 173-192.
- CARMINATI, E., M. J. R. WORTEL, W. SPAKMAN and R. SABADINI, 1998 The role of slab detachment processes in the opening of the western-central Mediterranean basins: some geological and geophysical evidence. *Earth and Planetary Science Letters* **160**: 651-665.
- CASAGRANDE, G., A. W. VARNAS, T. FOLEGOT and Y. STEPHAN, 2010 An original method for characterizing internal waves. *Ocean Modelling* **31**: 1-8.
- CASAGRANDE, G., A. W. VARNAS, Y. STEPHAN and T. FOLEGOT, 2009 Genesis of the coupling of internal wave modes in the Strait of Messina. *Journal of Marine Systems* **78**: S191-S204.
- CASALBORE, D., F. L. CHIOCCI, G. S. MUGNOZZA, P. TOMMASI and A. SPOSATO, 2011 Flash-flood hyperpycnal flows generating shallow-water landslides at Fiumara mouths in Western Messina Strait (Italy). *Marine Geophysical Research* **32**: 257-271.
- CATALANO, R., P. DISTEFANO, A. SULLI and F. P. VITALE, 1996 Paleogeography and structure of the central Mediterranean: Sicily and its offshore area. *Tectonophysics* **260**: 291-323.
- CATALANO, S., and G. DE GUIDI, 2003 Late Quaternary uplift of northeastern Sicily: relation with the active normal faulting deformation. *Journal of Geodynamics* **36**: 445-467.
- CATALANO, S., G. DE GUIDI, C. MONACO, G. TORTORICI and L. TORTORICI, 2003 Long-term behaviour of the late Quaternary normal faults in the Straits of Messina area (Calabrian arc): structural and morphological constraints. *Quaternary International* **101**: 81-91.
- CATALANO, S., G. DE GUIDI, C. MONACO, G. TORTORICI and L. TORTORICI, 2008 Active faulting and seismicity along the Siculo-Calabrian Rift Zone (Southern Italy). *Tectonophysics* **453**: 177-192.
- CHIARABBA, C., L. JOVANE and R. DISTEFANO, 2005 A new view of Italian seismicity using 20 years of instrumental recordings. *Tectonophysics* **395**: 251-268.
- CHIOCCI, F. L., and D. RIDENTE, 2011 Regional-scale seafloor mapping and geohazard assessment. The experience from the Italian project MaGIC (Marine Geohazards along the Italian Coasts). *Marine Geophysical Research* **32**: 13-23.
- COLANTONI, P., 1987 Marine geology of the Strait of Messina. Le Déroit de Messine (Italie) Évolution Tectono-Sédimentaire Récente (Pliocène et Quaternaire et Environmmt Actuel): 191-210.

- CONWAY, K. W., J. V. BARRIE, K. PICARD and B. D. BORNHOLD, 2012 Submarine channel evolution: active channels in fjords, British Columbia, Canada. *Geo-Marine Letters* **32**: 301-312.
- CPTIWORKINGGROUP., 2004 Catalogo Parametrico dei Terremoti Italiani, pp., <http://emidius.mi.ingv.it/CPTI/>.
- D'AGOSTINO, N., A. AVALLONE, D. CHELONI, E. D'ANASTASIO, S. MANTENUTO *et al.*, 2008 Active tectonics of the Adriatic region from GPS and earthquake slip vectors. *Journal of Geophysical Research-Solid Earth* **113**.
- D'AGOSTINO, N., E. D'ANASTASIO, A. GERVASI, I. GUERRA, M. R. NEDIMOVIC *et al.*, 2011 Forearc extension and slow rollback of the Calabrian Arc from GPS measurements. *Geophysical Research Letters* **38**.
- D'AGOSTINO, N., and G. SELVAGGI, 2004 Crustal motion along the Eurasia-Nubia plate boundary in the Calabrian Arc and Sicily and active extension in the Messina Straits from GPS measurements. *Journal of Geophysical Research-Solid Earth* **109**.
- D'AMICO, C., A. MESSINA, G. PUGLISI, A. ROTTURA and S. RUSSO, 1973 Confronti petrografici nel cristallino delle due sponde dello Stretto di Messina; implicazioni geodinamiche. *Bollettino della Societa Geologica Italiana* **92**: 939-953.
- D'AMICO, S., B. ORECCHIO, D. PRESTI, A. GERVASI, L. ZHU *et al.*, 2011 Testing the stability of moment tensor solutions for small earthquakes in the Calabro-Peloritan Arc region (Southern Italy). *Bollettino Di Geofisica Teorica Ed Applicata* **52**: 283-298.
- D'AMICO, S., B. ORECCHIO, D. PRESTI, L. P. ZHU, R. B. HERRMANN *et al.*, 2010 Broadband waveform inversion of moderate earthquakes in the Messina Straits, Southern Italy. *Physics of the Earth and Planetary Interiors* **179**: 97-106.
- DE NATALE, G., and F. PINGUE, 1991 A variable slip fault model for the 1908 Messina Straits (Italy) earthquake, by inversion of levelling data. *Geophysical Journal International* **104**: 73-84.
- DEFANT, A., 1940 Scilla e Cariddi e le correnti di marea nello Stretto di Messina. *Geofisica pura e applicata* **2**: 93-112.
- DEMETS, C., R. G. GORDON and D. F. ARGUS, 2010 Geologically current plate motions. *Geophysical Journal International* **181**: 1-80.
- DENATALE, G., and F. PINGUE, 1991 A Variable Slip Fault Model for the 1908 Messina Straits (Italy) Earthquake, by Inversion of Leveling Data. *Geophysical Journal International* **104**: 73-84.
- DEVOTI, J. A., D. W. ROSENTHAL, R. WU, A. L. ABRAMSON, B. M. STEINBERG *et al.*, 2008 Immune dysregulation and tumor-associated gene changes in recurrent respiratory papillomatosis: A paired microarray analysis. *Molecular Medicine* **14**: 608-617.
- DEVOTI, R., A. ESPOSITO, G. PIETRANTONIO, A. R. PISANI and F. RIGUZZI, 2011 Evidence of large scale deformation patterns from GPS data in the Italian subduction boundary. *Earth and Planetary Science Letters* **311**: 230-241.
- DI STEFANO, G., 1907 I pretesi grandi fenomeni di carreggiamento in Sicilia. *Rend. R. Acc. Lincei Cl. Sc. Fis. Mat. Nat* **16**: 375-381.
- DOGLIONI, C., F. INNOCENTI and G. MARIOTTI, 2001 Why Mt Etna? *Terra Nova* **13**: 25-31.
- DOGLIONI, C., M. LIGI, D. SCROCCA, S. BIGI, G. BORTOLUZZI *et al.*, 2012 The tectonic puzzle of the Messina area (Southern Italy): Insights from new seismic reflection data. *Scientific Reports* **2**.
- FACCENNA, C., T. W. BECKER, F. P. LUCENTE, L. JOLIVET and F. ROSSETTI, 2001 History of subduction and back-arc extension in the Central Mediterranean. *Geophysical Journal International* **145**: 809-820.
- FACCENNA, C., L. JOLIVET, C. PIROMALLO and A. MORELLI, 2003 Subduction and the depth of convection in the Mediterranean mantle. *Journal of Geophysical Research-Solid Earth* **108**.
- FACCENNA, C., P. MOLIN, B. ORECCHIO, V. OLIVETTI, O. BELLIER *et al.*, 2011 Topography of the Calabria subduction zone (Southern Italy): Clues for the origin of Mt. Etna. *Tectonics* **30**.

- FACCENNA, C., C. PIROMALLO, A. CRESPO-BLANC, L. JOLIVET and F. ROSSETTI, 2004 Lateral slab deformation and the origin of the western Mediterranean arcs. *Tectonics* **23**.
- FARRE, J. A., 1983 Breaching the shelfbreak: passage from youthful to mature phase in submarine canyon evolution.
- FAVALLI, M., E. BOSCHI, F. MAZZARINI and M. T. PARESCHI, 2009a Seismic and landslide source of the 1908 Straits of Messina tsunami (Sicily, Italy). *Geophysical Research Letters* **36**.
- FAVALLI, M., E. BOSCHI, F. MAZZARINI and M. T. PARESCHI, 2009b Seismic and landslide source of the 1908 Straits of Messina tsunami (Sicily, Italy). *Geophysical Research Letters* **36**.
- FERRANTI, L., C. MONACO, F. ANTONIOLI, L. MASCHIO, S. KERSHAW *et al.*, 2007 The contribution of regional uplift and coseismic slip to the vertical crustal motion in the Messina Straits, Southern Italy: Evidence from raised Late Holocene shorelines. *Journal of Geophysical Research-Solid Earth* **112**.
- FERRANTI, L., C. MONACO, D. MORELLI, F. ANTONIOLI and L. MASCHIO, 2008 Holocene activity of the Scilla Fault, Southern Calabria: Insights from coastal morphological and structural investigations. *Tectonophysics* **453**: 74-93.
- FIRTH, C., I. STEWART, W. MCGUIRE, S. KERSHAW and C. VITA-FINZI, 1996 Coastal elevation changes in eastern Sicily: implications for volcano instability at Mount Etna. Geological Society, London, Special Publications **110**: 153-167.
- FREPOLI, A., and A. AMATO, 2000 Fault plane solutions of crustal earthquakes in Southern Italy (1988-1995): seismotectonic implications.
- GALLAIS, F., D. GRAINDORGE, M.-A. GUTSCHER and D. KLAESCHEN, 2013 Propagation of a lithospheric tear fault (STEP) through the western boundary of the Calabrian accretionary wedge offshore eastern Sicily (Southern Italy). *Tectonophysics* **602**: 141-152.
- GALLI, P., F. GALADINI and D. PANTOSTI, 2008 Twenty years of paleoseismology in Italy. *Earth-Science Reviews* **88**: 89-117.
- GERARDI, F., M. S. BARBANO, P. M. DE MARTINI and D. PANTOSTI, 2008 Discrimination of Tsunami Sources (Earthquake versus Landslide) on the Basis of Historical Data in Eastern Sicily and Southern Calabria. *Bulletin of the Seismological Society of America* **98**: 2795-2805.
- GHISETTI, F., 1984a Recent Deformations and the Seismogenic Source in the Messina Strait (Southern Italy). *Tectonophysics* **109**: 191-208.
- GHISETTI, F., 1984b Recent deformations and the seismogenic source in the Messina Strait (Southern Italy). *Tectonophysics* **109**: 191-208.
- GHISETTI, F., 1992a Fault parameters in the Messina Strait (Southern Italy) and relations with the seismogenic source. *Tectonophysics* **210**: 117-133.
- GHISETTI, F., 1992b Fault Parameters in the Messina Strait (Southern Italy) and Relations with the Seismogenic Source. *Tectonophysics* **210**: 117-133.
- GHISETTI, F., and L. VEZZANI, 1982 Different Styles of Deformation in the Calabrian Arc (Southern Italy) Implications for a Seismotectonic Zoning. *Tectonophysics* **85**: 149-165.
- GHISETTI, F., and L. VEZZANI, 1984 Thin-skinned deformations of the western Sicily thrust belt and relationships with crustal shortening; mesostructural data on the Mt. Kumeta-Alcantara fault zone and related structures. *Bollettino della Societa Geologica Italiana* **103**: 129-157.
- GOES, S., D. GIARDINI, S. JENNY, C. HOLLENSTEIN, H. G. KAHLE *et al.*, 2004 A recent tectonic reorganization in the south-central Mediterranean. *Earth and Planetary Science Letters* **226**: 335-345.
- GOSWAMI, R., N. C. MITCHELL, A. ARGNANI and S. H. BROCKLEHURST, 2014 Geomorphology of the western Ionian Sea between Sicily and Calabria, Italy. *Geo-Marine Letters* **34**: 419-433.
- GOTO, C., Y. OGAWA, N. SHUTO and F. IMAMURA, 1997 *IUGG/IOC time project: Numerical method of tsunami simulation with the leap-frog scheme*. Unesco.

- GOVERS, R., and M. J. R. WORTEL, 2005 Lithosphere tearing at STEP faults: Response to edges of subduction zones. *Earth and Planetary Science Letters* **236**: 505-523.
- GROSS, F., S. KRASTEL, F. L. CHIOCCI, D. RIDENTE, J. BIALAS *et al.*, 2014 Evidence for Submarine Landslides Offshore Mt. Etna, Italy, pp. 307-316 in *Submarine Mass Movements and Their Consequences*. Springer.
- GUARNIERI, P., 2006 Plio-Quaternary segmentation of the south Tyrrhenian forearc basin. *International Journal of Earth Sciences* **95**: 107-118.
- GUARNIERI, P., and C. PIRROTTA, 2008 The response of drainage basins to the late Quaternary tectonics in the Sicilian side of the Messina Strait (NE Sicily). *Geomorphology* **95**: 260-273.
- GUEGUEN, E., C. DOGLIONI and M. FERNANDEZ, 1998 On the post-25 Ma geodynamic evolution of the western Mediterranean. *Tectonophysics* **298**: 259-269.
- GVIRTZMAN, Z., and A. NUR, 2001 Residual topography, lithospheric structure and sunken slabs in the central Mediterranean. *Earth and Planetary Science Letters* **187**: 117-130.
- HEIDARZADEH, M., M. D. PIROOZ, N. H. ZAKER and A. C. YALCINER, 2009 Preliminary estimation of the tsunami hazards associated with the Makran subduction zone at the northwestern Indian Ocean. *Natural hazards* **48**: 229-243.
- HIRN, A., R. NICOLICH, J. GALLART, M. LAIGLE and L. CERNOBORI, 1997 Roots of Etna volcano in faults of great earthquakes. *Earth and Planetary Science Letters* **148**: 171-191.
- HOLLENSTEIN, C., H. G. KAHLE, A. GEIGER, S. JENNY, S. GOES *et al.*, 2003 New GPS constraints on the Africa-Eurasia plate boundary zone in Southern Italy. *Geophysical Research Letters* **30**.
- JACQUES, E., C. MONACO, P. TAPPONNIER, L. TORTORICI and T. WINTER, 2001 Faulting and earthquake triggering during the 1783 Calabria seismic sequence. *Geophysical Journal International* **147**: 499-516.
- KEETLEY, J., and K. HILL, 2000 3D structural modeling of the Kutubu oilfields, Papua New Guinea, pp. 1446 in *American Association of Petroleum Geologists International Conference and Exhibition; Abstracts*.
- KRASTEL, S., C. ADAMI, J. BEIER, J. BIALAS, S. BIGELLA *et al.*, 2014 Seismogenic faults, landslides, and associated tsunamis off Southern Italy - Cruise No. M86/2 - December 27, 2011 - January 17, 2012 - Cartagena (Spain) - Brindisi (Italy) 10.2312/cr_m86_2.
- LAMBECK, K., and A. PURCELL, 2005 Sea-level change in the Mediterranean Sea since the LGM: model predictions for tectonically stable areas. *Quaternary Science Reviews* **24**: 1969-1988.
- LAVECCHIA, G., F. FERRARINI, R. DE NARDIS, F. VISINI and M. S. BARBANO, 2007 Active thrusting as a possible seismogenic source in Sicily (Southern Italy): Some insights from integrated structural-kinematic and seismological data. *Tectonophysics* **445**: 145-167.
- MALINVERNO, A., and W. B. F. RYAN, 1986 Extension in the Tyrrhenian Sea and Shortening in the Apennines as Result of Arc Migration Driven by Sinking of the Lithosphere. *Tectonics* **5**: 227-245.
- MARIOTTI, G., and C. DOGLIONI, 2000 The dip of the foreland monocline in the Alps and Apennines. *Earth and Planetary Science Letters* **181**: 191-202.
- MATTIA, M., M. PALANO, V. BRUNO and F. CANNAVO, 2009 Crustal motion along the Calabro-Peloritano Arc as imaged by twelve years of measurements on a dense GPS network. *Tectonophysics* **476**: 528-537.
- MERCALLI, G., 1909 *Contributo allo studio del terremoto calabro-messinese del 28 dicembre 1908*. Cooperativa tipografica.
- MIALL, A. D., 2000 Suggestions for researching and publishing regional stratigraphic research. *Sedimentary Geology* **132**: 1-3.
- MICHELINI, A., A. LOMAX, A. NARDI, A. ROSSI, B. PALOMBO *et al.*, 2005 A modern re-examination of the locations of the 1905 Calabria and the 1908 Messina Straits earthquakes, pp. 07909 in *Geophysical Research Abstracts*.

- MITCHELL, N. C., 2005 Interpreting long-profiles of canyons in the USA Atlantic continental slope. *Marine Geology* **214**: 75-99.
- MONACO, C., P. TAPPONNIER, L. TORTORICI and P. Y. GILLOT, 1997 Late Quaternary slip rates on the Acireale-Piedimonte normal faults and tectonic origin of Mt. Etna (Sicily). *Earth and Planetary Science Letters* **147**: 125-139.
- MONACO, C., and L. TORTORICI, 1995 Tectonic Role of Ophiolite-Bearing Terranes in the Development of the Southern Apennines Orogenic Belt. *Terra Nova* **7**: 153-160.
- MONACO, C., and L. TORTORICI, 2000a Active faulting in the Calabrian arc and eastern Sicily. *Journal of Geodynamics* **29**: 407-424.
- MONACO, C., and L. TORTORICI, 2000b Active faulting in the Calabrian arc and eastern Sicily. *Journal of Geodynamics* **29**: 407-424.
- MONACO, C., and L. TORTORICI, 2004 Faulting and effects of earthquakes on Minoan archaeological sites in Crete (Greece). *Tectonophysics* **382**: 103-116.
- MONACO, C., and L. TORTORICI, 2007 Active faulting and related tsunamis in eastern Sicily and southwestern Calabria. *Bollettino Di Geofisica Teorica Ed Applicata* **48**: 163-184.
- MONACO, C., L. TORTORICI, R. NICOLICH, L. CERNOBORI and M. COSTA, 1996 From collisional to rifted basins: An example from the southern Calabrian arc (Italy). *Tectonophysics* **266**: 233-249.
- MONTENAT, C., P. BARRIER and P. O. DESTEVOU, 1991 Some Aspects of the Recent Tectonics in the Strait of Messina, Italy. *Tectonophysics* **194**: 203-215.
- MONTONE, P., A. AMATO, A. FREPOLI, M. MARIUCCI and M. CESARO, 1997 Crustal stress regime in Italy. *Annals of Geophysics* **40**.
- MONTONE, P., M. T. MARIUCCI, S. PONDRELLI and A. AMATO, 2004 An improved stress map for Italy and surrounding regions (central Mediterranean). *Journal of Geophysical Research: Solid Earth* (1978–2012) **109**.
- MORGAN, J. K., E. SILVER, A. CAMERLENGHI, B. DUGAN, S. KIRBY *et al.*, 2009 Addressing geohazards through ocean drilling. *Sci Drill* **7**: 15-30.
- MULARGIA, F., P. BALDI, V. ACHILLI and F. BROCCIO, 1984a Recent Crustal Deformations and Tectonics of the Messina Strait Area. *Geophysical Journal of the Royal Astronomical Society* **76**: 369-381.
- MULARGIA, F., P. BALDI, V. ACHILLI and F. BROCCIO, 1984b Recent crustal deformations and tectonics of the Messina Strait area. *Geophysical Journal International* **76**: 369-381.
- MULARGIA, F., and E. BOSCHI, 1983 The 1908 Messina earthquake and related seismicity, pp. 493-518 in *Proceedings of the International School of Physics, Enrico Fermi*.
- MULDER, T., and J. P. M. SYVITSKI, 1995 Turbidity Currents Generated at River Mouths during Exceptional Discharges to the World Oceans. *Journal of Geology* **103**: 285-299.
- NERI, G., B. ORECCHIO, C. TOTARO, G. FALCONE and D. PRESTI, 2009 Subduction Beneath Southern Italy Close the Ending: Results from Seismic Tomography. *Seismological Research Letters* **80**: 63-70.
- NERI, M., V. ACOCELLA and B. BEHNCKE, 2004 The role of the Pernicana Fault System in the spreading of Mt. Etna (Italy) during the 2002–2003 eruption. *Bulletin of Volcanology* **66**: 417-430.
- OGNIBEN, L., A. PRATURLON and M. PAROTTO, 1973 *Structural Model of Italy: Scale 1: 1 000 000*. Grafica Editoriale Cartografica.
- OKADA, Y., 1985 Surface deformation due to shear and tensile faults in a half-space. *Bulletin of the seismological society of America* **75**: 1135-1154.
- OKAL, E. A., and C. E. SYNOLAKIS, 2003 A theoretical comparison of tsunamis from dislocations and landslides. *Pure and Applied Geophysics* **160**: 2177-2188.
- OLIVETTI, V., M. L. BALESTRIERI, C. FACCENNA, F. M. STUART and G. VIGNAROLI, 2010 Middle Miocene out-of-sequence thrusting and successive exhumation in the Peloritani Mountains,

- Sicily: Late stage evolution of an orogen unraveled by apatite fission track and (U-Th)/He thermochronometry. *Tectonics* **29**.
- OMORI, F., 1910 On the foreshocks of large earthquakes. *Rep. Imp. Earthq. Inves. Comm. A* **68**: 31-38.
- OMORI, F., 1911 On the recent sea-level variation at the Italian and Austrian mareograph stations, and on the cause of the Messina-Reggio Earthquake of 1908.
- PALANO, M., F. CANNAVO, L. FERRANTI, M. MATTIA and M. E. MAZZELLA, 2011 Strain and stress fields in the Southern Apennines (Italy) constrained by geodetic, seismological and borehole data. *Geophysical Journal International* **187**: 1270-1282.
- PALANO, M., L. FERRANTI, C. MONACO, M. MATTIA, M. ALOISI *et al.*, 2012 GPS velocity and strain fields in Sicily and southern Calabria, Italy: updated geodetic constraints on tectonic block interaction in the central Mediterranean. *Journal of Geophysical Research: Solid Earth* (1978–2012) **117**.
- PATACCA, E., R. SARTORI and P. SCANDONE, 1990 Tyrrhenian basin and Apenninic arcs: kinematic relations since late Tortonian times. *Mem. Soc. Geol. It* **45**: 425-451.
- PATACCA, E., and P. SCANDONE, 2007 Geology of the southern Apennines. *Bollettino della Società Geologica Italiana* **7**: 75-119.
- PEPE, F., G. BERTOTTI, F. CELLA and E. MARSELLA, 2000 Rifted margin formation in the south Tyrrhenian Sea: A high-resolution seismic profile across the north Sicily passive continental margin. *Tectonics* **19**: 241-257.
- PIATANESI, A., S. TINTI and E. BORTOLUCCI, 1999 Finite-element simulations of the 28 December 1908 Messina Straits (Southern Italy) tsunamis. *Physics and Chemistry of the Earth Part a-Solid Earth and Geodesy* **24**: 145-150.
- PINO, N. A., D. GIARDINI and E. BOSCHI, 2000 The December 28, 1908, Messina Straits, Southern Italy, earthquake: Waveform modeling of regional seismograms. *Journal of Geophysical Research-Solid Earth* **105**: 25473-25492.
- PINO, N. A., A. PIATANESI, G. VALENSISE and E. BOSCHI, 2009a The 28 December 1908 Messina Straits Earthquake (M(w)7.1): A Great Earthquake throughout a Century of Seismology. *Seismological Research Letters* **80**: 243-259.
- PINO, N. A., A. PIATANESI, G. VALENSISE and E. BOSCHI, 2009b The 28 December 1908 Messina Straits earthquake (Mw 7.1): A great earthquake throughout a century of seismology. *Seismological Research Letters* **80**: 243-259.
- PIPER, D. J. W., and W. R. NORMARK, 2009 Processes That Initiate Turbidity Currents and Their Influence on Turbidites: A Marine Geology Perspective. *Journal of Sedimentary Research* **79**: 347-362.
- PLATANIA, G., 1909 *Il maremoto dello stretto di Messina del 28 dicembre 1908*. società tipografica modenese.
- POLONIA, A., L. TORELLI, L. GASPERINI, S. ROMANO, S. VAIANI *et al.*, 2014 Active tectonics and seismic/tsunami hazard in the Messina Straits region: the Ionian and Alfeo/Etna fault systems. http://www.researchgate.net/profile/Luigi_Torelli/publication/269099383_Active_Tectonics_and_SeismicTsunami_Hazard_in_the_Messinian_Straits_Region_the_Ionian_and_AlfeoEtna_Fault_System_Atti_del_33_Convegno_Nazionale_GNGTS_Bologna_25-27_Novembre_2014_Tema_1_Geodinamica163-168/links/548074540cf2ccc7f8bd0559.pdf.
- POLONIA, A., L. TORELLI, P. MUSSONI, L. GASPERINI, A. ARTONI *et al.*, 2011a The Calabrian Arc subduction complex in the Ionian Sea: Regional architecture, active deformation, and seismic hazard. *Tectonics* **30**.
- POLONIA, A., L. TORELLI, P. MUSSONI, L. GASPERINI, A. ARTONI *et al.*, 2011b The Calabrian Arc subduction complex in the Ionian Sea: Regional architecture, active deformation, and seismic hazard. *Tectonics* **30**.

- PONDRELLI, S., S. SALIMBENI, G. EKSTROM, A. MORELLI, P. GASPERINI *et al.*, 2006 The Italian CMT dataset from 1977 to the present. *Physics of the Earth and Planetary Interiors* **159**: 286-303.
- RIDENTE, D., E. MARTORELLI, A. BOSMAN and F. L. CHIOCCI, 2014 High-resolution morpho-bathymetric imaging of the Messina Strait (Southern Italy). New insights on the 1908 earthquake and tsunami. *Geomorphology* **208**: 149-159.
- RIUSCETTI, M., and R. SCHICK, 1975 Earthquakes and tectonics in Southern Italy. *Boll. Geofis. teor. appl* **17**: 59-78.
- RUST, D., and S. KERSHAW, 2000 Holocene tectonic uplift patterns in northeastern Sicily: evidence from marine notches in coastal outcrops. *Marine Geology* **167**: 105-126.
- RYAN, W. B., and B. C. HEEZEN, 1965 Ionian Sea submarine canyons and the 1908 Messina turbidity current. *Geological Society of America Bulletin* **76**: 915-932.
- SANTORO, V. C., E. AMORE, L. CAVALLARO, G. COZZO and E. FOTI, 2002 Sand Waves in the Messina Strait, Italy. *Journal of Coastal Research*, <Go to ISI>://WOS:000209071900069: 640-653.
- SATAKE, K., and Y. TANIOKA, 2003 The July 1998 Papua New Guinea earthquake: Mechanism and quantification of unusual tsunami generation. *Pure and Applied Geophysics* **160**: 2087-2118.
- SCANDONE, R., F. BELLUCCI, L. LIRER and G. ROLANDI, 1991 The structure of the Campanian Plain and the activity of the Neapolitan volcanoes (Italy). *Journal of Volcanology and Geothermal Research* **48**: 1-31.
- SCARFI, L., H. LANGER and A. SCALTRITO, 2009 Seismicity, seismotectonics and crustal velocity structure of the Messina Strait (Italy). *Physics of the Earth and Planetary Interiors* **177**: 65-78.
- SCHICK, R., B. GEOPHYSIKER, R. SCHICK, F. GEOPHYSICIST, R. SCHICK *et al.*, 1977 *Eine seismotektonische bearbeitung des erdbebens von Messina im jahre 1908*. Bundesanstalt für Geowissenschaften und Rohstoffe.
- SCROCCA, D., E. CARMINATI and C. DOGLIONI, 2005 Deep structure of the southern Apennines, Italy: Thin-skinned or thick-skinned? *Tectonics* **24**.
- SEGUENZA, G., 1880 *Le formazioni terziarie nella provincia di Reggio (Calabria)*. Salviucci.
- SELLI, R., F. LUCCHINI, P. ROSSI, C. SAVELLI and M. DELMONTE, 1979 Geology and Petrochemistry of the Central Tyrrhenian Volcanos'. *Rapp. Comm. Int. Met. Medit* **25**: 26-61.
- SELVAGGI, G., 1998 Spatial distribution of horizontal seismic strain in the Apennines from historical earthquakes. *Annals of Geophysics* **41**.
- SERPELLONI, E., M. ANZIDEI, P. BALDI, G. CASULA and A. GALVANI, 2005 Crustal velocity and strain-rate fields in Italy and surrounding regions: new results from the analysis of permanent and non-permanent GPS networks. *Geophysical Journal International* **161**: 861-880.
- SERPELLONI, E., R. BÜRGMANN, M. ANZIDEI, P. BALDI, B. MASTROLEMBO VENTURA *et al.*, 2010 Strain accumulation across the Messina Straits and kinematics of Sicily and Calabria from GPS data and dislocation modeling. *Earth and Planetary Science Letters* **298**: 347-360.
- SERPELLONI, E., G. VANNUCCI, S. PONDRELLI, A. ARGNANI, G. CASULA *et al.*, 2007 Kinematics of the Western Africa-Eurasia plate boundary from focal mechanisms and GPS data. *Geophysical Journal International* **169**: 1180-1200.
- SHEPARD, F. P., 1972 Submarine Canyons. *Earth-Science Reviews* **8**: 1-&.
- SIROVICH, L., and F. PETTENATI, 1999 Seismotectonic outline of South-Eastern Sicily: an evaluation of available options for the earthquake fault rupture scenario. *Journal of Seismology* **3**: 213-233.
- SOLOV'EV, S. L., O. G. N. SOLOV'EVA, C. N. GO, K. S. KIM and N. A. SHCHETNIKOV, 2000 *Tsunamis in the Mediterranean Sea 2000 BC-2000 AD*. Springer.
- STEWART, I., A. CUNDY, S. KERSHAW and C. FIRTH, 1997a Holocene coastal uplift in the Taormina area, northeastern Sicily: implications for the southern prolongation of the Calabrian seismogenic belt. *Journal of Geodynamics* **24**: 37-50.

- STEWART, I. S., A. CUNDY, S. KERSHAW and C. FIRTH, 1997b Holocene coastal uplift in the Taormina area, northeastern Sicily: Implications for the southern prolongation of the Calabrian seismogenic belt. *Journal of Geodynamics* **24**: 37-50.
- SUPPASRI, A., S. KOSHIMURA and F. IMAMURA, 2011 Developing tsunami fragility curves based on the satellite remote sensing and the numerical modeling of the 2004 Indian Ocean tsunami in Thailand. *Natural Hazards and Earth System Science* **11**: 173-189.
- SYNOLAKIS, C. E., and E. N. BERNARD, 2006 Tsunami science before and beyond Boxing Day 2004. *Philosophical Transactions of the Royal Society A: Mathematical, Physical and Engineering Sciences* **364**: 2231-2265.
- TANSI, C., F. MUTO, S. CRITELLI and G. IOVINE, 2007 Neogene-Quaternary strike-slip tectonics in the central Calabrian Arc (Southern Italy). *Journal of Geodynamics* **43**: 393-414.
- TARAMELLI, T., 1911 Sull'origine dello Stretto di Messina. *Atti Società Italiana per il Progresso delle Scienze*, III Riunione, Roma: 29.
- TAYLOR, and FRANCIS, 2009 *The Messina Strait Bridge: A Challenge and a Dream*, pp. Oxford: CRC Press, Abingdon.
- TIBOR, G., T. M. NIEMI, Z. BEN-AVRAHAM, A. AL-ZOUBI, R. A. SADE *et al.*, 2010 Active tectonic morphology and submarine deformation of the northern Gulf of Eilat/Aqaba from analyses of multibeam data. *Geo-Marine Letters* **30**: 561-573.
- TINTI, S., and A. ARMIGLIATO, 2003a The use of scenarios to evaluate the tsunami impact in Southern Italy. *Marine Geology* **199**: 221-243.
- TINTI, S., and A. ARMIGLIATO, 2003b The use of scenarios to evaluate the tsunami impact in Southern Italy. *Marine Geology* **199**: 221-243.
- TINTI, S., A. ARMIGLIATO and E. BORTOLUCCI, 2001 Contribution of tsunami data analysis to constrain the seismic source: the case of the 1693 eastern Sicily earthquake. *Journal of Seismology* **5**: 41-61.
- TINTI, S., A. ARMIGLIATO, E. BORTOLUCCI and A. PIATANESI, 1999a Identification of the source fault of the 1908 Messina earthquake through Tsunami modelling. Is it a possible task? *Physics and Chemistry of the Earth Part B-Hydrology Oceans and Atmosphere* **24**: 417-421.
- TINTI, S., E. BORTOLUCCI and A. ARMIGLIATO, 1999b Numerical simulation of the landslide-induced tsunami of 1988 on Vulcano Island, Italy. *Bulletin of Volcanology* **61**: 121-137.
- TINTI, S., F. ZANIBONI, A. ARMIGLIATO, G. PAGNONI, S. GALLAZZI *et al.*, 2007 Tsunamigenic landslides in the western Corinth Gulf: numerical scenarios, pp. 405-414 in *Submarine Mass Movements and Their Consequences*. Springer.
- TORTORICI, L., C. MONACO, C. TANSI and O. COCINA, 1995 Recent and Active Tectonics in the Calabrian Arc (Southern Italy). *Tectonophysics* **243**: 37-55.
- UMHOFER, P. J., T. SCHWENNICKE, M. T. DEL MARGO, G. RUIZ-GERALDO, J. C. INGLE *et al.*, 2007 Transensional fault-termination basins: an important basin type illustrated by the Pliocene San Jose Island basin and related basins in the southern Gulf of California, Mexico. *Basin Research* **19**: 297-322.
- VALENSISE, G., R. BASILI and P. BURRATO, 2008 La sorgente del terremoto del 1908 nel quadro sismotettonico dello Stretto di Messina. Il Terremoto e il Maremoto del 28 dicembre 1908-Analisi sismologica, impatto, prospettive.
- VALENSISE, G., and D. PANTOSTI, 1992 A 125 Kyr-long geological record of seismic source repeatability: the Messina Straits (Southern Italy) and the 1908 earthquake (Ms 7.1/2). *Terra Nova* **4**: 472-483.
- VIGNAROLI, G., F. ROSSETTI, T. THEYE and C. FACCENNA, 2008 Styles and regimes of orogenic thickening in the Peloritani Mountains (Sicily, Italy): new constraints on the tectono-metamorphic evolution of the Apennine belt. *Geological Magazine* **145**: 552-569.

- VITI, M., E. MANTOVANI, D. BABBUCCI and C. TAMBURELLI, 2011a Plate kinematics and geodynamics in the Central Mediterranean. *Journal of Geodynamics* **51**: 190-204.
- VITI, M., E. MANTOVANI, D. BABBUCCI and C. TAMBURELLI, 2011b Plate kinematics and geodynamics in the Central Mediterranean. *Journal of Geodynamics* **51**: 190-204.
- WARN-VARNAS, A., J. HAWKINS, P. K. SMOLARKIEWICZ, S. A. CHIN-BING, D. KING *et al.*, 2007 Solitary wave effects north of Strait of Messina. *Ocean Modelling* **18**: 97-121.
- WELLS, D. L., and K. J. COPPERSMITH, 1994 New Empirical Relationships among Magnitude, Rupture Length, Rupture Width, Rupture Area, and Surface Displacement. *Bulletin of the Seismological Society of America* **84**: 974-1002.
- WESTAWAY, R., 1992 Seismic Moment Summation for Historical Earthquakes in Italy - Tectonic Implications. *Journal of Geophysical Research-Solid Earth* **97**: 15437-15464.
- WESTAWAY, R., 1993 Quaternary Uplift of Southern Italy. *Journal of Geophysical Research-Solid Earth* **98**: 21741-21772.
- WHITE, N., J. JACKSON and D. MCKENZIE, 1986 The relationship between the geometry of normal faults and that of the sedimentary layers in their hanging walls. *Journal of Structural Geology* **8**: 897-909.
- WORTEL, M. J. R., and W. SPAKMAN, 2000 Geophysics - Subduction and slab detachment in the Mediterranean-Carpathian region. *Science* **290**: 1910-1917.
- YALÇINER, A., E. PELINOVSKY, T. TALIPOVA, A. KURKIN, A. KOZELKOV *et al.*, 2004 Tsunamis in the Black Sea: comparison of the historical, instrumental, and numerical data. *Journal of Geophysical Research: Oceans* (1978–2012) **109**.
- ZEILON, N., 1912 On the seiches of the Gullmar Fjord. *Sv. Hydrogr. Biol. Komm. Skr.* **5**: 1-49.
- ZOLLO, A., A. EMOLO, A. HERRERO and L. IMPROTA, 1999 High frequency strong ground motion modelling in the Catania area associated with the Ibleo-Maltese fault system. *Journal of Seismology* **3**: 279-+.

ACKNOWLEDGEMENTS

First and foremost, I would like to thank my supervisor Prof. Dr. Sebastian Krastel. For me, it has been an honour for me to work as a Ph.D. student with him. He has taught me, both consciously and unconsciously, how good geoscience can be done. I appreciate all his contributions of time, ideas, and funding to make my Ph.D. experience productive and stimulating. The joy and enthusiasm he has for his research was contagious and motivational for me, even during tough time in the Ph.D. pursuit. I am thankful for the excellent example he has provided as a successful scientist and professor. I am not outstanding enough, but he did not give up on me. Thanks for his believe in me. Secondly, I want to thank my second supervisor Prof. Dr. Jan-Hinrich Behrmann. He has given me a lot of nice suggestions and instructions to my works, especially when I was completely confused. I like his preciseness and straightforwardness. I appreciated the cooperation of our Italian cooperators, Francesco Chiocci and Domenico Ridente as well as Sapienza University of Rome. It was them who proposed this project that we could have this opportunity to learn more things and get a doctor degree. Thanks very much.

The members of our research group have contributed immensely to my personal and professional time at CAU. The group has been a source of friendships as well as good advice and collaboration. I am grateful to our group's administrative assistants who kept us organized and was always ready to help.

I would like to acknowledge Dr. Deniz Cukur who worked as a postdoc in our group until last year. I very much appreciated his enthusiasm, intensity, willingness, and amazing ability to do research and to be a successful scientist. We always sat together to talk about scientific questions. To be honest, when I started my work, I was a completely new member in this research field. It was Deniz who gave me the first guidance. I learnt nearly every software that we need from him, especially the "2D Move", and had occupied numerous Saturdays of him. Thanks for his kindness and help. At the end of last October, he got a permanent position in KIGAM (Korea Institute of Geoscience and Mineral Resources). I congratulate to him!

Dr. Mohammad Heidarzadeh is a co-author of one of my manuscripts. We worked in the same office for about one year. During that time, he gave me many suggestions to my work and how to become a doctor. Although he moved to Japan in the last year, which is a pity thing for me, we still keep in touch to perfect our work.

Julia Schwab and Felix Gross, who are also Ph.D. students of my professor, helped me a lot on my living in Kiel and study in GEOMAR (Helmholtz-Zentrum für Ozeanforschung Kiel) and CAU, such as registration in the university, being familiar with the environments of GEOMAR and the university, etc. When I had any confusion in my work, I was willing to ask them. Their friendly and kindness impressed me very much. Thanks for their help.

Other past and present group members that I have had the pleasure to work with or alongside of are Dr. Katja Lindhorst, M.Sc. Irena Schulten, M.Sc. Mathias Meyer, M.Sc. Julio Beier, and numerous others who have come through the lab. Thanks for all the courses I attended and teachers who gave these courses. Thanks for all the teachers who work in the university used to give me help.

My time at CAU was made enjoyable in large part due to many friends and groups that became a part of my life. I am grateful for time spent with roommates and friends, and for many other people and memories.

I gratefully acknowledge the funding sources that made my Ph.D. work possible. I was funded by China Scholarship Council for my first 3 years and was funded by Kiel University for another 9 months. Thanks again for my professor's help when I applied for this additional fund.

For this dissertation, I would like to thank my reading committee members: Prof. Dr. Sebastian Krastel-Gudegast and Prof. Dr. Jan-Hinrich Behrmann for their time, interest, and helpful comments. I would also like to thank the members of my oral defense committee, Prof. Dr. Martin Wahl, Prof. Dr. Sebastian Krastel-Gudegast, Prof. Dr. Jan-Hinrich Behrmann, and PD Dr. Michael Stipp for their time and insightful questions.

Lastly, I would like to thank my family for all their love and encouragement. For my parents who raised me with a love of life and supported me in all my pursuits. Thanks for my aunts and uncles. Without their guarantee, I could not get fund from our government. Thanks to them. Thanks.

Lili Fu

Christian-Albrechts-Universität zu Kiel

September 2015

CURRICULUM VITAE

BASIC INFORMATION

Name: 付莉莉 / Lili Fu

Gender: Female

Date of Birth: 21.08.1980

Place of Birth: Jilin City, Jilin Province, P. R. China

Marital Status: Unmarried

Educational Level: Master of Science

EDUCATION

11.2011 - Present:

PhD candidate of Marine Geosciences, funded by China Scholarship Council (CSC)

12.2012-Present, Institut für Geowissenschaften, Christian-Albrechts Universität zu Kiel

11.2011-11.2012, GEOMAR | Helmholtz-Zentrum für Ozeanforschung Kiel

Supervisor: Prof. Dr. Sebastian Krastel, Prof. Dr. Jan-Hinrich Behrmann

09.2008 – 07.2011:

Master's degree of Marine Geology

Institute of Estuarine and Coastal Zone, College of Marine Geo-science, Ocean University of China

Supervisor: 冯秀丽 博士 教授 / Prof. Dr. Xiuli Feng

09.1999 – 07.2003:

Bachelor's degree of Geographical Science

College of Tourism and Geographical Science, Jilin Normal University

WORK EXPERIENCES

08.2003 - 07.2008

Full-Time High School Geography Teacher

No.3 High School of Deqing County, Zhejiang Province